THE EXTENDED HIGH-ORDER SANDWICH PANEL THEORY

A Thesis
Presented to
The Academic Faculty

by

Catherine N. Phan

In Partial Fulfillment
of the Requirements for the Degree
Doctor of Philosophy in the
School of Aerospace Engineering

Georgia Institute of Technology
May 2012

THE EXTENDED HIGH-ORDER SANDWICH PANEL THEORY

Approved by:

Professor George A. Kardomateas,
Advisor
School of Aerospace Engineering
Georgia Institute of Technology

Professor Yeoshua Frostig
School of Civil Engineering
Engineering
Technion Institute of Israel

Professor Dewey H. Hodges
School of Aerospace Engineering
Georgia Institute of Technology

Professor Victor Birman
School of Mechanical Engineering
Missouri Institute of Technology

Professor Massimo Ruzzene
School of Aerospace Engineering
Georgia Institute of Technology

Date Approved: 15 12 2011

To my parents,

Ban and Loan Phan.

ACKNOWLEDGEMENTS

I want to thank my committee, for each of their individual suggestions that have helped me to explore this topic more deeply. Their guidance and dedication to the advancement of knowledge is commendable. I am especially grateful to my advisor and mentor Professor Kardomateas for always playing a positive supportive role in our research together and for all the great advice on research, getting published, and life in general. His work in providing elasticity solutions for orthotropic material sandwich panels have been invaluable in the validation of the new present theory. I am also grateful to have worked with and to know Professor Frostig. His enthusiasm for sandwich composites is infectious and I have been inspired to really look at the physical meaning of this theory and its results. Thank you to Professor Hodges for introducing me to the work of Berdichevsky and the Variational Asymptotic method, a topic I will continue to investigate further. Thank you to Professor Ruzzene for giving me advice on what challenges need to be addressed when comparing the new theory for dynamic problems. Thank you to Professor Birman for also being such a positive role in my committee and reminding me that practical application is important. Also I would like to thank Dr. Mark Battley, Senior Research Associate at the Center for Advanced Composites Materials (CACM) in Auckland, NZ, and soon to be Dr. Nathan Bailey for allowing me to come to beautiful New Zealand and teaching me how to make sandwich panels and conduct impact experiments. Their help gave me first hand experience in experimentally validating the new extended high-order sandwich panel theory.

The financial support of the Office of Naval Research and the interest and encouragement of the Grant Monitor, Dr. Y.D.S. Rajapakse, are both gratefully acknowledged. In addition, I want to thank NSF and the Royal Society of New Zealand for funding my research collaboration efforts at the CACM.

Lastly, I would like to thank Michael Brian Ward for his support and patience throughout my PhD work.

TABLE OF CONTENTS

LIST OF TABLES

LIST OF FIGURES

SUMMARY

The contribution of this thesis is an extended high-order sandwich panel theory (EHSAPT) for sandwich beams/wide panels, in which the axial stresses are taken into account as well as the shear and transverse normal stresses in the core, and its validation. The general nonlinear formulation of EHSAPT is given in Chapter 2. Validation of the present theory is made by comparison with elasticity solutions and experimental data. The accuracy of EHSAPT is assessed for the standard class of structural analysis problems which include: static loading, static instability (global buckling and wrinkling), free vibrations, and dynamic loading. In Chapter 3 the static response to a half-sine distributed load applied to the top face sheet of a simply supported sandwich beam/wide panel is solved. Validation is made with elasticity, and Euler-Bernoulli beam, first order shear deformation theory, and HSAPT were also included for comparison. In Chapter 4 the static global buckling critical load is determined for a simply supported sandwich beam/wide panel under edgewise loading. Validation is made with elasticity, and Allen's formula and HSAPT are included for comparison. In Chapter 5 the static wrinkling critical load of a simply supported sandwich beam/wide panel is investigated. Validation includes comparison with elasticity, experimental results reported in literature, and recently acquired experimental results. Results using Hoff-Mautner's wrinkling formula and HSAPT are also shown. In Chapter 6 the free vibrations of a simply supported sandwich beam/wide panel are explored, and the predicted antisymmetric and symmetric natural frequencies are compared to experimental results found in the literature and with elasticity. The last validation of EHSAPT is made for the dynamic response to a half-sine distributed

load with an exponential time decay applied to the top face sheet of a simply supported sandwich beam. Results are compared with elasticity. The response from using HSAPT is also shown. Chapter 8 presents results from an impact experiment upon a sandwich panel and comparison with EHSAPT. Finally, Chapter 9 gives overall comments on the future work that can be done with EHSAPT.

CHAPTER I

INTRODUCTION AND LITERATURE REVIEW

Typical sandwich panels consist of two stiff metallic or composite thin face sheets separated by a thick, lightweight core. The core could be a stiff honeycomb, soft foam, or anything in between. This configuration gives the sandwich material system high stiffness and strength, low weight, and high-energy absorption capability. As a result of these desirable properties, sandwich structures have found applications in the construction of aerospace vehicles, naval vehicles, wind turbines and civil infrastructure. Structures in these applications may be subjected to highly transient loads such as blast, gusts, or impact, with surface pressure spread over the entire structure or over a concentrated area. A good understanding of the response of suddenly loaded sandwich structural configurations is essential in ensuring their integrity.

It is common in the analysis of sandwich panels to neglect the transverse deformation of the core [33, 2, 38]. An early theory of sandwich structures, commonly known as the First-Order Shear Deformation Theory (FOSDT), refines classic beam/plate theories by taking into account the shear rigidity of the core, but this theory still assumes that longitudinal deformation is linear in the thickness coordinate and the core is infinitely rigid in the transverse direction. FOSDT assumes a uniform shear strain through the height of the panel. Though this model is simple, its application is acceptable when the sandwich core is very stiff vertically and statically loaded. In general, and especially in modern sandwich panels with cores of foam type, the core is flexible in all directions. Hence, the assumption of a stiff core in the vertical direction is violated, but the assumption of negligible in-plane stresses is still valid due to low in-plane rigidity with respect to that of the face sheets. When the core

is not very stiff in the vertical direction, the FOSDT gives inaccurate predictions for the transverse displacement under quasi-static loading [31]. More importantly, experimental results [16, 21, 28, 37, 40] have shown that the core can undergo significant transverse deformation when the sandwich structure experiences a sudden, impulsive loading and the core plays an important role in the absorption of the impact energy. Therefore, a more accurate sandwich panel model should account for the transverse compressibility of the core. Consideration of the core compressibility implies that the displacements of the upper and lower face sheets may not be identical. Another important issue is the accurate representation of the core shear, which is a key component in sandwich analysis since cores are typically of very low modulus and thus transverse shear has a significant influence on the structural behavior.

Many refined theories exist in which various assumptions are made in order to better model the stress, strain, and displacement distribution throughout the thickness of a composite. Berdichevsky [3, 4] offers an approximate universal asymptotic theory for linear and nonlinear sandwich beams and plates with geometric and material symmetry about the mid-plane of the structure subject to static loads. This theory can give accurate results for the structural response to a static loading or even to a dynamic loading of long-duration, but is not suitable for highly transient loading problems.

Numerous equivalent single layer, layer-wise, zig-zag, and mixed layer-wise theories have been proposed for the analysis of sandwich beams [1] and plates [8]. These theories typically make the same assumption in each layer regarding the distribution of displacements and/or stresses through the thickness coordinate z, and enforce compatibility and/or traction continuity at the interfaces. Layer-wise theories with displacement and stress assumptions of $\mathrm{O}(z^2)$ to $\mathrm{O}(z^4)$ presented in [8] give accurate displacements, stresses (longitudinal and shear), and natural frequencies compared to elastostatic and elastodynamic benchmarks; however, transverse normal stress/strain

results were not shown. Furthermore, these theories are often presented in an integral sense because they rely on symbolic mathematical software to evaluate a particular application [7].

Other theories do not make the same displacement/stress distribution assumption for each layer of the sandwich. Hohe et al. [19] developed a model for sandwich plates in which the transverse normal stress is constant along the transverse coordinate, z, and the shearing stress is first order in z. A compressible sandwich panel theory must allow for at least a linear distribution of transverse stress through the height of the core if transverse loading is applied to just one face. Li and Kardomateas [27] explored a higher-order theory for plates in which the transverse normal stress in the core is of third order in z, and the shear stress in the core is of fourth order in z. This theory gave inaccurate transverse stress distributions through the core for a quasi-statically loaded problem.

In 1992, Frostig et al. developed the High-order Sandwich Panel Theory (HSAPT), a compressible core theory which accounts for the transverse and shear stresses in the core but neglects the in-plane stresses in the core [15]. Neglecting the in-plane stresses in the core results in a constant shear stress distribution through the thickness of the core which has been shown to be a good approximation for sandwich constructions with very soft cores undergoing quasi-static loading [31]. Neglecting the axial stresses in the core reduces the static equilibrium equation of elasticity to the following:

$$\cancelto{0}{\frac{\partial \sigma_{xx}}{\partial x}} + \frac{\partial \tau_{xz}}{\partial z} = 0 \tag{1}$$

Therefore a constant shear stress distribution through the thickness of the core is a good approximation for sandwich constructions with very soft cores in static problems [31]. However, for dynamic problems the right hand side is no longer zero but equal to the density of the core times the axial acceleration of the core. Therefore, in dynamic problems, if the core's density and axial acceleration are not negligible, the shear

stress may not always be constant through the thickness.

The static formulation of HSAPT has been used to solve numerous problems. Comparison of HSAPT with elasticity [36] and experiment [5] has shown that HSAPT accurately predicts displacements and axial strain concentrations in the faces adjacent to supports and concentrated load regions. With regard to the core, however, though HSAPT is a good approximate theory away from supports, and concentrated load regions, it can show inaccurate shear stress and axial strain through-thickness distributions adjacent to regions of concentrated loads and supports [36]. HSAPT has been used to study the global buckling and wrinkling behavior of soft core sandwich composite beams [13] and plates [11].

There are two models of HSAPT that exist in literature for dynamic problems. The original model [14] is a mixed formulation in which the five unknowns are from generalized displacement varialbes are: the two axial displacements at the top and bottom face sheet $u_0^t(x,t)$, $u_0^b(x,t)$, and the two transverse displacements at the top and bottom face sheets $w^t(x,t)$, $w^b(x,t)$, plus the uniform shear stress in the core $\tau^c(x)$. In the mixed formulation model, the accelerations are assumed to vary linearly through the core. The second model is a displacement-based formulation in which the five generalized displacement variables are: $u_0^t(x,t)$, $u_0^b(x,t)$, $w^t(x,t)$, $w^b(x,t)$, and the mid-core transverse displacement $w_0^c(x,t)$ (instead of the shear stress $\tau^c(x)$). In this latter model, the accelerations in the core are allowed to be nonlinear through the core. The mixed formulation of HSAPT has been used to study the free vibrations of sandwich beams in [14, 35]. The mixed and displacement based formulations of HSAPT have been used to study free vibrations of sandwich plates in [34].

The theories mentioned above make the usual assumption that the axial rigidity in the core can be neglected for sandwich beams/wide panels with very soft cores compared to the face sheets. Under some circumstances, such as improvement of impact rigidity of the sandwich panel or introduction of axial loads into the core, the effect

of the axial rigidity of the core should be considered. Frostig [12] suggested a computational model that takes into account the axial rigidity of the core for sandwich beams/wide panels for stretchable electronic applications. Furthermore, the assumption of constant shear stress through through the height of the core is one that is reduced from static equilibrium when the axial stresses in the core are neglected (see Eqn. (1)). Dynamic equilibrium equations in which the axial inertial terms of the core are included will not yield a constant shear stress distribution through the height of the core. For these reasons, the formulation and validation of the extended high-order sandwich panel theory (EHSAPT) for beams/wide panels in which the axial rigidity of the core is included is the focus of this thesis.

CHAPTER II

GENERAL NONLINEAR FORMULATION OF EHSAPT

Figure 1 shows a sandwich beam/wide panel of length a with a core of thickness $2c$ and top and bottom face sheet thicknesses f_t and f_b, respectively. The width of the panel is b. A Cartesian coordinate system (x, y, z) is defined at one end of the panel and its origin is placed at the middle of the core. The y-direction is not shown, but is pointed into the page. Only loading in the x-z plane is considered to act on the panel which solely causes displacements in the x and z directions designated by u and w, respectively. Therefore any displacements, strains, stresses, or loads dependent upon y are not considered. The superscripts t, b, and c shall refer to the top face sheet, bottom face sheet, and core, respectively. The subscript 0 refers to the middle surface of the corresponding phase.

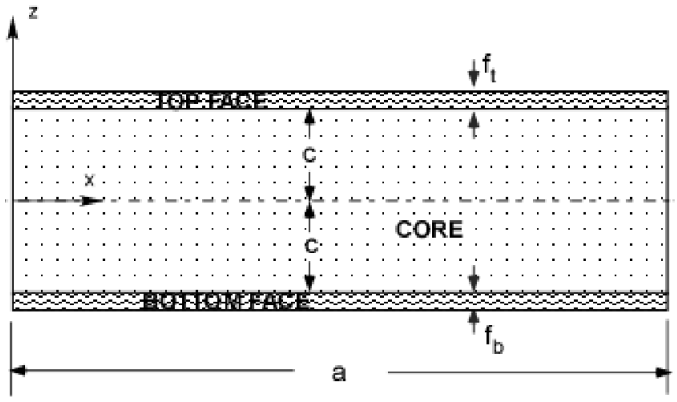

Figure 1: Definition of the sandwich configuration

The displacement fields of the top and bottom face sheets are are assumed to satisfy the Euler-Bernoulli assumptions: that plane sections remain plane and perpendicular to the constituent's deformed axis, and that sections are infinitely rigid in the y and z-directions. Therefore, the displacement field for the top face sheet,

$c \leq z \leq c + f_t$, is:

$$w^t(x,z,t) = w^t(x,t) \; ; \qquad u^t(x,z,t) = u_0^t(x,t) - \left(z - c - \frac{f_t}{2}\right) w_{,x}^t(x,t) \tag{2a}$$

and for the bottom face sheet, $-(c + f_b) \leq z \leq -c$:

$$w^b(x,z,t) = w^b(x,t) \; ; \qquad u^b(x,z,t) = u_0^b(x,t) - \left(z + c + \frac{f_b}{2}\right) w_{,x}^b(x,t) \tag{2b}$$

Since large displacements and moderate rotations are considered the non-linear strains in the face sheets read:

$$\epsilon_{xx}^{t,b}(x,z,t) = u_{,x}^{t,b}(x,z,t) + \frac{1}{2} w_{,x}^{t,b}(x,t)^2 \tag{3}$$

If a linear analysis is pursued, the second (squared) term in Eqn. (3) is neglected.

While the face sheets can change their length only longitudinally, the core can change its height and length. The displacement fields considered for the core follow the resulting fields that are in the HSAPT model (see Frostig et al. [15]), and they read:

$$w^c(x,z,t) = w_0^c(x,t) + w_1^c(x,t) z + w_2^c(x,t) z^2 \tag{4a}$$

$$u^c(x,z,t) = u_0^c(x,t) + \phi_0^c(x,t) z + u_2^c(x,t) z^2 + u_3^c(x,t) z^3 \tag{4b}$$

where w_0^c and u_0^c are the transverse and in-plane displacements, respectively, ϕ_0^c is the slope at the centroid of the core, while w_1^c, w_2^c are the transverse unknown functions and u_2^c, u_3^c are the in-plane unknown functions to be determined by enforcing compatibility of the displacements at the upper, $z = c$, and lower, $z = -c$, face-core interfaces. Hence, using the compatibility condition in the transverse direction at the upper and the lower face core interfaces (same core and face sheet transverse displacement) yields the following distribution of the transverse displacement:

$$w^c(x,z,t) = \left(-\frac{z}{2c} + \frac{z^2}{2c^2}\right) w^b(x,t) + \left(1 - \frac{z^2}{c^2}\right) w_0^c(x,t) + \left(\frac{z}{2c} + \frac{z^2}{2c^2}\right) w^t(x,t) \tag{5a}$$

The in-plane displacement of the core $u^c(x,z,t)$, is determined through the fulfillment of the compatibility conditions of the in-plane direction, see second equations in Eqns.

(2a) and (2b) at $z = c$ and $-c$ (same core and face sheet in-plane displacement at the interface). Hence, after some algebraic manipulation they read:

$$\begin{aligned} u^c(x,z,t) =& z\left(1-\frac{z^2}{c^2}\right)\phi_0^c(x,t) + \frac{z^2}{2c^2}\left(1-\frac{z}{c}\right)u_0^b + \left(1-\frac{z^2}{c^2}\right)u_0^c + \frac{z^2}{2c^2}\left(1+\frac{z}{c}\right)u_0^t \\ &+ \frac{f_b z^2}{4c^2}\left(-1+\frac{z}{c}\right)w_{,x}^b + \frac{f_t z^2}{4c^2}\left(1+\frac{z}{c}\right)w_{,x}^t \end{aligned} \tag{5b}$$

Therefore, this theory is in terms of seven generalized displacement variables (unknown functions of x and t): two for the top face sheet, w_0^t, u_0^t, two for the bottom face sheet, w_0^b, u_0^b, and three for the core, w_0^c, u_0^c and ϕ_0^c. The strains can be obtained from the displacements using the linear strain-displacement relations. Hence, the transverse normal strain is:

$$\epsilon_{zz}^c = \frac{\partial w^c}{\partial z} = \left(\frac{z}{c^2}-\frac{1}{2c}\right)w^b - \frac{2z}{c^2}w_0^c + \left(\frac{z}{c^2}+\frac{1}{2c}\right)w^t \tag{6a}$$

and the shear strain

$$\begin{aligned} \gamma_{zx}^c = \frac{\partial u^c}{\partial z} + \frac{\partial w^c}{\partial x} =& \left(1-\frac{3z^2}{c^2}\right)\phi_0^c + \left(\frac{z}{c^2}-\frac{3z^2}{2c^3}\right)u_0^b - \left(\frac{2z}{c^2}\right)u_0^c + \left(\frac{z}{c^2}+\frac{3z^2}{2c^3}\right)u_0^t + \\ & \left[-\left(\frac{c+f_b}{2c^2}\right)z + \left(\frac{2c+3f_b}{4c^3}\right)z^2\right]w_{,x}^b + \left(1-\frac{z^2}{c^2}\right)w_{0,x}^c + \\ & \left[\left(\frac{c+f_t}{2c^2}\right)z + \left(\frac{2c+3f_t}{4c^3}\right)z^2\right]w_{,x}^t \end{aligned} \tag{6b}$$

There is also a linear axial plane strain in the core

$$\epsilon_{xx}^c = \frac{\partial u^c}{\partial x} \tag{6c}$$

which has the same structure as Eqn. (5b), but with the generalized function coordinates replaced by one order higher derivative with respect to x. Nonlinear in-plane strains in the core are neglected due to the core's low in-plane rigidity as compared with that of the face sheets.

In the following $C_{ij}^{t,b,c}$ are the corresponding stiffness constants where we have used the notation $1 \equiv x$, $3 \equiv z$, and $55 \equiv xz$. Only orthotropic materials are considered.

For the face sheets, the transverse stress that acts in the plane of the cross-section, $\sigma_{zz}^{t,b}$, is much smaller than the axial stresses $\sigma_{xx}^{t,b}$. When this stress component in the plane of the cross-section is assumed to be null, the constitutive laws lead to the following *reduced Hooke's law*:

$$\sigma_{xx}^{t,b} = C_{11}^{t,b}\epsilon_{xx}^{t,b} \tag{7}$$

where, in terms of the Young's modulus, $E_1^{t,b}$ the stiffness constant for a beam/wide panel is: $C_{11}^{t,b} = E_1^{t,b}$.

We also assume an orthotropic core with stress-strain relations:

$$\begin{Bmatrix} \sigma_{xx}^c \\ \sigma_{zz}^c \\ \tau_{xz}^c \end{Bmatrix} = \begin{bmatrix} C_{11}^c & C_{13}^c & 0 \\ C_{13}^c & C_{33}^c & 0 \\ 0 & 0 & C_{55}^c \end{bmatrix} \begin{Bmatrix} \epsilon_{xx}^c \\ \epsilon_{zz}^c \\ \gamma_{xz}^c \end{Bmatrix} \tag{8a}$$

where the components C_{ij}^c in Eqn. (8a) is the inverse of the compliance matrix, whose components a_{ij}^c are expressed in terms of the Young's and shear moduli and Poisson's ratio of the core as:

$$a_{11}^c = \frac{1}{E_1^c}; \quad a_{13}^c = -\frac{\nu_{31}^c}{E_3^c}; \quad a_{33}^c = \quad \frac{1}{E_3^c}; \quad a_{55}^c = \frac{1}{G_{31}^c} \tag{8b}$$

The equations of motion and appropriate boundary conditions are derived from Hamilton's principle:

$$\int_{t_1}^{t_2} \delta(U + V - T)dt = 0 \tag{9a}$$

where U is the strain energy of the sandwich panel, V is the potential due to the applied loading, and T is the kinetic energy. The first variation of the strain energy of the sandwich panel is:

$$\begin{aligned} \delta U = \int_0^a \Bigg[& \int_{-c+f_b}^{-c} b\ \sigma_{xx}^b \delta\epsilon_{xx}^b dz + \int_{-c}^{c} b\left(\sigma_{xx}^c \delta\epsilon_{xx}^c + \sigma_{zz}^c \delta\epsilon_{zz}^c + \tau_{zx}^c \delta\gamma_{zx}^c\right) dz \\ & + \int_{c}^{c+f_t} b\ \sigma_{xx}^t \delta\epsilon_{xx}^t dz \Bigg] dx \end{aligned} \tag{9b}$$

and the first variation of the external potential due to several general loading conditions shown in Figure 2 is:

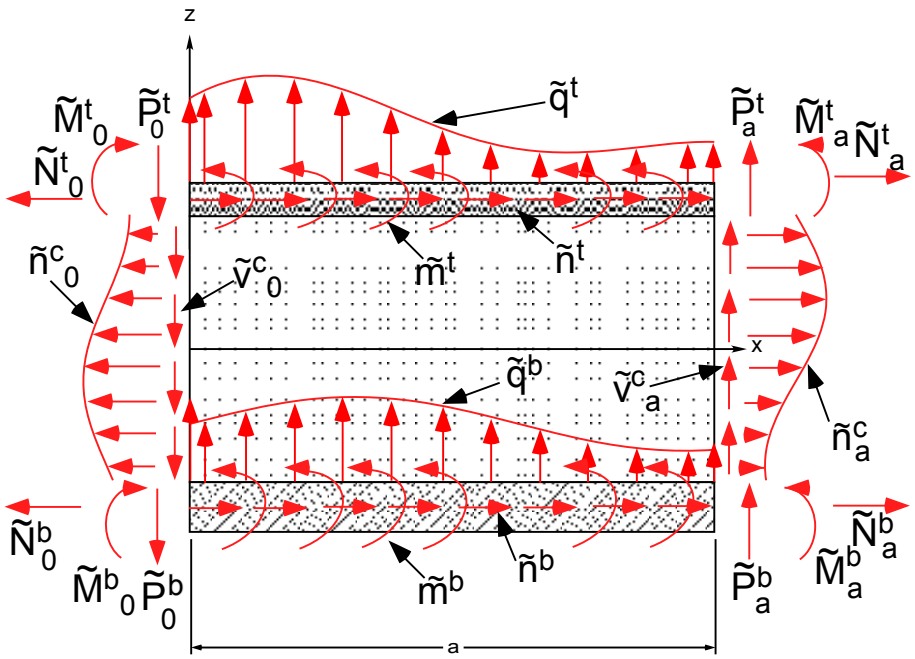

Figure 2: General loading on sandwich panel. Distributed loading of the core is only shown at the edges.

$$
\begin{aligned}
\delta V = &- \int_0^a \int_0^b \left(\widetilde{n}^t \delta u_0^t + \widetilde{n}^b \delta u_0^b + \widetilde{q}^t \delta w^t + \widetilde{q}^b \delta w^b + \widetilde{m}^t \delta w^t_{,x} + \widetilde{m}^b \delta w^b_{,x} \right) dy\, dx \\
&+ \widetilde{N}_0^t(t) \delta u_0^t(0,t) - \widetilde{N}_a^t(t) \delta u_0^t(a,t) \\
&+ \widetilde{N}_0^b(t) \delta u_0^b(0,t) - \widetilde{N}_a^b(t) \delta u_0^b(a,t) \\
&+ \widetilde{P}_0^t(t) \delta w^t(0,t) - \widetilde{P}_a^t(t) \delta w^t(a,t) \\
&+ \widetilde{P}_0^b(t) \delta w^b(0,t) - \widetilde{P}_a^b(t) \delta w^b(a,t) \\
&+ \widetilde{M}_0^t(t) \delta w^t_{,x}(0,t) - \widetilde{M}_a^t(t) \delta w^t_{,x}(a,t) \\
&+ \widetilde{M}_0^b(t) \delta w^b_{,x}(0,t) - \widetilde{M}_a^b(t) \delta w^b_{,x}(a,t) \\
&- \int_0^b \int_{-c}^c \left(\widetilde{n}^c \delta u^c + \widetilde{v}^c \delta w^c \right) dz\, dy \Bigg]_{x=0}^{a}
\end{aligned}
\tag{9c}
$$

where $\widetilde{n}^{t,b}$ is the distributed in-plane force (along x), $\widetilde{q}^{t,b}$ is the distributed transverse force (along z) and $\widetilde{m}^{t,b}$ is the distributed moment on the top and bottom face sheets. Moreover, $\widetilde{N}_0^{t,b}$ and $\widetilde{N}_a^{t,b}$ are the end axial force at $x = 0$ and $x = a$ respectively, $\widetilde{P}_0^{t,b}$ and $\widetilde{P}_a^{t,b}$ are the end shear force at $x = 0$ and $x = a$ respectively, and $\widetilde{M}_0^{t,b}$ and $\widetilde{M}_a^{t,b}$

are the end moment at the top and bottom face sheets at the ends $x = 0$ and $x = a$, respectively. Please notice the positive sense of the applied concentrated end loads is chosen to be in the same direction as their equivalent end stress resultants. In addition, $\widetilde{n}^c$ is the distributed end axial force and $\widetilde{v}^c$ is the end distributed shear force applied at the ends of the core at $x = 0$ and $x = a$. All the external loads considered are uniformly distributed in the y-direction. Since the face sheets and the core do not exhibit bend-twist coupling the external loads considered only cause deformations in the x-z plane.

In the following we assume that b is constant and $\widetilde{n}^c$ and $\widetilde{v}^c$ are constant and they are only applied at the edges of the beam. In this case,

$$\int_{-c}^{c} b\ \widetilde{n}^c \delta u^c dz = \widetilde{n}^c bc \left[\frac{1}{3}\left(\delta u_0^b + \delta u_0^t\right) + \frac{4}{3}\left(\delta u_0^c\right) - \frac{f_b}{6}\delta w_{,x}^b + \frac{f_t}{6}\delta w_{,x}^t\right] \tag{9d}$$

$$\int_{-c}^{c} b\ \widetilde{v}^c \delta w^c dz = \widetilde{v}^c bc \left(\frac{1}{3}\delta w^b + \frac{4}{3}\delta w_0^c + \frac{1}{3}\delta w^t\right) \tag{9e}$$

Of course, the theory can admit any variation of $\widetilde{n}^c$ and $\widetilde{v}^c$ along z; for example, a bending moment on the core would correspond to a linear variation of $\widetilde{n}^c$ with respect to z. However, for most practical purposes, loads are applied to the face sheets and not the core.

The first variation of the kinetic energy is:

$$\begin{aligned}\delta T = \int_0^a \Bigg(&\int_{-(c+f_b)}^{-c} b\ \rho^b(\dot{u}^b\delta\dot{u}^b + \dot{w}^b\delta\dot{w}^b)dz + \int_{-c}^{c} b\ \rho^c(\dot{u}^c\delta\dot{u}^c + \dot{w}^c\delta\dot{w}^c)dz \\ &+ \int_{c}^{c+f_t} b\ \rho^t(\dot{u}^t\delta\dot{u}^t + +\dot{w}^t\delta\dot{w}^t)dz\Bigg)\ dx\end{aligned} \tag{10}$$

For the sandwich panels made out of orthotropic materials, we can substitute the stresses in terms of the strains from the constitutive relations, Eqns. (7) and (8a), and then the strains, Eqns. (3) and (6), in terms of the displacements profiles, Eqns. (2) and (5), and finally apply the variational principle, Eqns. (9); thus we can write a set of non-linear governing equations in terms of the seven unknown generalized displacement variables as follows:

Top face sheet:

$$\begin{aligned}\delta u_0^t: \quad & \Bigg[-\left(\frac{4}{5}C_{55}^c + \frac{2c^2}{35}C_{11}^c\frac{\partial^2}{\partial x^2} - \frac{2c^2\rho^c}{35}\frac{\partial^2}{\partial t^2}\right)\phi_0^c - \left(\frac{7}{30c}C_{55}^c + \frac{c}{35}C_{11}^c\frac{\partial^2}{\partial x^2} - \frac{c\rho^c}{35}\frac{\partial^2}{\partial t^2}\right)u_0^b \\ & - \left(\frac{4}{3c}C_{55}^c + \frac{2c}{15}C_{11}^c\frac{\partial^2}{\partial x^2} - \frac{2c\rho^c}{15}\frac{\partial^2}{\partial t^2}\right)u_0^c + \left[\frac{47}{30c}C_{55}^c - \alpha_1^t\frac{\partial^2}{\partial x^2} + \left(\frac{6c\rho^c}{35} + f_t\rho^t\right)\frac{\partial^2}{\partial t^2}\right]u_0^t \\ & - \left(\alpha_2^b\frac{\partial}{\partial x} - \frac{cf_b}{70}C_{11}^c\frac{\partial^3}{\partial x^3} + \frac{cf_b\rho^c}{70}\frac{\partial^3}{\partial x\partial t^2}\right)w^b + \left(\beta_1\frac{\partial}{\partial x}\right)w_0^c \\ & + \left(\alpha_3^t\frac{\partial}{\partial x} - \frac{3cf_t}{35}C_{11}^c\frac{\partial^3}{\partial x^3} + \frac{3cf_t\rho^c}{35}\frac{\partial^3}{\partial x\partial t^2}\right)w^t\Bigg]b = \widetilde{n}^t + F_u^t\end{aligned} \tag{11a}$$

where F_u^t is the nonlinear term:

$$F_u^t = C_{11}^t b f_t w_{,x}^t w_{,xx}^t \tag{11b}$$

and $\widetilde{p}^t$ is the distributed in-plane force (along x) at the top face, and

$$\begin{aligned}\delta w^t: \quad & \Bigg[\left(\alpha_4^t\frac{\partial}{\partial x} + \frac{c^2f_t}{35}C_{11}^c\frac{\partial^3}{\partial x^3} - \frac{c^2f_t\rho^c}{35}\frac{\partial^3}{\partial x\partial t^2}\right)\phi_0^c + \left(\alpha_5^t\frac{\partial}{\partial x} + \frac{cf_t}{70}C_{11}^c\frac{\partial^3}{\partial x^3} - \frac{cf_t\rho^c}{70}\frac{\partial^3}{\partial x\partial t^2}\right)u_0^b \\ & + \left(\alpha_6^t\frac{\partial}{\partial x} + \frac{cf_t}{15}C_{11}^c\frac{\partial^3}{\partial x^3} - \frac{cf_t\rho^c}{15}\frac{\partial^3}{\partial x\partial t^2}\right)u_0^c + \left(-\alpha_3^t\frac{\partial}{\partial x} + \frac{3cf_t}{35}C_{11}^c\frac{\partial^3}{\partial x^3} - \frac{3cf_t\rho^c}{35}\frac{\partial^3}{\partial x\partial t^2}\right)u_0^t \\ & + \left(\frac{1}{6c}C_{33}^c + \beta_2\frac{\partial^2}{\partial x^2} - \frac{cf_bf_t}{140}C_{11}^c\frac{\partial^4}{\partial x^4} - \frac{c\rho^c}{15}\frac{\partial^2}{\partial t^2} + \frac{cf_bf_t\rho^c}{140}\frac{\partial^4}{\partial x^2\partial t^2}\right)w^b \\ & + \left(-\frac{4}{3c}C_{33}^c + \alpha_7^t\frac{\partial^2}{\partial x^2} + \frac{2c\rho^c}{15}\frac{\partial^2}{\partial t^2}\right)w_0^c \\ & + \left(\frac{7}{6c}C_{33}^c + \alpha_8^t\frac{\partial^2}{\partial x^2} + \alpha_9^t\frac{\partial^4}{\partial x^4} + \left(\frac{4c\rho^c}{15} + f_t\rho^t\right)\frac{\partial^2}{\partial t^2} - \left(\frac{3cf_t^2\rho^c}{70} + \frac{f_t^3\rho^t}{12}\right)\frac{\partial^4}{\partial x^2\partial t^2}\right)w^t\Bigg]b \\ & = \widetilde{q}^t - \widetilde{m}_{,x}^t + F_w^t\end{aligned} \tag{12a}$$

where F_w^t is the nonlinear term:

$$F_w^t = C_{11}^t b f_t\left[w_{,x}^t u_{0,xx}^t + u_{0,x}^t w_{,xx}^t + \frac{3}{2}(w_{,x}^t)^2 w_{,xx}^t\right] \tag{12b}$$

and $\widetilde{q}^t$ is the distributed transverse force and $\widetilde{m}^t$ is the distributed moment along the top face sheet.

Core:

$$\delta u_0^c: \quad \Bigg[-\left(\frac{4}{3c}C_{55}^c + \frac{2c}{15}C_{11}^c\frac{\partial^2}{\partial x^2} - \frac{2c\rho^c}{15}\frac{\partial^2}{\partial t^2}\right)u_0^b + \left(\frac{8}{3c}C_{55}^c - \frac{16c}{15}C_{11}^c\frac{\partial^2}{\partial x^2} + \frac{16c\rho^c}{15}\frac{\partial^2}{\partial t^2}\right)u_0^c$$
$$-\left(\frac{4}{3c}C_{55}^c + \frac{2c}{15}C_{11}^c\frac{\partial^2}{\partial x^2} - \frac{2c\rho^c}{15}\frac{\partial^2}{\partial t^2}\right)u_0^t + \left(\alpha_6^b\frac{\partial}{\partial x} + \frac{cf_b}{15}C_{11}^c\frac{\partial^3}{\partial x^3} - \frac{cf_b\rho^c}{15}\frac{\partial^3}{\partial x\partial t^2}\right)w^b$$
$$-\left(\alpha_6^t\frac{\partial}{\partial x} + \frac{cf_t}{15}C_{11}^c\frac{\partial^3}{\partial x^3} - \frac{cf_t\rho^c}{15}\frac{\partial^3}{\partial x\partial t^2}\right)w^t\Bigg]b = 0 \tag{13}$$

$$\delta\phi_0^c: \quad \Bigg[\left(\frac{8c}{5}C_{55}^c - \frac{16c^3}{105}C_{11}^c\frac{\partial^2}{\partial x^2} + \frac{16c^3\rho^c}{105}\frac{\partial^2}{\partial t^2}\right)\phi_0^c + \left(\frac{4}{5}C_{55}^c + \frac{2c^2}{35}C_{11}^c\frac{\partial^2}{\partial x^2} - \frac{2c^2\rho^c}{35}\frac{\partial^2}{\partial t^2}\right)u_0^b$$
$$-\left(\frac{4}{5}C_{55}^c + \frac{2c^2}{35}C_{11}^c\frac{\partial^2}{\partial x^2} - \frac{2c^2\rho^c}{35}\frac{\partial^2}{\partial t^2}\right)u_0^t - \left(\alpha_4^b\frac{\partial}{\partial x} + \frac{c^2f_b}{35}C_{11}^c\frac{\partial^3}{\partial x^3} - \frac{c^2f_b\rho^c}{35}\frac{\partial^3}{\partial x\partial t^2}\right)w^b$$
$$+\left(\beta_3\frac{\partial}{\partial x}\right)w_0^c - \left(\alpha_4^t\frac{\partial}{\partial x} + \frac{c^2f_t}{35}C_{11}^c\frac{\partial^3}{\partial x^3} - \frac{c^2f_t\rho^c}{35}\frac{\partial^3}{\partial x\partial t^2}\right)w^t\Bigg]b = 0 \tag{14}$$

$$\delta w_0^c: \quad \Bigg[-\left(\beta_3\frac{\partial}{\partial x}\right)\phi_0^c + \left(\beta_1\frac{\partial}{\partial x}\right)u_0^b - \left(\beta_1\frac{\partial}{\partial x}\right)u_0^t + \left(-\frac{4}{3c}C_{33}^c + \alpha_7^b\frac{\partial^2}{\partial x^2} + \frac{2c\rho^c}{15}\frac{\partial^2}{\partial t^2}\right)w^b$$
$$+\left(\frac{8}{3c}C_{33}^c - \frac{16c}{15}C_{55}^c\frac{\partial^2}{\partial x^2} + \frac{16c\rho^c}{15}\frac{\partial^2}{\partial t^2}\right)w_0^c + \left(-\frac{4}{3c}C_{33}^c + \alpha_7^t\frac{\partial^2}{\partial x^2} + \frac{2c\rho^c}{15}\frac{\partial^2}{\partial t^2}\right)w^t\Bigg]b = 0 \tag{15}$$

Bottom face sheet:

$$\delta u_0^b: \quad \Bigg[\left(\frac{4}{5}C_{55}^c + \frac{2c^2}{35}C_{11}^c\frac{\partial^2}{\partial x^2} - \frac{2c^2\rho^c}{35}\frac{\partial^2}{\partial t^2}\right)\phi_0^c + \left(\frac{47}{30c}C_{55}^c - \alpha_1^b\frac{\partial^2}{\partial x^2} + \left(\frac{6c\rho^c}{35} + f_b\rho^b\right)\frac{\partial^2}{\partial t^2}\right)u_0^b$$
$$-\left(\frac{4}{3c}C_{55}^c + \frac{2c}{15}C_{11}^c\frac{\partial^2}{\partial x^2} - \frac{2c\rho^c}{15}\frac{\partial^2}{\partial t^2}\right)u_0^c - \left(\frac{7}{30c}C_{55}^c + \frac{c}{35}C_{11}^c\frac{\partial^2}{\partial x^2} - \frac{c\rho^c}{35}\frac{\partial^2}{\partial t^2}\right)u_0^t$$
$$+\left(-\alpha_3^b\frac{\partial}{\partial x} + \frac{3cf_b}{35}C_{11}^c\frac{\partial^3}{\partial x^3} - \frac{3cf_b\rho^c}{35}\frac{\partial^3}{\partial x\partial t^2}\right)w^b - \left(\beta_1\frac{\partial}{\partial x}\right)w_0^c$$
$$+\left(\alpha_2^t\frac{\partial}{\partial x} - \frac{cf_t}{70}C_{11}^c\frac{\partial^3}{\partial x^3} + \frac{cf_t\rho^c}{70}\frac{\partial^3}{\partial x\partial t^2}\right)w^t\Bigg]b = \widetilde{n}^b + \hat{F}_u^b \tag{16a}$$

where F_u^b is the nonlinear term:

$$F_u^b = C_{11}^b b f_b w_{,x}^b w_{,xx}^b \tag{16b}$$

and $\widetilde{p}^b$ is the distributed in-plane force (along x) at the bottom face.

$$\begin{aligned}\delta w^b: \quad & \left[\left(\alpha_4^b\frac{\partial}{\partial x}+\frac{c^2 f_b}{35}C_{11}^c\frac{\partial^3}{\partial x^3}-\frac{c^2 f_b\rho^c}{35}\frac{\partial^3}{\partial x\partial t^2}\right)\phi_0^c+\left(\alpha_3^b\frac{\partial}{\partial x}-\frac{3cf_b}{35}C_{11}^c\frac{\partial^3}{\partial x^3}+\frac{3cf_b\rho^c}{35}\frac{\partial^3}{\partial x\partial t^2}\right)u_0^b\right.\\
&-\left(\alpha_6^b\frac{\partial}{\partial x}+\frac{cf_b}{15}C_{11}^c\frac{\partial^3}{\partial x^3}-\frac{cf_b\rho^c}{15}\frac{\partial^3}{\partial x\partial t^2}\right)u_0^c-\left(\alpha_5^b\frac{\partial}{\partial x}+\frac{cf_b}{70}C_{11}^c\frac{\partial^3}{\partial x^3}-\frac{cf_b\rho^c}{70}\frac{\partial^3}{\partial x\partial t^2}\right)u_0^t\\
&+\left(\frac{7}{6c}C_{33}^c+\alpha_8^b\frac{\partial^2}{\partial x^2}+\alpha_9^b\frac{\partial^4}{\partial x^4}+\left(\frac{4c\rho^c}{15}+f_b\rho^b\right)\frac{\partial^2}{\partial t^2}-\left(\frac{3cf_b^2\rho^c}{70}+\frac{f_b^3\rho^b}{12}\right)\frac{\partial^4}{\partial x^2\partial t^2}\right)w^b\\
&+\left(-\frac{4}{3c}C_{33}^c+\alpha_7^b\frac{\partial^2}{\partial x^2}+\frac{2c\rho^c}{15}\frac{\partial^2}{\partial t^2}\right)w_0^c\\
&\left.+\left(\frac{1}{6c}C_{33}^c+\beta_2\frac{\partial^2}{\partial x^2}-\frac{cf_bf_t}{140}C_{11}^c\frac{\partial^4}{\partial x^4}-\frac{c\rho^c}{15}\frac{\partial^2}{\partial t^2}+\frac{cf_bf_t\rho^c}{140}\frac{\partial^4}{\partial x^2\partial t^2}\right)w^t\right]b\\
&=\widetilde{q}^b-\widetilde{m}_{,x}^b+F_w^b\end{aligned}\tag{17a}$$

where F_w^b is the nonlinear term:

$$F_w^b=C_{11}^b b f_b\left[w_{,x}^b u_{0,xx}^b+u_{0,x}^b w_{,xx}^b+\frac{3}{2}(w_{,x}^b)^2 w_{,xx}^b\right]\tag{17b}$$

and $\widetilde{q}^b$ is the distributed transverse force and $\widetilde{m}^b$ is the distributed moment applied along the bottom face sheet. In the above expressions, the following constants are defined:

$$\alpha_1^i=\frac{6c}{35}C_{11}^c+f_iC_{11}^i\ ;\qquad \alpha_2^i=\frac{1}{30}C_{13}^c+\left(\frac{1}{30}-\frac{7f_i}{60c}\right)C_{55}^c\tag{18a}$$

$$\alpha_3^i=-\frac{11}{30}C_{13}^c+\left(\frac{19}{30}+\frac{47f_i}{60c}\right)C_{55}^c\ ;\qquad \alpha_4^i=\frac{4c}{15}C_{13}^c+\left(\frac{4c}{15}+\frac{2f_i}{5}\right)C_{55}^c\ ,\tag{18b}$$

$$\alpha_5^i=-\alpha_2^i\ ;\qquad \alpha_6^i=\frac{2}{3}C_{13}^c+\left(\frac{2}{3}+\frac{2f_i}{3c}\right)C_{55}^c\tag{18c}$$

$$\alpha_7^i=-\frac{f_i}{5}C_{13}^c-\left(\frac{2c}{15}+\frac{f_i}{5}\right)C_{55}^c\ ,\tag{18d}$$

$$\alpha_8^i=\frac{11f_i}{30}C_{13}^c-\left(\frac{4c}{15}+\frac{19f_i}{30}+\frac{47{f_i}^2}{120c}\right)C_{55}^c\ ,\tag{18e}$$

$$\alpha_9^i=\frac{{f_i}^3}{12}C_{11}^i+\frac{3c{f_i}^2}{70}C_{11}^c\tag{18f}$$

and

$$\beta_1=\frac{2}{5}(C_{13}^c+C_{55}^c)\tag{19a}$$

$$\beta_2 = \frac{f_b + f_t}{60} C_{13}^c + \left(\frac{c}{15} + \frac{f_b + f_t}{60} - \frac{7 f_b f_t}{120 c} \right) C_{55}^c \tag{19b}$$

The corresponding boundary conditions at $x = 0$ and a, read as follows (at each end there are nine boundary conditions, three for each face sheet and three for the core):

For the top face sheet:

(i) *Either* $\delta u_0^t = 0$ *or*,

$$\begin{aligned} &\left[\left(\frac{2c^2}{35} C_{11}^c \frac{\partial}{\partial x} \right) \phi_0^c + \left(\frac{c}{35} C_{11}^c \frac{\partial}{\partial x} \right) u_0^b + \left(\frac{2c}{15} C_{11}^c \frac{\partial}{\partial x} \right) u_0^c + \left(\alpha_1^t \frac{\partial}{\partial x} \right) u_0^t \right. \\ &\left. + \left(\frac{1}{30} C_{13}^c - \frac{c f_b}{70} C_{11}^c \frac{\partial^2}{\partial x^2} \right) w^b - \left(\frac{2}{5} C_{13}^c \right) w_0^c + \left(\frac{11}{30} C_{13}^c + \frac{3 c f_t}{35} C_{11}^c \frac{\partial^2}{\partial x^2} \right) w^t \right] b \\ &= \widetilde{N}^t + \frac{\widetilde{n}^c c}{3} + B_u^t \end{aligned} \tag{20a}$$

where $\widetilde{N}^t$ is the end axial force at the top face and $\widetilde{n}^c$ is the end axial force at the the core (at the end $x = 0$ or $x = a$) and the nonlinear term

$$B_u^t = -\frac{f_t b}{2} C_{11}^t (w_{,x}^t)^2 \tag{20b}$$

(ii) *Either* $\delta w^t = 0$ *or*,

$$\begin{aligned} &\left(- \left[\frac{2(2c + 3f_t)}{15} C_{55}^c + \frac{c^2 f_t}{35} C_{11}^c \frac{\partial^2}{\partial x^2} \right] \phi_0^c + \left[\frac{(2c - 7f_t)}{60c} C_{55}^c - \frac{c f_t}{70} C_{11}^c \frac{\partial^2}{\partial x^2} \right] u_0^b \right. \\ &- \left[\frac{2(c + f_t)}{3c} C_{55}^c + \frac{c f_t}{15} C_{11}^c \frac{\partial^2}{\partial x^2} \right] u_0^c + \left[\frac{(38c + 47f_t)}{60c} C_{55}^c - \frac{3 c f_t}{35} C_{11}^c \frac{\partial^2}{\partial x^2} \right] u_0^t \\ &+ \left[\left(\frac{f_b}{60} C_{13}^c - \beta_2 \right) \frac{\partial}{\partial x} + \frac{c f_b f_t}{140} C_{11}^c \frac{\partial^3}{\partial x^3} \right] w^b - \left(\alpha_7^t \frac{\partial}{\partial x} \right) w_0^c \\ &\left. + \left[\left(\frac{11 f_t}{60} C_{13}^c - \alpha_8^t \right) \frac{\partial}{\partial x} - \alpha_9^t \frac{\partial^3}{\partial x^3} \right] w^t + L_w^t \right) b = \\ &= \widetilde{P}^t + \widetilde{m}^t + \frac{\widetilde{v}^c c}{3} + B_w^t \end{aligned} \tag{21a}$$

where L_w^t are the inertial terms in the boundary condition:

$$\begin{aligned} L_w^t = &\frac{f_t}{420} \left[35 f_t^2 \rho^t \frac{\partial^3 w^t}{\partial x \partial t^2} + \rho^c \left(12 c^2 \frac{\partial^2 \phi_0^c}{\partial t^2} + 6c \frac{\partial^2 u_0^b}{\partial t^2} + 28c \frac{\partial^2 u_0^c}{\partial t^2} + 36c \frac{\partial^2 u_0^t}{\partial t^2} \right. \right. \\ &\left. \left. - 3 c f_b \frac{\partial^3 w^b}{\partial x \partial t^2} + 18 c f_t \frac{\partial^3 w^t}{\partial x \partial t^2} \right) \right] \end{aligned} \tag{21b}$$

B_w^t is the nonlinear term:

$$B_w^t = -\frac{f_t}{2} C_{11}^t w_{,x}^t \left[2u_{0,x}^t + (w_{,x}^t)^2\right] \tag{21c}$$

and $\widetilde{P}^t$ is the end shear force at the top face and $\widetilde{v}^c$ is the end shear force at the core (at the end $x = 0$ or $x = a$).

(iii) *Either* $\delta w_{,x}^t = 0$ or,

$$\left[\left(\frac{c^2 f_t}{35} C_{11}^c \frac{\partial}{\partial x}\right)\phi_0^c + \left(\frac{c f_t}{70} C_{11}^c \frac{\partial}{\partial x}\right)u_0^b + \left(\frac{c f_t}{15} C_{11}^c \frac{\partial}{\partial x}\right)u_0^c + \left(\frac{3c f_t}{35} C_{11}^c \frac{\partial}{\partial x}\right)u_0^t \right.$$
$$\left. + \left(\frac{f_t}{60} C_{13}^c - \frac{c f_b f_t}{140} C_{11}^c \frac{\partial^2}{\partial x^2}\right)w^b - \left(\frac{f_t}{5} C_{13}^c\right)w_0^c + \left(\frac{11 f_t}{60} C_{13}^c + \alpha_9^t \frac{\partial^2}{\partial x^2}\right)w^t\right] b = \widetilde{M}^t + \frac{\widetilde{n}^c c f_t}{6} \tag{22}$$

where $\widetilde{M}^t$ is the end moment at the top face (at the end $x = 0$ or $x = a$).

For the core:

(i) *Either* $\delta u_0^c = 0$ *or*,

$$\left[\left(\frac{2c}{15} C_{11}^c \frac{\partial}{\partial x}\right)u_0^b + \left(\frac{16c}{15} C_{11}^c \frac{\partial}{\partial x}\right)u_0^c + \left(\frac{2c}{15} C_{11}^c \frac{\partial}{\partial x}\right)u_0^t \right.$$
$$\left. - \left(\frac{2}{3} C_{13}^c + \frac{c f_b}{15} C_{11}^c \frac{\partial^2}{\partial x^2}\right)w^b + \left(\frac{2}{3} C_{13}^c + \frac{c f_t}{15} C_{11}^c \frac{\partial^2}{\partial x^2}\right)w^t\right] b = \frac{4\widetilde{n}^c c}{3} \tag{23}$$

(ii) *Either* $\delta \phi_0^c = 0$ *or*,

$$\left[\left(\frac{16c^3}{105} C_{11}^c \frac{\partial}{\partial x}\right)\phi_0^c - \left(\frac{2c^2}{35} C_{11}^c \frac{\partial}{\partial x}\right)u_0^b + \left(\frac{2c^2}{35} C_{11}^c \frac{\partial}{\partial x}\right)u_0^t + \left(\frac{4c}{15} C_{13}^c + \frac{c^2 f_b}{35} C_{11}^c \frac{\partial^2}{\partial x^2}\right)w^b \right.$$
$$\left. - \left(\frac{8c}{15} C_{13}^c\right)w_0^c + \left(\frac{4c}{15} C_{13}^c + \frac{c^2 f_t}{35} C_{11}^c \frac{\partial^2}{\partial x^2}\right)w^t\right] b = 0 \tag{24}$$

(iii) *Either* $\delta w_0^c = 0$ *or*,

$$C_{55}^c b\left[\frac{8c}{15}\phi_0^c - \frac{2}{5}u_0^b + \frac{2}{5}u_0^t + \frac{(2c + 3f_b)}{15}w_{,x}^b + \frac{16c}{15}w_{0,x}^c + \frac{(2c + 3f_t)}{15}w_{,x}^t\right] = \frac{4}{3}\widetilde{v}^c c \tag{25}$$

For the bottom face sheet:

(i) *Either* $\delta u_0^b = 0$ *or*,

$$\begin{aligned}
&\Big[-\left(\frac{2c^2}{35}C_{11}^c\frac{\partial}{\partial x}\right)\phi_0^c + \left(\alpha_1^b\frac{\partial}{\partial x}\right)u_0^b + \left(\frac{2c}{15}C_{11}^c\frac{\partial}{\partial x}\right)u_0^c + \left(\frac{c}{35}C_{11}^c\frac{\partial}{\partial x}\right)u_0^t \\
&- \left(\frac{11}{30}C_{13}^c + \frac{3cf_b}{35}C_{11}^c\frac{\partial^2}{\partial x^2}\right)w^b + \left(\frac{2}{5}C_{13}^c\right)w_0^c + \left(-\frac{1}{30}C_{13}^c + \frac{cf_t}{70}C_{11}^c\frac{\partial^2}{\partial x^2}\right)w^t\Big] \\
&= \widetilde{N}^b + \frac{\widetilde{n}^c c}{3} + B_u^b
\end{aligned} \tag{26a}$$

where $\widetilde{N}^b$ is the end axial force at the bottom face and the nonlinear term,

$$B_u^b = -\frac{f_b b}{2}C_{11}^b(w_{,x}^b)^2 \tag{26b}$$

(ii) *Either* $\delta w^b = 0$ *or*,

$$\begin{aligned}
&\Bigg(-\left[\frac{2(2c+3f_b)}{15}C_{55}^c + \frac{c^2 f_b}{35}C_{11}^c\frac{\partial^2}{\partial x^2}\right]\phi_0^c + \left[-\frac{(38c-47f_b)}{60c}C_{55}^c + \frac{3cf_b}{35}C_{11}^c\frac{\partial^2}{\partial x^2}\right]u_0^b \\
&+ \left[\frac{2(c+f_b)}{3c}C_{55}^c + \frac{cf_b}{15}C_{11}^c\frac{\partial^2}{\partial x^2}\right]u_0^c + \left[\frac{(-2c+7f_b)}{60c}C_{55}^c + \frac{cf_b}{70}C_{11}^c\frac{\partial^2}{\partial x^2}\right]u_0^t \\
&+ \left[\left(\frac{11f_b}{60}C_{13}^c - \alpha_8^b\right)\frac{\partial}{\partial x} - \alpha_9^b\frac{\partial^3}{\partial x^3}\right]w^b - \left(\alpha_7^b\frac{\partial}{\partial x}\right)w_0^c \\
&+ \left[\left(\frac{f_t}{60}C_{13}^c - \beta_2\right)\frac{\partial}{\partial x} + \frac{cf_b f_t}{140}C_{11}^c\frac{\partial^3}{\partial x^3}\right]w^t + L_w^b\Bigg)b \\
&= \widetilde{P}^b + \widetilde{m}^b + \frac{\widetilde{v}^c c}{3} + B_w^b
\end{aligned} \tag{27a}$$

where L_w^b are the inertial terms in the boundary condition:

$$\begin{aligned}
L_w^b = &\frac{f_b}{420}\Bigg[35f_b^2\rho^b\frac{\partial^3 w^b}{\partial x\partial t^2} + \rho^c\Bigg(12c^2\rho^c\frac{\partial^2\phi_0^c}{\partial t^2} - 36c\frac{\partial^2 u_0^b}{\partial t^2} - 28c\frac{\partial^2 u_0^c}{\partial t^2} - 6c\frac{\partial^2 u_0^t}{\partial t^2} \\
&+18cf_b\frac{\partial^3 w^b}{\partial x\partial t^2} - 3cf_t\frac{\partial^3 w^t}{\partial x\partial t^2}\Bigg)\Bigg]
\end{aligned} \tag{27b}$$

where B_w^b is the nonlinear term:

$$B_w^b = -\frac{f_b b}{2}C_{11}^b w_{,x}^b\left[2u_{0,x}^b + (w_{,x}^b)^2\right] \tag{27c}$$

and $\widetilde{P}^b$ is the end shear force at bottom face.

(iii) *Either* $\delta w^b_{,x} = 0$ *or*,

$$\left[\left(\frac{c^2 f_b}{35} C^c_{11} \frac{\partial}{\partial x}\right)\phi^c_0 - \left(\frac{3cf_b}{35} C^c_{11} \frac{\partial}{\partial x}\right)u^b_0 - \left(\frac{cf_b}{15} C^c_{11} \frac{\partial}{\partial x}\right)u^c_0 - \left(\frac{cf_b}{70} C^c_{11} \frac{\partial}{\partial x}\right)u^t_0 + \left(\frac{11 f_b}{60} C^c_{13} + \alpha^b_9 \frac{\partial^2}{\partial x^2}\right)w^b - \left(\frac{f_b}{5} C^c_{13}\right)w^c_0 + \left(\frac{f_b}{60} C^c_{13} - \frac{cf_b f_t}{140} C^c_{11} \frac{\partial^2}{\partial x^2}\right)w^t\right] b = \widetilde{M}^b - \frac{\widetilde{n}^c c f_b}{6} \tag{28}$$

where $\widetilde{M}^b$ is the end moment at the bottom face. The superscript $\widetilde{}$ denotes in the above equations the known external boundary values.

Hamilton's principle results in seven coupled partial differential equations, Eqns. (11)-(17), four of which are nonlinear due to the consideration of large displacements and moderate rotations of the face sheets. The order of the equations of motion is 18 in x, and second order in time. Therefore, there are 18 boundary conditions, 9 at each end at $x = 0$ and $x = a$ given by Eqns. (20)-(28). Since the rotations of the face sheets are assumed to be the derivatives of the transverse displacements with respect to x, there exists inertial terms L^t_w and L^b_w in the boundary conditions in Eqns. (21a) and (27a). The 7 generalized displacement variables of EHSAPT are: $u^t_0(x,t)$, $u^c_0(x,t)$, $u^b_0(x,t)$, $\phi^c_0(x,t)$, $w^t(x,t)$, $w^c_0(x,t)$, and $w^b(x,t)$.

We have also made use of the definitions of the axial stress resultants of the top face, bottom face, and core respectively, $N^{t,b,c}$, where these are defined as:

$$N^t(x,t) = \int_c^{c+f_t} b\sigma^t_{xx} dz = C^t_{11} b f_t \epsilon^t_{xx} \ , \quad N^b_x(x,t) = \int_{-c-f_b}^{-c} b\sigma^b_{xx} dz = C^b_{11} b f_b \epsilon^b_{xx} \ , \tag{29a}$$

$$N^c_x(x,t) = \int_{-c}^{c} b\sigma^c_{xx} dz = C^c_{13} b(w^t - w^b) + \frac{bcC^c_{11}}{3}\left(u^b_{0,x} + 4u^c_{0,x} + u^t_{0,x} + \frac{f_t}{2} w^t_{,xx} - \frac{f_b}{2} w^b_{,xx}\right) \ , \tag{29b}$$

and where the nonlinear axial strains $\epsilon^{t,b}_{xx}$ are given in Eqn. (3).

Also, $M^{t,b,c}$ are the moment stress resultants of the top face, bottom face, and core about their own centroids, respectively, and are defined as:

$$M^t(x,t) = -\int_c^{c+f_t} b\sigma^t_{xx}\left(z - c - \frac{f_t}{2}\right) dz = C^t_{11} \frac{b f_t^3}{12} w^t_{,xx} \ , \tag{29c}$$

$$M^b(x,t) = -\int_{-c-f_b}^{-c} b\sigma_{xx}^b \left(z + c + \frac{f_b}{2}\right) dz = C_{11}^b \frac{b f_b^3}{12} w_{,xx}^b \ , \tag{29d}$$

$$\begin{aligned} M^c(x,t) = -\int_{-c}^{c} b\sigma_{xx}^c z dz = &-\frac{2cbC_{13}^c}{3}\left(w^b - 2w_0^c + w^t\right) \\ &-\frac{bc^2C_{11}^c}{30}\left[8c\phi_{0,x}^c + 6(u_{0,x}^t - u_{0,x}^b) + 3(f_b w_{,xx}^b + f_t w_{,xx}^t)\right] \end{aligned} \tag{29e}$$

Finally, V^c is the shear stress resultant of the core and is defined as:

$$\begin{aligned} V^c(x,t) = &\int_{-c}^{c} b\tau_{zx}^c dz = \\ &C_{55}^c b\left[\left(u_0^t - u_0^b\right) + \frac{c}{3}\left(w_{0,x}^b + w_{0,x}^t\right) + \frac{1}{2}\left(f_b w_{0,x}^b + f_t w_{0,x}^t\right) + 8cw_{0,x}^c\right] \ . \end{aligned} \tag{29f}$$

The general nonlinear governing equations and boundary conditions of EHSAPT rewritten in terms of the stress resultants and the generalized coordinates are listed in Appendix C. This formulation is useful when using the perturbation approach for solving stability problems as demonstrated in Chapters 4 and 5.

CHAPTER III

STATIC LOADING PROBLEM

The solution to a simply-supported sandwich panel under the transversely applied static load:

$$\widetilde{q}^t(x) = q_0 \sin \frac{\pi x}{a} \ . \tag{30}$$

using the linear formulation of EHSAPT will be shown. The accuracy of EHSAPT or any new composite model can be readily assessed if an elasticity solution exists. Indeed, Pagano [30] presented the three-dimensional elasticity solution for a laminated or sandwich beam for the case of a positive discriminant of the quadratic characteristic equation, which is formed from the orthotropic material constants, and only when these two real roots are positive. The isotropic case, in which there are two equal real roots, was also outlined. Recently, Kardomateas and Phan [25] extended the Pagano [30] solution to the case of (i) negative discriminant, which results in two complex conjugate roots of the quadratic equation and (ii) positive discriminant but with real negative roots. The case of a negative discriminant is actually frequently encountered in sandwich construction where the orthotropic core is stiffer in the transverse than the in-plane directions. Results from this elasticity solution showed that the core transverse shear is nearly constant for the very soft cores but it acquires a pronounced distribution, nearly parabolic, as the stiffness of the core increased. The transverse normal strain in the core was found to be nearly linear in z. It should be mentioned that elasticity solutions that address the complex roots for the two-dimensional case (plate) have already been presented by Zenkour [41] and Demasi [9]; however the present formulation of EHSAPT deals with a beam (one-dimensional) configuration.

In the next section, the static formulation of EHSAPT will be solved. The numerical results for several typical sandwich panel configurations with orthotropic phases will be compared with the results using the elasticity solution [25], the classical model and the first order shear model as well as the Frostig et al. high-order sandwich panel theory [15].

3.1 Solution Procedure

In this case, the boundary conditions for $x = 0,\ a$ are the three kinematic conditions:

$$w^t = w^b = w_0^c = 0 \tag{31}$$

and the right hand sides of the six natural boundary conditions in (20a), (22), (23), (24), (26a), and (28) are equal to zero.

All these are satisfied by displacements in the form:

$$u_0^t = U_0^t \cos\frac{\pi x}{a}\ ; \quad u_0^c = U_0^c \cos\frac{\pi x}{a}\ ; \quad \phi_0^c = \Phi_0^c \cos\frac{\pi x}{a}\ ; \quad u_0^b = U_0^b \cos\frac{\pi x}{a}\ , \tag{32a}$$

$$w^t = W^t \sin\frac{\pi x}{a}\ ; \quad w_0^c = W_0^c \sin\frac{\pi x}{a}\ ; \quad w^b = W^b \sin\frac{\pi x}{a}\ . \tag{32b}$$

We consider the static linear problem, which means that the load is applied quasi-statically such that the inertial terms can be neglected, and displacements are small so nonlinear terms $F_{u,w}^{t,b}$ in the governing differential equations and the nonlinear terms $B_w^{t,b}$ in the boundary conditions can be neglected.

Substituting Eqn. (32) into Eqns. (11)-(17) results in a system of seven linear equations for the seven unknown constants U_0^t, U_0^c, Φ_0^c, U_0^b, W^t, W_0^c, W^b.

3.2 Numerical case study

We shall consider sandwich configurations consisting of faces made out of either graphite/epoxy or e-glass/polyester unidirectional composite and core made out of either hexagonal glass/phenolic honeycomb or balsa wood. The moduli and Poisson's ratios for these materials are given in Table 1.

Table 1: Material properties. Moduli data are in GPa

	Graphite Epoxy FACE	E-Glass Polyester FACE	Balsa Wood CORE	Glass-Phenolic Honeycomb CORE
E_1	181.0	40.0	0.671	0.032
E_2	10.3	10.0	0.158	0.032
E_3	10.3	10.0	7.72	0.300
G_{23}	5.96	3.5	0.312	0.048
G_{31}	7.17	4.5	0.312	0.048
G_{12}	7.17	4.5	0.200	0.013
ν_{32}	0.40	0.40	0.49	0.25
ν_{31}	0.016	0.26	0.23	0.25
ν_{12}	0.277	0.065	0.66	0.25

The two face sheets are assumed identical with thickness $f_t = f_b = f = 2$ mm. The core thickness is $2c = 16$ mm. The total thickness of the panel is defined as $h_{tot} = 2f + 2c$ and the length of the beam is $a = 20h_{tot}$ and width $b = 1$ m. The load parameter $q_0 = 10^9$ N/m.

In the following results, the displacements are normalized with

$$w_{norm} = \frac{3q_0a^4}{2\pi^4 E_1^f b f^3} \ . \tag{33}$$

and the stresses with q_0/b.

Plotted in Figure 3 is the normalized displacement at the top face sheet as a function of x, for the case of Graphite/Epoxy faces and Glass Phenolic Honeycomb core; this core is very soft compared to the faces with an in-plane Young's modulus ratio of $E_1^c/E_1^f < 0.001$. In this figure, we also show the predictions of the simple Classical beam theory (CL), which does not include transverse shear, as well as the First Order Shear theories (FOSD); for the latter, there are two versions: one that is based only on the core shear stiffness (FOSD(c)) and one that includes the face sheet stiffnesses (FOSD(f)). Both are outlined in Appendix A. In addition, we show the predictions of the High-Order sandwich panel theory (HSAPT). This theory, which is based on an assumption that the in-plane rigidity of the core is neglected and yields a constant shear stress and zero axial stress in the core, is outlined in Appendix B.

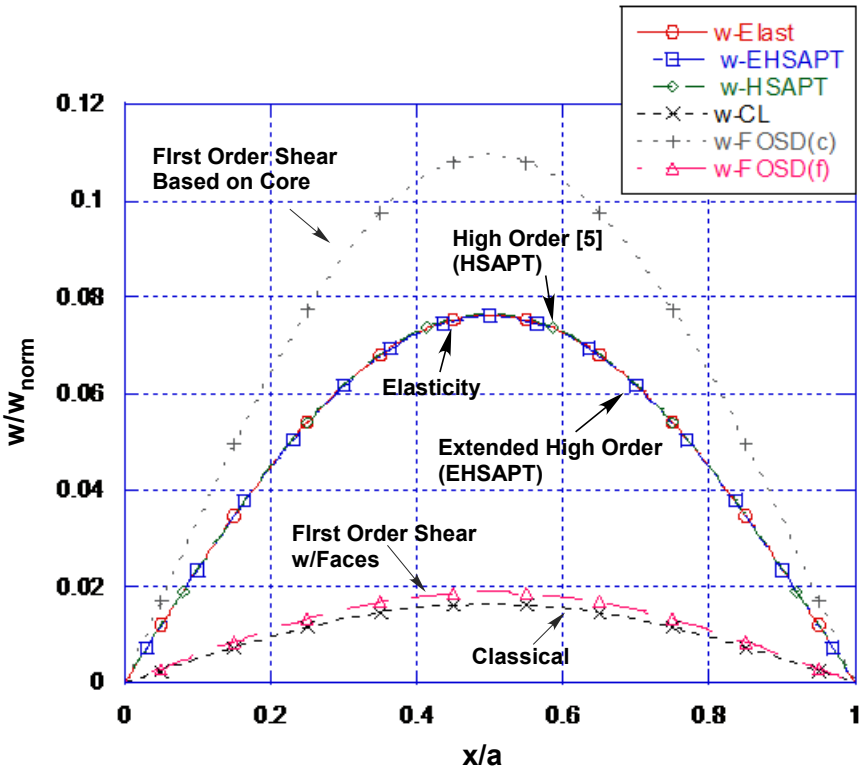

Figure 3: Transverse Displacement, w, at the top, $z = c + f$, for the case of Graphite/Epoxy faces and Glass Phenolic Honeycomb core.

From Figure 3, we can see that both the Classical and FOSD (both versions) seem to be inadequate. The Classical theory is too non-conservative and the First Order Shear theory with face sheets included can hardly make a difference. On the other hand, the FOSD theory where shear is assumed to be carried exclusively by the core is too conservative; this clearly demonstrates the need for higher order theories in dealing with sandwich structures. In this regard, both the Frostig et al. HSAPT [15] and the present EHSAPT theories give a displacement profile which is essentially identical to the elasticity solution. In Figure 3 we can also readily observe the large effect of transverse shear, which is an important feature of sandwich structures. The distribution of the axial stress in the core, σ_{xx}, as a function of z at the mid-span location, $x = a/2$ (where the bending moment is maximum), is plotted in Figure 4, again for the case of Graphite/Epoxy faces and Glass Phenolic Honeycomb core.

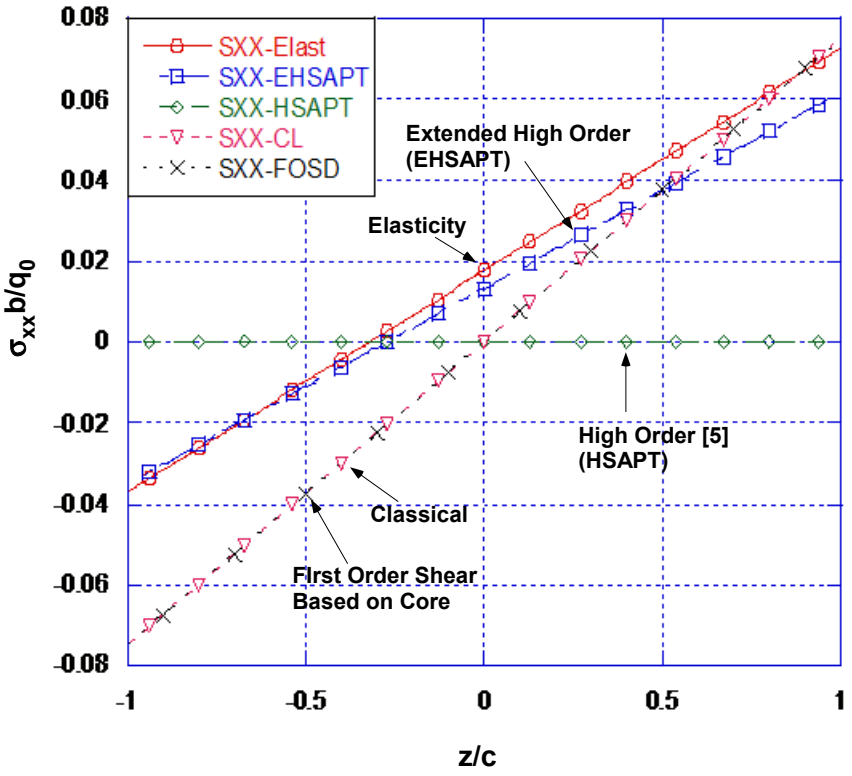

Figure 4: Through-thickness distribution in the core of the axial stress, σ_{xx}, at $x = a/2$ for the case of Graphite/Epoxy faces and Glass Phenolic Honeycomb core.

The present Extended High Order theory predicts a stress very close to the elasticity. Note that HSAPT neglects the axial rigidity of the core that yields a zero axial stress. The Classical and FOSD theories give practically identical predictions but they are in appreciable error by comparison to the elasticity, with the error increasing towards the lower end of the core ($z = -c$). All curves are linear. Notice also that for the elasticity and the Extended High Order theory there is not a symmetry with regard to the mid line ($z = 0$) unlike the Classical and FOSD theories. Even though the sandwich panel has symmetric geometry and material lay-up, the axis of zero axial stress does not occur at the centroid of the core. This is a high-order effect that EHSAPT captures.

The through-thickness distribution of the transverse normal stress in the core, σ_{zz},

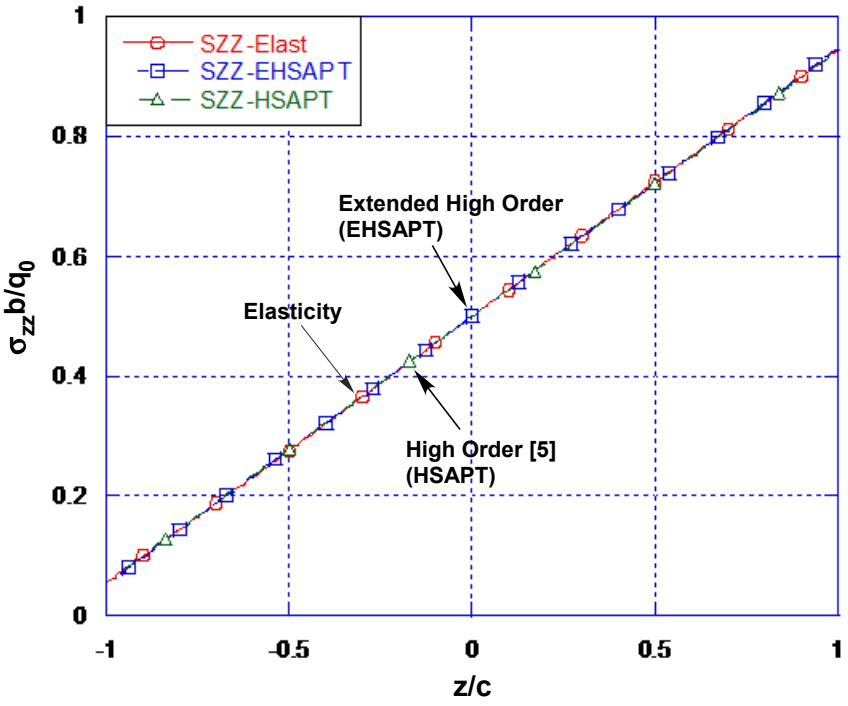

Figure 5: Through-thickness distribution in the core of the transverse normal stress, σ_{zz}, at $x = a/2$ for the case of E-glass/Polyester faces and Balsa Wood core.

at the midspan location, $x = a/2$, is shown in Figure 5 for the case of E-glass/Polyester faces and Balsa Wood core. The E-glass/Balsa lay-up represents a panel in which the core is moderately stiff with an in-plane Young's modulus ratio of $E_1^c/E_1^f \sim 0.02$. Only the profiles using elasticity and the Frostig et al. [15] and the Extended High Order theories are presented, since the First Order Shear theory and the Classical theory consider the core incompressible, i.e. zero σ_{zz}. Both high-order theories are practically coinciding with the elasticity curve and all are nearly linear. However, the theories differ when the transverse normal strain is examined in Figure 6 with the present Extended High Order theory being very close to the elasticity.

Figures 7 and 8 show the through-thickness distribution of the transverse shear stress in the core, τ_{xz}, at $x = a/10$, i.e. near the ends where shearing is expected to be significant, for the cases of Graphite/Epoxy faces and Glass Phenolic Honeycomb core (Figure 7) and E-glass/Polyester faces and Balsa Wood core (Figure 8). For

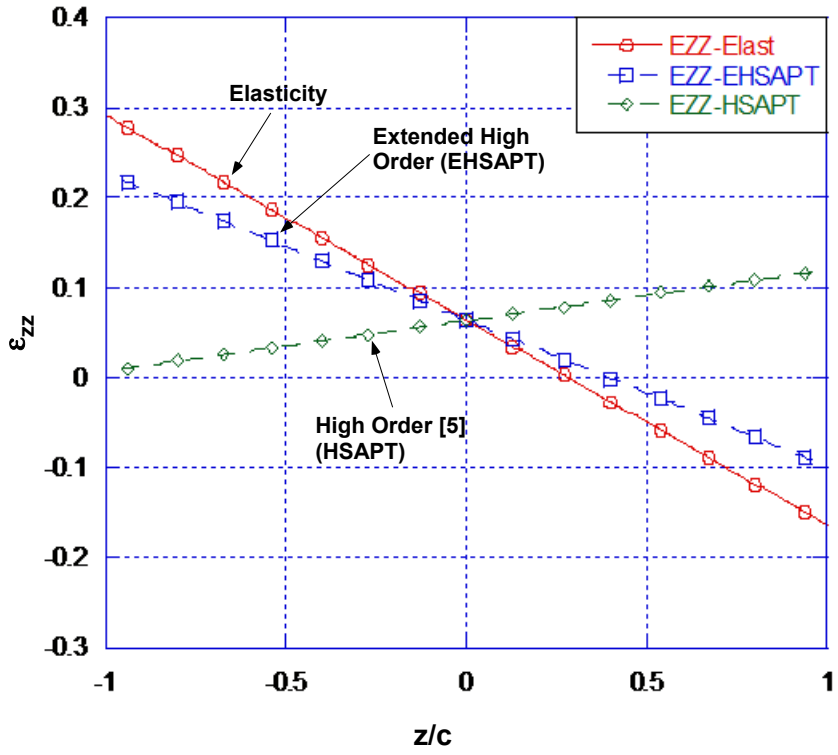

Figure 6: Through-thickness distribution in the core of the transverse normal strain, ϵ_{zz}, at $x = a/2$ for the case of E-glass/Polyester faces and Balsa Wood core.

the very soft core case of Figure 8, the shearing stress is nearly constant and thus for all theories the difference from elasticity is practically negligible. Indeed, the elasticity data show that the range of the shearing stress variation is about 0.05% of the maximum value, i.e. the shearing stress is practically constant. This case of a very soft core would justify the neglect of the in-plane rigidity of the core that is associated with constant shear stresses in the core, made in the Frostig et al. [15] theory. Still, in Figure 7 one can see that the EHSAPT is practically identical to the elasticity whereas the HSAPT shows more difference.

For the case of the E-glass/Polyester faces and Balsa Wood core, however, the shear stress shows a noticeable distribution (about 5%) through the thickness, which is very nicely captured by the present Extended High Order theory, which is practically identical to the elasticity. For this sandwich configuration, it is obvious that a theory

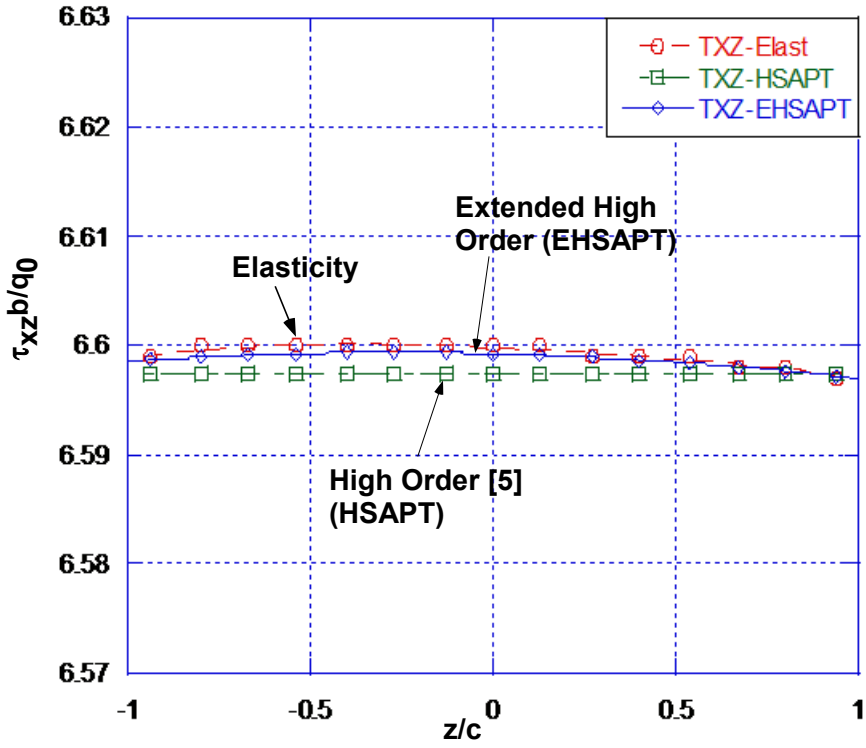

Figure 7: Through-thickness distribution in the core of the transverse shear stress, τ_{xz}, at $x = a/10$ for the case of Graphite/Epoxy faces and Glass Phenolic Honeycomb.

based on a constant shearing stress assumption (HSAPT) would not capture this distribution.

This issue is further explored by considering a sandwich construction in which both the face sheets and the core are isotropic. By varying the moduli ratio, we can accordingly increase the shear stress range in the core. Thus, we assume that the face sheets are made out of isotropic Aluminum Alloy with $E_f = 100$ GPa and the core is made out of isotropic material having a modulus E_c such that the ratio E_f/E_c assumes the values of 50, 5 and 2. The Poisson's ratios are assumed $\nu_f = \nu_c = 0.30$. Figure 9 shows the shear stress distribution through the thickness. For the moduli ratio of 2 the range is very large, with the maximum over minimum shear stress ratio

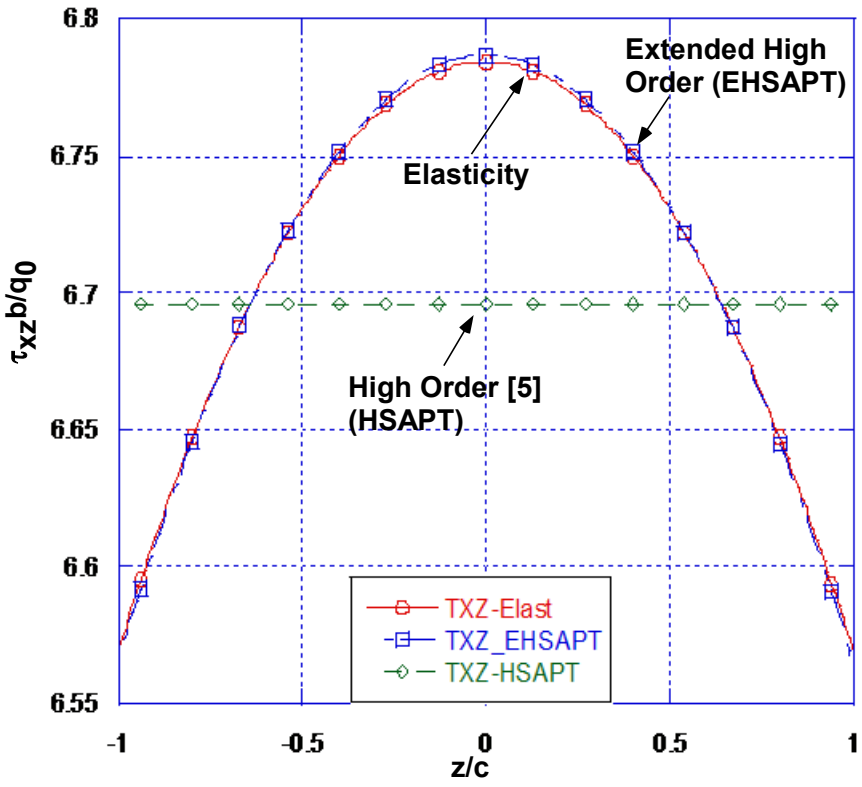

Figure 8: Through-thickness distribution in the core of the transverse shear stress, τ_{xz}, at $x = a/10$ for the case of E-glass/Polyester faces and Balsa Wood core.

being about 2. On the contrary, for the moduli ratio of 50, the shear stress range is very small, with the corresponding maximum over minimum shear stress ratio being only about 1.04. The present Extended High Order theory is capable of capturing the shear stress profile in all cases, even the most demanding case of $E_f/E_c = 2$, and in all cases yields results that are practically identical to those from the elasticity solution. On the contrary, a constant shear stress assumption would be applicable only for the large ratios of E_f/E_c.

Carrera and Brischetto [8] have shown that equivalent single layer sandwich plate theories have significant problems in terms of accuracy for very high skin-to-core stiffness ratios. Although we cannot make a direct comparison with their data, since

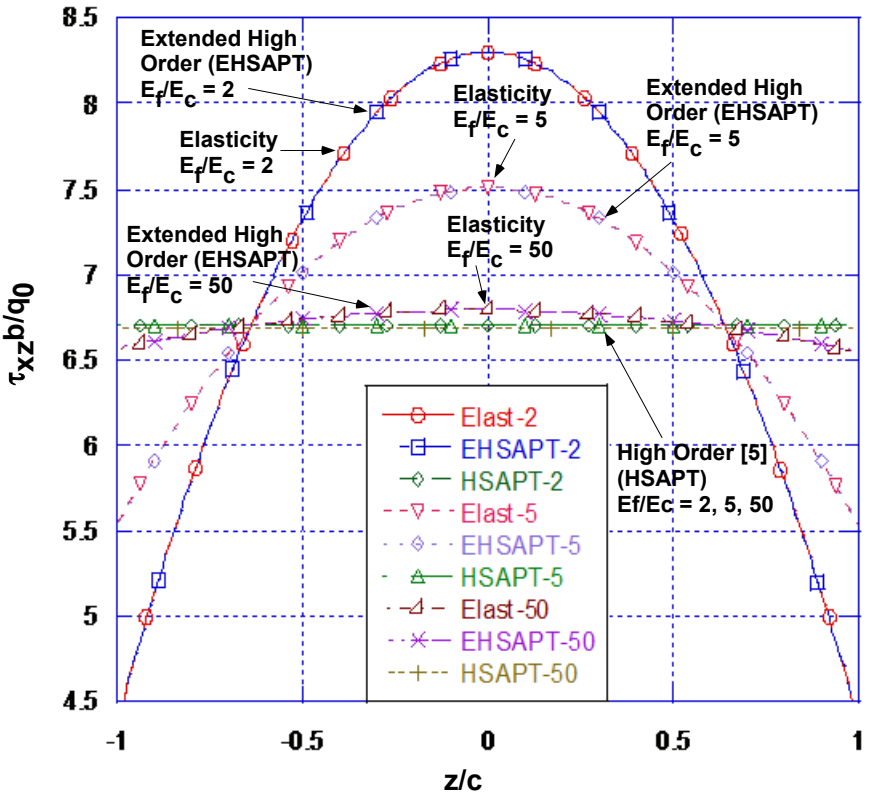

Figure 9: Through-thickness distribution in the core of the transverse shear stress, τ_{xz}, at $z = a/10$ for the case of isotropic Aluminum Alloy faces and a wide range of isotropic cores.

the study in [8] was done for plates, a similar table as Table 28 in [8] was made to numerically assess the accuracy of EHSAPT with respect to elasticity for the distributed loading problem shown in this paper. The widely followed First Order Shear Deformation theory (FOSD) is also shown.

The material and geometry configurations were taken from [8]; each face sheet has a thickness f_t=f_b=f=0.1 m, the total core thickness is $2c$= 0.8m, and the total height h_{tot}=f_t + f_b + $2c$. A range of beam lengths, a, is examined, as denoted by the parameter LTR = a/h_{tot}; this range of LTRs is {4, 10, 100, 1000}. The core is isotropic with modulus E_c=1 GPa and Poisson's ratio $\nu_c = 0.3$. A range of isotropic faces with modulus E_f and Poisson's ratio $\nu_f = 0.3$ is examined, as denoted by the parameter FCSR = E_f/E_c; this range of FCSRs is 7.3 times {10^1, 10^4, 10^6 and 10^8}.

Table 2: Normalized transverse displacement at mid-core ($x = a/2,\ z = 0$); R=FCSR/LTR

FCSR	LTR	4	10	100	1000
$7.3E+01$	R	18.25	7.3	0.73	0.073
	elasticity	0.0892	0.0269	0.0148	0.0147
	EHSAPT	0.0907	0.0284	0.0163	0.0162
	FOSD	0.1321	0.0337	0.0152	0.0150
$7.3E+04$	R	18250	7300	730	73
	elasticity	3.418	2.805	0.1333	0.0161
	EHSAPT	3.725	3.013	0.1351	0.0176
	FOSD	117.09	18.747	0.2023	0.0169
$7.3E+06$	R	1.825E+06	7.3E+05	7.3E+04	7.3E+03
	elasticity	3.576	3.619	2.811	0.1333
	EHSAPT	3.914	3.973	3.021	0.1351
	FOSD	1.171E+04	1873.0	18.748	0.2023
$7.3E+08$	R	1.825E+08	7.3E+07	7.3E+06	7.3E+05
	elasticity	3.577	3.630	3.629	2.811
	EHSAPT	3.916	3.987	3.987	3.021
	FOSD	1.171E+06	1.873E+05	1873.0	18.748

Tables 2 and 3 show the value of the normalized mid-span transverse displacement at the mid-plane ($x = a/2,\ z = 0$) and at the top face sheet ($x = a/2,\ z = c + ft/2$), respectively. The transverse displacements at the mid-plane and top locations are presented to show the compressibility of the core (i.e. when the two displacements are not equal). The elasticity data in the two tables show that sandwich configurations with high FCSR and low LTR combinations exhibit the most compressibility for this particular static problem. For example, for FCSR=$7.3 * 10^8$ and LTR=4, the top face sheet has about twice as much displacement as that of the mid-plane. As FCSR gets smaller (i.e. the core and face sheet properties become more similar) and the LTR becomes higher (i.e. the beam becomes longer) the two displacements become practically the same. Both tables also show that the FOSD theory is highly inaccurate in predicting transverse displacement for all cases except for the low FCSR and high LTR combinations. On the contrary, with regard to the two transverse displacements, the EHSAPT provides results that are consistently close to those of

Table 3: Normalized transverse displacement at top face ($x = a/2$, $z = c + f_t/2$); R=FCSR/LTR

FCSR	LTR	4	10	100	1000
$7.3E+01$	R	18.25	7.3	0.73	0.073
	elasticity	0.0932	0.0270	0.0148	0.0147
	EHSAPT	0.0956	0.0285	0.0163	0.0162
	FOSD	0.1321	0.0337	0.0152	0.0150
$7.3E+04$	R	18250	7300	730	73
	elasticity	5.098	2.883	0.1333	0.0161
	EHSAPT	5.664	3.108	0.1351	0.0176
	FOSD	117.09	18.747	0.2023	0.0169
$7.3E+06$	R	1.825E+06	7.3E+05	7.3E+04	7.3E+03
	elasticity	7.244	6.038	2.812	0.1333
	EHSAPT	7.952	6.725	3.022	0.1351
	FOSD	1.171E+04	1873.0	18.748	0.2023
$7.3E+08$	R	1.825E+08	7.3E+07	7.3E+06	7.3E+05
	elasticity	7.291	7.263	3.698	2.811
	EHSAPT	7.999	7.981	4.071	3.021
	FOSD	1.171E+06	1.873E+05	1873.0	18.748

elasticity theory with the deviation from elasticity theory not exceeding 11%; in many cases the EHSAPT is very accurate ($< 2\%$ deviation from elasticity). It should be noted that Tables 2a and 2b only give transverse displacement data for two locations and don't capture the entire transverse displacement profile through the thickness.

Table 4 shows the the mid-plane normalized shear stress at (x=$a/10$, $z = 0$). The EHSAPT is very accurate for low FCSR and the full range of LTRs, practically coinciding with elasticity; for the more demanding cases of higher FCSRs, the EHSAPT is still quite accurate with the deviation from elasticity not exceeding 10%. On the contrary, the FOSD is inaccurate in predicting shear stress for all cases; for the high FSCRs and low LTRs, the FOSD stress values are, again, many orders of magnitude that of elasticity. This numerical assessment (although not exhaustive since it considers a fixed face-sheet-to-total-thickness ratio f/h_{tot}= 0.1 and does not consider orthotropic materials) gives further insight into the accuracy of EHSAPT with respect to elasticity.

Table 4: Normalized shear stress, τ_{xz}/q_0, at mid-core ($x = a/2$, $z = 0$); R=FCSR/LTR

FCSR	LTR	4	10	100	1000
$7.3E+01$	R	18.25	7.3	0.73	0.073
	elasticity	1.327	3.373	33.828	338.29
	EHSAPT	1.327	3.373	33.828	338.29
	FOSD	1.816	4.541	45.410	454.10
$7.3E+04$	R	18250	7300	730	73
	elasticity	0.0602	0.7651	32.406	334.88
	EHSAPT	0.0656	0.8217	32.501	334.89
	FOSD	1.8164	4.5410	45.410	454.10
$7.3E+06$	R	1.825E+06	7.3E+05	7.3E+04	7.3E+03
	elasticity	6.300E-4	9.890E-3	7.657	324.05
	EHSAPT	6.890E-4	1.085E-2	8.229	325.01
	FOSD	1.816	4.541	45.410	454.10
$7.3E+08$	R	1.825E+08	7.3E+07	7.3E+06	7.3E+05
	elasticity	6.301E-6	9.914E-5	0.0990	76.575
	EHSAPT	6.894E-6	1.089E-4	0.1087	82.289
	FOSD	1.816	4.541	45.410	454.10

3.3 Conclusions

Results have been presented for the case of transverse loading of a simply supported sandwich beam by comparison to the elasticity, the Classical sandwich beam theory, the FOSD theory and the HSAPT model, see Frostig et al. [15], for different face sheet and core material combinations. The results show that the present extended high-order theory is very close to the elasticity solution in terms of both the displacements and the transverse stress or strain, as well as axial stress through the core, and, in addition, the shear stress distributions in the core for core materials ranging from very soft to almost half the stiffness of the face sheets. In particular, it captures the very large range of core shear stress and the nearly parabolic profile in the cases of cores that are not "soft".

CHAPTER IV

STATIC GLOBAL BUCKLING

The solution procedure using EHSAPT to determine the global buckling behavior for a general asymmetric sandwich beam/wide plate with different face sheet materials and face sheet thicknesses is presented. We have used EHSAPT to solve for three cases:

Case (a): The axial load is applied exclusively to the face sheets. Large displacements in the core are neglected (linear strain-displacement relations are modeled in the core).

Case (b): Uniform axial strain is imposed through the entire height of the beam. Again, large displacements in the core are neglected (linear strain-displacement relations are modeling in the core).

Case (c): Uniform axial strain is imposed through the entire height of the beam. Now, large displacements in the core are considered (nonlinear strain-displacement relations are modeled in the core).

Cases (a) and (b) make use of the general nonlinear EHSAPT formulation given in Chapter 2, while case (c) involves including non-linear axial strains in the core that were not in the original formulation. It will be shown that the critical *global* buckling load is nearly identical for cases (a) and (c) for a range of core materials and geometry configurations but case (a) loading involves a simpler solution process. Moreover, this critical load is very close to the elasticity prediction. Therefore, this chapter will show in detail the solution procedure for finding the critical load of the case (a) loading.

As a benchmark, an elasticity solution for the global buckling of a sandwich beam/wide plate was presented by Kardomateas (2010) [24]. In this paper, two formulas were found to be the most accurate (by comparing to elasticity). These were (a) the formula derived by Allen (1969) [2] for thick faces (note that there also exist a corresponding formula by Allen for thin faces, but this was less accurate) and (b) the Engesser's (1891) [10] critical load formula where the shear correction factor used is the one derived for sandwich sections by Huang and Kardomateas (2002) [20]. The latter shear correction formula is not exclusively based on the shear modulus of the core, but instead includes the shear modulus of the faces and the extensional modulus of the core, therefore, it can account for sandwich constructions with stiffer cores and/or more compliant faces. In the analysis we shall use the Allen's thick faces formula as a representative of the simple formulas to compare with the High Order theory results. Frostig's proof that this formula would be the direct result of the HSAPT for the case of an incompressible core will also be shown.

First the solution procedure for solving cases (a), (b), and (c), respectively, for a simply-supported sandwich beam with general asymmetric geometry is presented. Then results are shown for a soft and a moderate core sandwich configurations with symmetric geometry, followed by conclusions.

4.1 Three Solution Approaches

Here we make use of the static formulation of EHSAPT that is written out in terms of its stress resultants and generalized coordinate (see Appendix C).

4.1.1 Case (a): Loading on the Face Sheets with Linear Axial Strains in the Core

In this case, $\widetilde{N}^t$ and $\widetilde{N}^b$ are applied on the top and bottom face sheets, respectively, such that the axial strains are equal on the top and bottom faces, and the net axial loading on each side of the beam is $-P$.

Imposing the condition of the same axial strain and the condition that the sum of the loads on the top and bottom face sheets equals $-P$ provides two equations for the unknown axial loads, which are found to be:

$$\widetilde{N}_p^t = -\kappa^t P \ ; \qquad \widetilde{N}_p^b = -\kappa^b P \ , \tag{34a}$$

where

$$\kappa^t = \frac{a_{11}^b f_t}{a_{11}^t f_b + a_{11}^b f_t} \ , \qquad \kappa^b = \frac{a_{11}^t f_b}{a_{11}^t f_b + a_{11}^b f_t} \ , \tag{34b}$$

and $a_{11}^i = 1/E_1^i$ is the compliance constant of the corresponding face sheet $(i = t, b)$.

The critical load for an asymmetric geometry and material configuration can be determined using the perturbation approach:

$$N^i(x) = N_p^i(x) + \xi N_s^i(x), \qquad (i = t, b, c) \tag{35a}$$

$$u_0^i(x) = u_p(x) + \xi u_{0s}^i(x), \quad w_0^i(x) = \xi w_{0s}^i(x) \qquad (i = t, b) \tag{35b}$$

$$M^i(x) = \xi M_s^i(x), \qquad (i = t, b, c) \tag{35c}$$

$$u_0^c(x) = \xi u_{0s}^c(x), \quad \phi_0^c(x) = \xi \phi_{0s}^c(x), \quad w_0^c = w_{0s}^c(x), \quad V^c(x) = \xi V_s^c(x) \ . \tag{35d}$$

The additional subscript p stands for primary, or the prebuckled state, while the additional subscript s stands for secondary, or the perturbed state, and ξ is an infinitesimally small quantity.

By considering Eqns. (34) and substituting the displacements, the stress resultants of the face sheets, Eqn. (35a), can be written as:

$$N^i = -\kappa^i P + \xi \left(C_{11}^i f_i u_{0s,x}^i \right) \qquad (i = t, b) \tag{36}$$

We assume global buckling modes for the simply-supported beam, as follows:

$$u_{0s}^{t,b,c} = U_0^{t,b,c} \cos \frac{\pi x}{a} \ ; \qquad \phi_{0s}^c = \Phi_0^c \cos \frac{\pi x}{a} \ , \tag{37a}$$

$$w_s^{t,b} = W^{t,b} \sin \frac{\pi x}{a}; \quad w_{0s}^c = W_0^c \sin \frac{\pi x}{a} \tag{37b}$$

Substitution of the secondary terms into the buckled state equations leads to seven algebraic equations, and these are:

$$\delta u_0^t: \quad U_0^b\left(-\frac{7}{30c}C_{55}^c+\frac{c\pi^2}{35a^2}C_{11}^c\right)+U_{0n}^c\left(-\frac{4}{3c}C_{55}^c+\frac{2c\pi^2}{15a^2}C_{11}^c\right)$$
$$+\Phi_0^c\left(-\frac{4}{5}C_{55}^c+\frac{2c^2\pi^2}{35a^2}C_{11}^c\right)+U_0^t\left(\frac{47}{30c}C_{55}^c+\frac{6c\pi^2}{35a^2}C_{11}^c+\frac{f_t\pi^2}{a^2}C_{11}^t\right)$$
$$+W^b\left(-\frac{cf_b\pi^3}{70a^3}C_{11}^c-\eta_2^b\frac{\pi}{a}\right)+W_0^c\frac{\pi\beta_1}{a}+W^t\left(\frac{3cf_t\pi^3}{35a^3}C_{11}^c+\eta_3^t\frac{\pi}{a}\right)=0 \tag{38a}$$

$$\delta w_0^t: \quad U_0^b\left(\frac{cf_t\pi^3}{70a^3}C_{11}^c+\eta_2^t\frac{\pi}{a}\right)+U_0^c\left(\frac{cf_t\pi^3}{15a^3}C_{11}^c-\eta_6^t\frac{\pi}{a}\right)+\Phi_0^c\left(\frac{c^2f_t\pi^3}{35a^3}C_{11}^c-\eta_4^t\frac{\pi}{a}\right)$$
$$+U_0^t\left(\frac{3cf_t\pi^3}{35a^3}C_{11}^c+\frac{\pi}{a}\eta_3^t\right)+W^b\left(\frac{C_{33}^c}{6c}-\frac{cf_bf_t\pi^4}{140a^4}C_{11}^c-\beta_2\frac{\pi^2}{a^2}\right)+W_0^c\left(-\frac{4}{3c}C_{33}^c-\eta_7^t\frac{\pi^2}{a^2}\right)$$
$$+W^t\left(-\kappa^tP\frac{\pi^2}{a^2}+\frac{7}{6c}C_{33}^c+\frac{3cf_t^2\pi^4}{70a^4}C_{11}^c+\frac{f_t^3\pi^4}{12a^4}C_{11}^t-\eta_8^t\frac{\pi^2}{a^2}\right)=0 \tag{38b}$$

$$\delta u_0^c: \quad U_0^b\left(-\frac{4}{3c}C_{55}^c+\frac{2c\pi^2}{15a^2}C_{11}^c\right)+U_0^c\left(\frac{8}{3c}C_{55}^c+\frac{16c\pi^2}{15a^2}C_{11}^c\right)+U_0^t\left(-\frac{4}{3c}C_{55}^c+\frac{2c\pi^2}{15a^2}C_{11}^c\right)$$
$$+W^b\left(\frac{\eta_6^b\pi}{a}-\frac{cf_b\pi^3}{15a^3}C_{11}^c\right)+W_0^t\left(\frac{cf_t\pi^3}{15a^3}C_{11}^c-\frac{\eta_6^t\pi}{a}\right)=0 \tag{38c}$$

$$\delta\phi_0^c: \quad U_0^b\left(\frac{4}{5}C_{55}^c-\frac{2c^2\pi^2}{35a^2}C_{11}^c\right)+\Phi_0^c\left(\frac{8c}{5}C_{55}^c+\frac{16c^3\pi^2}{105a^2}C_{11}^c\right)+U_0^t\left(-\frac{4}{5}C_{55}^c+\frac{2c^2\pi^2}{35a^2}C_{11}^c\right)$$
$$+W^b\left(\frac{c^2f_b\pi^3}{35a^3}C_{11}^c-\frac{\eta_4^b\pi}{a}\right)+W_{0n}^c\left(\frac{4c\beta_1\pi}{3a}\right)+W_0^t\left(\frac{c^2f_t\pi^3}{35a^3}C_{11}^c-\frac{\eta_4^t\pi}{a}\right)=0 \tag{38d}$$

$$\delta w_0^c: \quad -U_0^b\left(\frac{\beta_1\pi}{a}\right)+\Phi_0^c\left(\frac{4c\beta_1\pi}{3a}\right)+U_0^t\left(\frac{\beta_1\pi}{a}\right)-W^b\left(\frac{4}{3c}C_{33}^c+\frac{\eta_7^i\pi^2}{a^2}\right)$$
$$+W_0^c\left(\frac{8}{3c}C_{33}^c+\frac{16c\pi^2}{15a^2}C_{55}^c\right)-W^t\left(\frac{4}{3c}C_{33}^c+\frac{\eta_7^i\pi^2}{a^2}\right)=0 \tag{38e}$$

$$\delta u_0^b: \quad U_0^b\left(\frac{47}{30c}C_{55}^c+\frac{6c\pi^2}{35a^2}C_{11}^c+f_b\frac{\pi^2}{a^2}C_{11}^b\right)+U_0^c\left(-\frac{4}{3c}C_{55}^c+\frac{2c\pi^2}{15a^2}C_{11}^c\right)$$
$$+\Phi_0^c\left(\frac{4}{5}C_{55}^c-\frac{2c^2\pi^2}{35a^2}C_{11}^c\right)+U_0^t\left(-\frac{7}{30c}C_{55}^c+\frac{c\pi^2}{35a^2}C_{11}^c\right)+W^b\left(-\frac{3cf_b\pi^3}{35a^3}C_{11}^c-\eta_3^b\frac{\pi}{a}\right)$$
$$-W_0^c\left(\frac{\pi}{a}\beta_1\right)+W_0^t\left(\frac{cf_t\pi^3}{70a^3}C_{11}^c+\eta_2^t\frac{\pi}{a}\right)=0 \tag{38f}$$

$$\delta w_0^b: \quad U_0^b\left(-\frac{3cf_b\pi^3}{35a^3}C_{11}^c-\eta_3^b\frac{\pi}{a}\right)+U_0^c\left(-\frac{cf_b\pi^3}{15a^3}C_{11}^c-\eta_6^b\frac{\pi}{a}\right)+\Phi_{0n}^c\left(\frac{c^2f_b\pi^3}{35a^3}C_{11}^c-\eta_4^b\frac{\pi}{a}\right)$$
$$+U_0^t\left(-\frac{cf_b\pi^3}{70a^3}C_{11}^c-\eta_2^b\frac{\pi}{a}\right)+W^b\left(-\kappa^bP\frac{\pi^2}{a^2}+\frac{7}{6c}C_{33}^c+\frac{3cf_b^2\pi^4}{70a^4}C_{11}^c+\frac{f_b^3\pi^4}{12a^4}C_{11}^b-\eta_8^b\frac{\pi^2}{a^2}\right)$$
$$+W_0^c\left(-\frac{4}{3c}C_{33}^c-\eta_7^b\frac{\pi^2}{a^2}\right)+W^t\left(\frac{C_{33}^c}{6c}-\frac{cf_bf_t\pi^4}{140a^4}C_{11}^c-\beta_2\frac{\pi^2}{a^2}\right)=0 \tag{38g}$$

Notice that the loading P (eigenvalue) appears in the δw_0^t Eqn. (38b) in the term W^t and in the δw_0^b Eqn. (38g) in the term W^b.

The equations can be cast in matrix form:

$$\{[K_{LC}]-\frac{\pi^2}{a^2}\lfloor G_a\rfloor[\ I\ ]\}\{U\}=\{0\} \tag{39}$$

$[K_{LC}]$ is a 7x7 matrix involving material stiffnesses and sandwich dimensions, and each element is given in Appendix D. The subscript LC denotes that the sandwich system has linear strains in the core. Later in this study another matrix, the K_{NLC} will represent additional terms that account for nonlinear axial strains in the core. The loading vector is represented by $\lfloor G_a\rfloor=\lfloor 0,0,0,0,\kappa^bP,0,\kappa^tP\rfloor$, if the equations of the system are written in the order of Eqns. (16a), (13), (14), (11), (17a), (15), (12a), respectively. Seven unknown displacement amplitudes make up the vector $\{U\}=\lfloor U_0^b,U_0^c,\Phi_0^c,U_0^t,W^b,W_0^c,W^t\rfloor^T$. The critical load is determined by finding the value of P for which the system has a nontrivial solution, or finding P by zeroing the determinant:

$$\det\{[K_{LC}]-\frac{\pi^2}{a^2}\lfloor G_a\rfloor[\ I\ ]\}=0\ . \tag{40}$$

4.1.2 Case (b): Uniform Strain Loading with Linear Axial Strains in the Core

In this case, both face sheets and the core have the same axial strain $\epsilon^i_{xxp} = \sigma^i_{xxp}/C^i_{11}$ for $i = t, b, c$, and imposing that the net stress resultant at each end is $-P$, gives:

$$\widetilde{N}^t = -\kappa^t P \ ; \qquad \widetilde{N}^b = -\kappa^b P \ ; \qquad \widetilde{n}^c = -\kappa^c \frac{P}{2c} \ , \tag{41a}$$

where

$$\kappa^t = \frac{a^b_{11} a^c_{11} f_t}{a^b_{11} a^t_{11} 2c + a^b_{11} a^c_{11} f_t + a^t_{11} a^c_{11} f_b} \ , \quad \kappa^b = \frac{a^t_{11} a^c_{11} f_b}{a^b_{11} a^t_{11} 2c + a^b_{11} a^c_{11} f_t + a^t_{11} a^c_{11} f_b} \ , \tag{41b}$$

$$\kappa^c = \frac{a^t_{11} a^b_{11} 2c}{a^b_{11} a^t_{11} 2c + a^b_{11} a^c_{11} f_t + a^t_{11} a^c_{11} f_b} \ . \tag{41c}$$

and $a^i_{11} = 1/E^i_1$ is the compliance of the top or bottom face or core ($i = t, b, c$).

When a uniform strain exists in the core, the face sheets have a nonzero transverse displacement at the primary state, which is due to the Poisson's effect on the core during compression (as opposed to the previous case). Thus, the top and bottom face sheets have primary state transverse displacements that are equal, yet opposite in direction, i.e. w_p and $-w_p$, respectively; furthermore they are constant along x. Moreover, when the loading is uniform strain, the axial displacement at the primary state in the face sheets and the core is the same, denoted by u_p. Therefore, in this case the displacements in the perturbation approach are

$$u^i_0(x) = u_p(x) + \xi u^i_{0s}(x) \qquad (i = t, b, c) \tag{42a}$$

$$\phi^c_0(x) = \xi \phi^c_{0s}(x) \ , \tag{42b}$$

$$w^t(x) = w_p + \xi W^t_s(x) \ , \tag{42c}$$

$$w^c_0(x) = \xi w^c_{0s}(x) \ , \tag{42d}$$

$$w^b(x) = -w_p + \xi W^b_s(x) \ . \tag{42e}$$

Since the axial stresses at the primary state are

$$\sigma^i_{xxp} = C^i_{11} u_{p,x} \ , \ i = t, b \quad \text{and} \quad \sigma^c_{xxp} = C^c_{11} u_{p,x} + C^c_{13} \frac{w_p}{c} \ , \tag{43a}$$

the following relations hold true at the primary state:

$$C^t_{11} f^t u_{p,x} = -\kappa^t P \ ; \quad C^b_{11} f^b u_{p,x} = -\kappa^b P \ ; \quad 2C^c_{13} w_p + 2c C^c_{11} u_{p,x} = -\kappa^c P \ . \tag{43b}$$

These relationships are also confirmed by solving the pre-buckling state equations.

Substituting these displacements into the EHSAPT governing equations again, leads to the same system of equations as for case (a), but this time the $\kappa^{t,b}$ are given by Eqn. (41b) and include the contribution of the core.

Therefore, the critical load can be determined by solving the buckled state Eqns. (38) which can be set in the form:

$$\{[K_{LC}] - \frac{\pi^2}{a^2} \lfloor G_b \rfloor [\ I\ ]\} \{U\} = \{0\} \tag{44a}$$

where $[K_{LC}]$ is the same as that given in Case (a) because the core still has linear axial strains, but now $\lfloor G_b \rfloor = \lfloor 0, 0, 0, 0, \kappa^b P, 0, \kappa^t P \rfloor$ where the κ^i's are those given in this section, Eqns. (41b). Note that even though there is a distributed axial load on the core, $\widetilde{n}^c = -\kappa^c P/(2c)$, it is not present in the loading vector because nonlinear axial strains in the core were neglected. Again, the critical load is determined by solving the value of P which gives a nontrivial solution to the buckled state equations, i.e. by zeroing the determinant:

$$\det\{[K_{LC}] - \frac{\pi^2}{a^2} \lfloor G_b \rfloor [\ I\ ]\} = 0 \ . \tag{44b}$$

4.1.3 Case (c): Uniform Strain Loading with Non-Linear Axial Strains in the Core

If the nonlinear axial strain in the core is considered, the axial load appears in the "buckled state" equations for the core as well. The nonlinear axial strain for the core

is

$$\epsilon^c_{xx}(x,z) = u^c_{,x}(x,z) + \frac{1}{2}\left[w^c_{,x}(x,z)\right]^2 \ , \tag{45}$$

The axial stress resultant N^c, Eqn. (29b) in Chapter 2, is based on the assumption of linear strains for the core. When nonlinear strains are included in the core, the following term is added to Eqn. (3):

$$N^c_{NL} = \frac{c}{15}C^c_{11}\left[2w^b_{,x}w^c_{0,x} - w^b_{,x}w^t_{,x} + 2(w^b_{,x})^2 + 2w^c_{0,x}w^t_{,x} + 8(w^c_{0,x})^2 + 2(w^t_{0,x})^2\right] \ . \tag{46}$$

Again, the moment stress resultant of the core M^c, Eqn. (29e) in Chapter 2, is based on the assumption of linear strains for the core. When nonlinear strains are included in the core, the following term is added to (29e):

$$M^c_{NL} = \frac{c^2}{30}C^c_{11}\left(w^b_{,x} - w^t_{,x}\right)\left(3w^b_{,x} + 4w^c_{0,x} + 3w^t_{,x}\right) \ . \tag{47}$$

and involves many terms if expanded out in terms of the unknown displacement variables. We would like to note that the solution procedure for this case becomes quite complicated because both primary and secondary unknown displacement variables appear in the buckled state set of equations. Later the results section will show that the extra work required to solve both sets of equations did not make significant gains in accuracy. We shall summarize the solution procedure for this case, which involves the perturbation approach with the same assumed deformation as in Case (b), and neglecting higher order terms of ξ. The resulting buckled state equations is:

$$\{[K_{LC}] + [K_{NLC}] - \frac{\pi^2}{a^2}\lfloor G_c \rfloor [\ I\ ]\}\{U\} = \{0\} \ , \tag{48a}$$

where $[K_{LC}]$ is the same as in Cases (a) and (b), and $[K_{NLC}]$ contains the additional terms that account for nonlinear axial strains in the core:

$$K_{NLC} = \frac{\pi^2}{a^2}\left(cC_{11}^c u_{p,x} + C_{13}^c w_p\right) \begin{bmatrix} 0 & 0 & 0 & 0 & 0 & 0 & 0 \\ 0 & 0 & 0 & 0 & 0 & 0 & 0 \\ 0 & 0 & 0 & 0 & 0 & 0 & 0 \\ 0 & 0 & 0 & 0 & 0 & 0 & 0 \\ 0 & 0 & 0 & 0 & \frac{4}{15} & \frac{2}{15} & -\frac{1}{15} \\ 0 & 0 & 0 & 0 & \frac{2}{15} & -\frac{14}{15} & \frac{2}{15} \\ 0 & 0 & 0 & 0 & -\frac{1}{15} & \frac{2}{15} & \frac{4}{15} \end{bmatrix} . \tag{48b}$$

Note that $[K_{NLC}]$ depends on the primary state displacements, in particular, on $u_{p,x}$, (the x-derivative of the uniform axial displacement) and w_p (the uniform transverse displacement of the top face sheet due to the Poisson's effect in the axially loaded core), see case (b). The solution to the primary state displacements can be obtained by solving the prebuckled-state equations and are:

$$u_p = -\frac{\kappa^t P}{C_{11}^t}x = -\frac{\kappa^b P}{C_{11}^b}x = -\frac{\kappa^c P}{C_{11}^c}x \tag{48c}$$

$$w_p = -\frac{cC_{13}^c}{C_{33}^c}u_{p,x} \tag{48d}$$

Now that the nonlinear axial strain of the core is considered, not only the loading on the face sheets but also the loading on the core appears in the force vector:

$$G_c = [0, 0, 0, 0, \kappa^t P, \kappa^c P, \kappa^b P]^t \tag{48e}$$

Again, the critical load is determined by solving the value of P which gives a nontrivial solution to the buckled state equations, i.e. by zeroing the determinant:

$$\det\{[K_{LC}] + [K_{NLC}] - \frac{\pi^2}{a^2}\lfloor G_c \rfloor [\ I\ ]\} = 0\ . \tag{48f}$$

Finally, it should be noted that the solution procedure results in a usual eigenvalue problem and subsequently zeroing out a determinant. For Cases (a) and (b), this results in a characteristic equation that is quadratic in P, and for Case (c) it results in a cubic equation in P.

4.2 Numerical case study

We consider a sandwich configuration with symmetric geometry ($f_t = f_b = f$) and same face sheet material, leading to the loading condition $\widetilde{N}^t = \widetilde{N}^b = -P/2$ on the top and bottom face sheets for Case (a) (loading on face sheets) and $\widetilde{N}^t = \widetilde{N}^b = -\kappa^f P$ and $\widetilde{n}^c = -\kappa^c P/(2c)$ for Cases (b) and (c) (Uniform Strain, Linear and Nonlinear Core, respectively), where the κ's are given in Eqns. (41b) and (41c).

Two material system sandwich configurations will be considered: (i) carbon/epoxy unidirectional faces with hexagonal glass/phenolic honeycomb, which represents a sandwich with a very Soft Core (axial stiffness of core very small compared to that of the face sheets, $E_1^c/E_1^f < 0.001$) and (ii) e-glass/polyester unidirectional faces with balsa wood core, which represents a sandwich with a Moderate Core (E_1^c/E_1^f on the order of 0.01). The moduli and Poisson's ratios for these materials were given in Table 1 of Chapter 3.

The total thickness is considered constant at $h_{tot} = 2f + 2c = 30$ mm, the length over total thickness $a/h_{tot} = 30$, and we examine a range of face thicknesses defined by the ratio of face sheet thickness over total thickness, f/h_{tot}, between 0.02 and 0.20.

The results will be produced for (i) the simple sandwich buckling formula of Allen (thick faces version), which has been proven to be the most accurate among the simple sandwich buckling formulas, and which considers the transverse shear effects of the core, (ii) the High Order Sandwich Panel theory (HSAPT), which takes into account the core's transverse shear and also the core's transverse compressibility effects but neglects the core's axial stiffness effects and (iii) the present Extended High Order Sandwich Panel Theory (EHSAPT), which takes into account all three effects, namely the core's transverse shear and transverse compressibility effects as well as the core's axial stiffness effects. The benchmark values are the critical loads from the elasticity solution (Kardomateas, 2010) [24]. The global critical loads for the Allen thick faces formula and the HSAPT are given in Appendix E. The results are normalized with

the Euler load, P_{E0}:

$$P_{E0} = \frac{\pi^2}{a^2} 2 \left[E_f \frac{f^3}{12} + E_f f \left(\frac{f}{2} + c \right)^2 + E_c \frac{c^3}{3} \right] . \tag{49a}$$

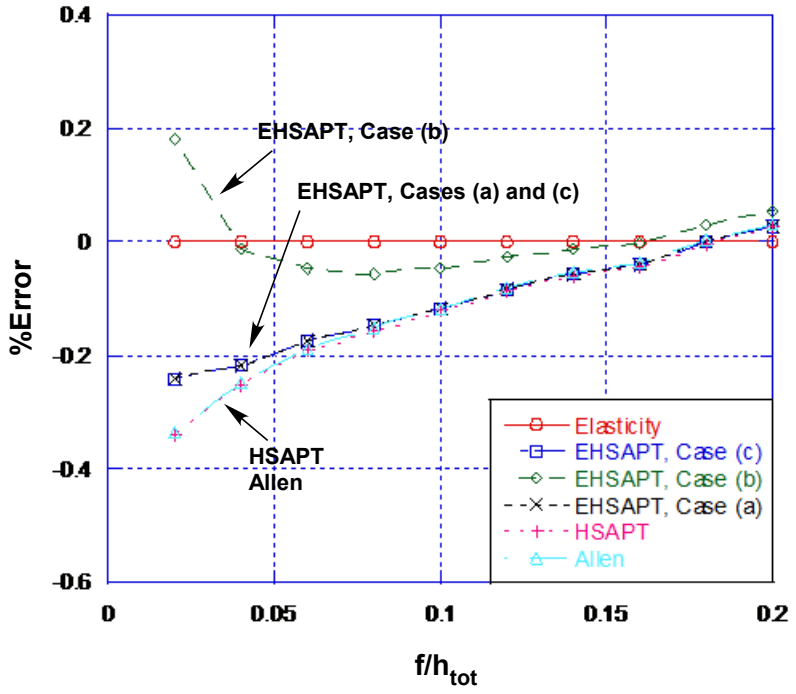

Figure 10: Percent Error (from elasticity) for the Critical Load of the various theories for the case of Soft Core and length $a = 30h_{tot}$.

Figure 10 shows the comparison of the theories to elasticity for the case of Soft Core and length ratio a/h_{tot}=30, as an Error %, calculated as

$$Error\% = \frac{P_{cr,theory} - P_{cr,elasticity}}{P_{cr,elasticity}} * 100 . \tag{49b}$$

We can see that the errors are of the order of $\pm 0.5\%$, very small, i.e. for this sandwich configuration all predictions are very close to the elasticity. For this material system, the Allen thick faces formula, the HSAPT and the EHSAPT Cases (a) (Loading on Faces, Linear Core) and (c) (Uniform Strain, Non-Linear Core) are all conservative and give practically identical results for the entire range of face sheet thicknesses. On the contrary, the EHSAPT Case (b) (Uniform Strain, Linear Core)

approach is less conservative and even becomes non-conservative for the very small ratios of f/h_{tot}. It should also be noted that the critical loads are significantly less than the Euler critical load, thus showing the importance of transverse shear in sandwich structures.

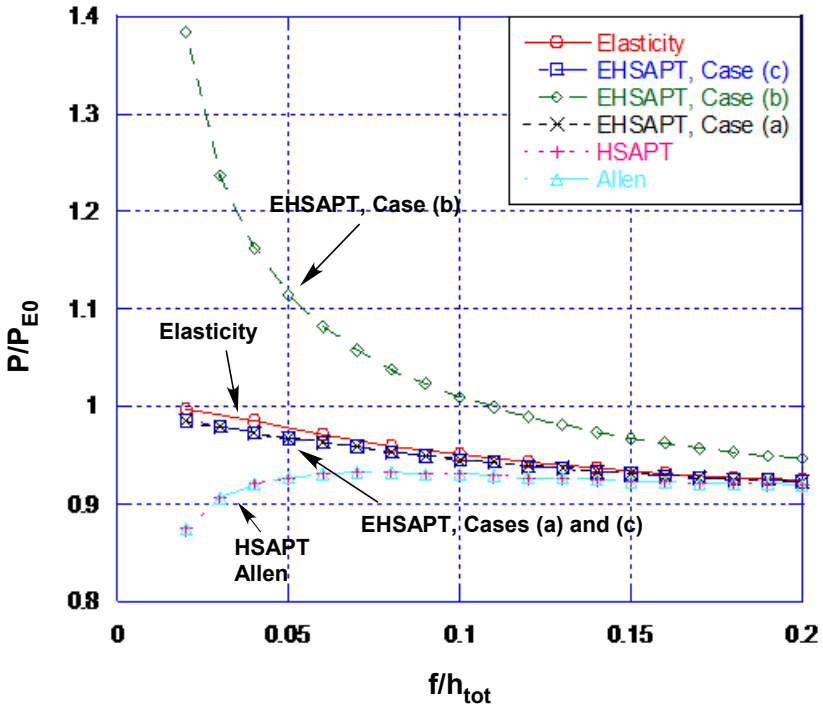

Figure 11: Critical Load (normalized with the Euler load) for the various theories for the case of Moderate Core and length $a = 30h_{tot}$.

Figure 11 shows that for the Moderate Core sandwich and length ratio a/h_{tot}=30, the theories diverge as the face sheet thickness becomes thinner compared to the overall thickness of the sandwich cross-section. The Allen's formula and the HSAPT give almost identical results and are the most conservative and can be as much as 15% below the elasticity value. The EHSAPT Cases (a) (Loading on Faces, Linear Core) and (c) (Uniform Strain, Non-Linear Core) are the most accurate, within 1% of the elasticity value, and on the conservative side. The EHSAPT Case (b) (Uniform Strain, Linear Core) is quite non-conservative, and can be as much as 40% above the

elasticity value, i.e. it is the most inaccurate. This result shows the importance of including the nonlinear axial strain in the core for the actual uniform strain loading solution. However, it is also remarkable that the simplified approach of Case (a) (Loading on Faces, Linear Core) is identical to the most complex approach taken with the EHSAPT Case (c) (Uniform Strain, Non-Linear Core).

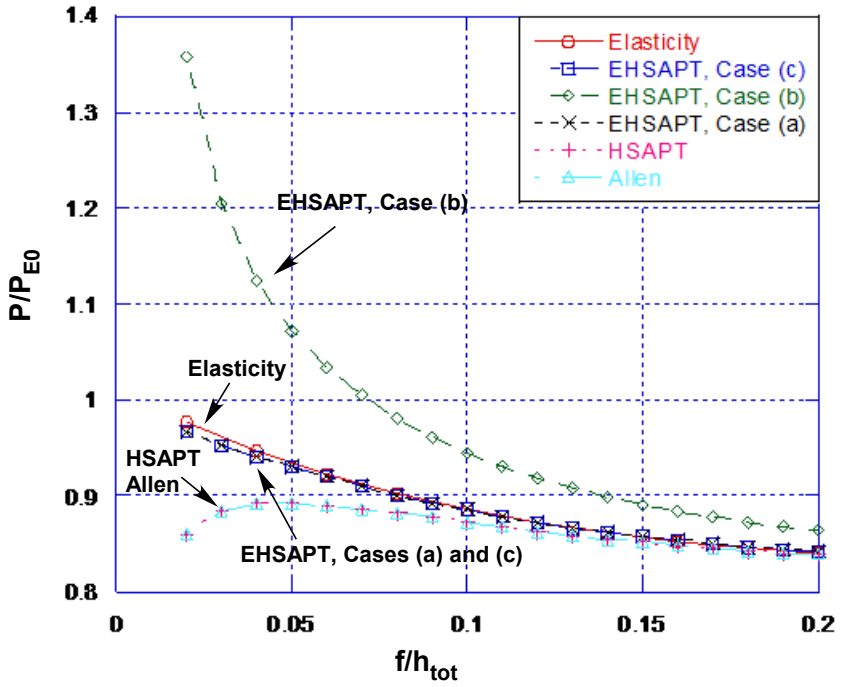

Figure 12: Critical Load (normalized with the Euler load) for the various theories for the case of Moderate Core and length $a = 20h_{tot}$.

Figures 12 and 13 show the effect of length for the Moderate Core configuration, i.e. results for $a/h_{tot} = 20$ and 10 respectively. For these shorter beam configurations, the EHSAPT Cases (a) and (c) are consistently close to the elasticity solution for the entire range of the face sheet thicknesses, and stay within about 1% error, i.e the most accurate. The other theories all diverge from elasticity for small f/h_{tot}. The Allen thick faces formula and the HSAPT are again identical and most conservative, and the EHSAPT Case (b) is again non-conservative and most inaccurate. Moreover, as the

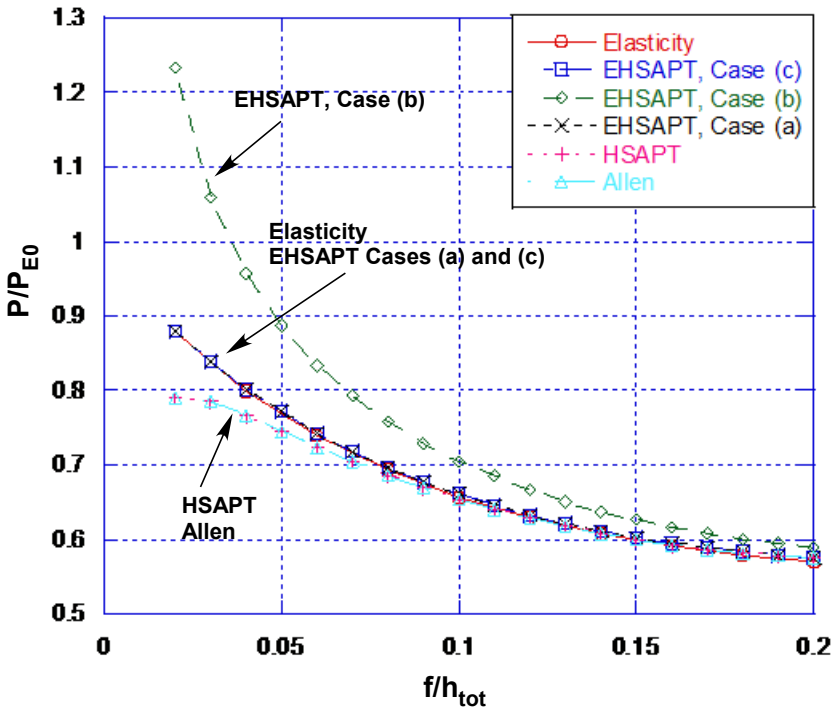

Figure 13: Critical Load (normalized with the Euler load) for the various theories for the case of Moderate Core and length $a = 10h_{tot}$.

beam length decreases, in all cases the predictions become somewhat less conservative. For the soft core configuration the EHSAPT, HSAPT, and Allen formula all predict practically the same critical load for all three length cases examined.

Thus, we can conclude that, when we deal with the critical load of sandwich structures, the present EHSAPT produces results very close to the elasticity for a wide range of cores, as opposed to the other theories of formulas, which seem to be accurate only when the core is very soft. It is important, however, how this theory is implemented, in the sense that this high accuracy is obtained for either Case (a) (Loading on Faces, Linear Core) or Case (c) (Uniform Strain, Non-Linear Core), but not for Case (b) (Uniform Strain, Linear Core).

An argument that explains the apparent inaccuracy of Case (b) can be made as follows: In Case (b), loads are distributed to both the faces and the core, but the

load vector G_b has only the stress resultants from the faces and does not have a contribution from the core, thus the loads of G_b would sum to a value less than the applied load P. On the contrary, in Case (c), the load vector G_c has stress resultants from both faces and the core (because now nonlinear strains are considered in the core) and these stress resultants would sum to P. In Case (a), loads were only applied to the faces, so although the load vector G_a contains only the stress resultants in the faces, these would again sum up to P.

Finally, a common observation in all these plots is that the Allen thick faces formula and the HSAPT give almost identical predictions. In fact, it can be proven that the HSAPT critical load resuces to that of the Allen thick faces formula if only transverse shear effects are included (i.e. the HSAPT applied without the core's transverse compressibility effects). This derivation is outlined in Appendix E.

4.3 Conclusions

The following conclusions are drawn by comparing the critical loads from these different theories to the benchmark critical load predicted by elasticity:

(1) The EHSAPT Cases (a) (Loading on the Faces and Linear Core) and Case (c) (Uniform Strain, Non-Linear Core) are nearly identical for both the Soft Core and Moderate Core configurations.

(2) For the Soft Core sandwich configurations ($E_1^c/E_1^f \leq 0.001$) all three theories (Allen thick faces formula, HSAPT and EHSAPT) predict the critical load within 1% of the critical load from elasticity.

(3) For the Moderate Core sandwich configurations ($E_1^c/E_1^f \leq 0.01$), the EHSAPT Cases (a) (Loading on the Faces and Linear Core) and Case (c) (Uniform Strain, Non-Linear Core) are consistently within about 1% of the critical load from elasticity. On the contrary, the Allen thick faces formula, the HSAPT, and the

EHSAPT Case (b) (Uniform Strain and Linear Core) diverge from elasticity for smaller f/h_{tot}. But the Allen thick faces formula and the HSAPT, diverge to more conservative values whereas the EHSAPT Case (b) (Uniform Strain and Linear Core) diverges to more nonconservative values for the smaller values of the ratio f/h_{tot} (i.e. thinner faces). The latter is also the least accurate and can be in significant error for these small f/h_{tot} ratios.

(4) In applying the various theories, it is important how the compressive loading is implemented, in the sense that Loading on the Faces with a Linear Core assumption gives almost identical results to the most complex case of Uniform Strain loading and a Non-Linear Core assumption, but certainly not for Uniform Strain loading and Linear Core assumption, for which quite inaccurate results can be obtained for moderate cores.

CHAPTER V

STATIC WRINKLING

The core compressibility has an important influence in the phenomenon known as face wrinkling or local buckling. Wrinkling is a local instability phenomenon characterized by short-wave buckling of the faces as opposed to global column buckling (Euler buckling) as depicted in Figure 14. Typically, wrinkling loads are lower than Euler Global buckling loads when the face sheets are very thin compared to the overall thickness of the panel. Wrinkling modes can be either symmetric or asymmetric as shown in Figure 14. Several formulas can be found in literature for the critical

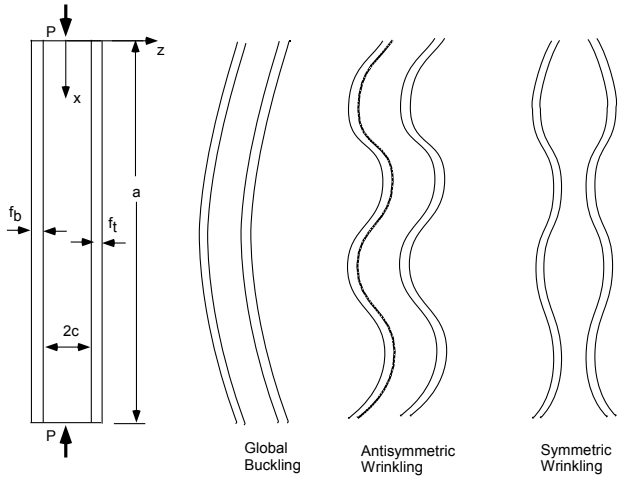

Figure 14: Global Buckling vs Wrinkling.

wrinkling load. A whole chapter is devoted to these different formulas in Carlsson and Kardomateas [6]. Most notable among the simple formulas is the Hoff-Mautner formula [18] and the Allen [2] formula and the former will be used in comparing with our results.

Another relevant study is an analytical model derived by Vonach and Rammerstorfer [39] that leads to a single explicit equation for the critical wrinkling load

of sandwich plates with isotropic faces and thick orthotropic cores. The authors performed a parametric study which showed that for highly orthotropic cores (e.g. honeycombs) wrinkling depends strongly on the in-plane stiffness of the core. Their results matched numerical solutions well for very thick cores that can be assumed infinitely thick, and no interaction between the face sheets exist. This finding is important because the main difference between the recent EHSAPT and the earlier HSAPT is that the latter does not account for the in-plane stiffness of the core.

Validation of the wrinkling results from the high order theories can be achieved by comparing to the elasticity solution for the wrinkling of a sandwich beam/wide plate, which was derived by Kardomateas [23]. In addition, validation can be achieved by comparing to experimental wrinkling loads. Historically, the success of comparisons of experimental results to analytical wrinkling models has been limited. Several semi-empirical derivations have been compared to various sandwich structure examples however obtaining good correlation has been hampered by inadequate testing conditions, conservative material assumptions and manufacturing flaws [26]. Due to the sensitivity of buckling instability to the bond between the face sheet and core constituent, many aspects of material manufacturing and specimen preparation affect the variations in test results for determining the critical wrinkling stress. Wrinkling failure is a common failure mode for sandwich structures with thin face sheets and lightweight cores. During experimental tests sandwich structures may display no or little post wrinkling load capacity, therefore catastrophic failure is common. Additionally, wrinkling refers to a local instability where the buckling wavelengths are typically less than the core thickness, making detection and capture of such buckling modes difficult.

In this section the critical wrinkling load is determined using the nonlinear differential equations of the new EHSAPT. The case study of a simply supported (S-S) sandwich beam undergoing compressive edgewise loading with symmetric geometry

and same face sheet materials is used for validation with two different experiments. The first set of these experiments was performed recently by Postdoctoral student Nathan Bailey and Senior Research Associate Dr. Mark Battley at the Center for Advanced Composite Materials (Auckland University, Auckland, NZ) using a thin skin sandwich structure commonly used in interior aircraft structures, namely Glass Face/Nomex Honeycomb Core. The second set of experiments are the ones performed by Norris et al [29] Aluminum face/Granulated-cork core specimens.

In section 4 the global buckling of sandwich beams/ wide panels using three different solution procedures were presented using the EHSAPT [32]. It was found that the EHSAPT Cases PFLC (Loading on Faces, Linear Core) and USNLC (Uniform Strain, Non-Linear Core) are nearly identical for both the soft Core and moderate core configurations and both are very close to elasticity predictions whereas case USLC (Uniform Strain, Linear Core) diverges from elasticity to more nonconservative values for moderate cores. These loading conditions are depicted in Figure 15.

This section presents the EHSAPT wrinkling formulations. Two methods of solving the EHSAPT differential equations for wrinkling were undertaken, the PFLC (Loading on Faces, Linear Core) and USNLC (Uniform Strain, Non-Linear Core) as described above. The two methods were investigated to see if the two approaches would result in different wrinkling loads. Next the simple wrinkling formulas that will be used for comparison are described. The results from the EHSAPT are compared with these simple wrinkling formulas, as well as with the critical wrinkling loads from elasticity. Moreover, compression experiments were recently conducted on Glass Face/Nomex Honeycomb Core by Mr. Nathan Bailey and Dr. Mark Battley at the Center for Advanced Composite Materials at University of Auckland, NZ. Their experimental test setup is described followed by the results and conclusions.

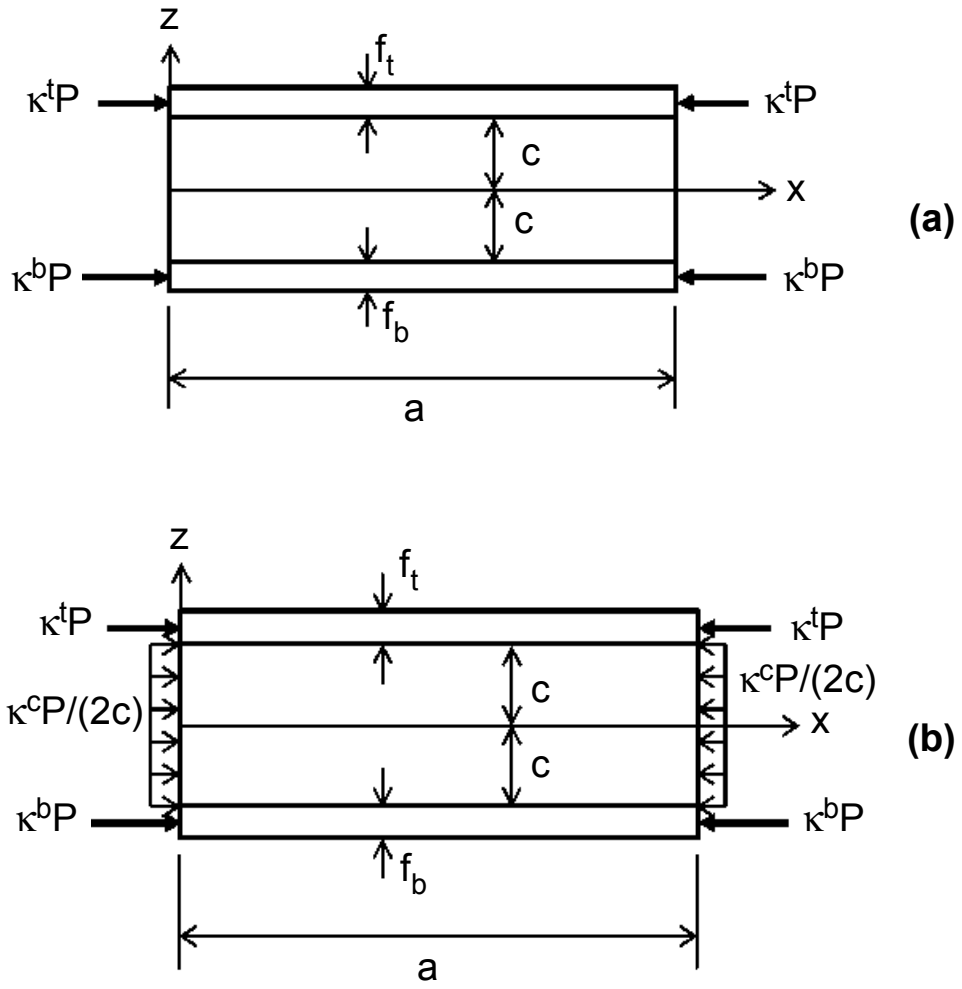

Figure 15: The two loading cases: (a) Loading on Faces, Linear Core (PFLC); (b) Uniform Strain, Nonlinear Core (USNLC).

5.1 Two solution approaches using EHSAPT

In Chapter 4 the critical global buckling load was determined using EHSAPT. The two most accurate approaches were case (a), in which concentrated compressive loads were applied on the face sheets and the linear strains in the core were used, and case (c), in which an edgewise loading was applied throughout the height of core and nonlinear axial strains had to be taken into account in order to provide accurate results. These two solution approaches are used again, now for the study of high-order wrinkling. In this chapter case (a) is referred to as the PFLC approach for loading P

on the Face sheets and having Linear strains in the Core, see Figure 15a. Case (c) is referred to as USNLC for Uniform Strain loading and NonLinear strains in the Core, see Figure 15b.

The PFLC and USNLC solution approaches are exactly the same as that described in sections 4.1.1 and 4.1.3, respectively, except that the global buckling mode described by terms $\frac{\pi}{a}$ from the trigonometric functions that describe the buckled shape need to replaced with the high-order wrinkling mode $\frac{n\pi}{a}$. The wave number n is the number of half-sine waves that would appear in the wrinkled shape once the sandwich beam/ wide panel has reached its critical load. In order to find out the critical wrinkling load and mode, the solution to $n = 1$ to a high enough value N needs to be solved and sorted. The lowest load and its corresponding mode number is the critical condition at which the beam/ wide panel will wrinkle.

5.2 Critical Wrinkling Load from the HSAPT and other Wrinkling Formulas

The wrinkling formulas from HSAPT are derived in [13]. In the case of a symmetrical construction in which the two skins are identical, the symmetric wrinkling critical load from the HSAPT in is:

$$P_{cr,HSAPT,symm} = \frac{2[E^c_{33} \ + c\ (EI)\ \alpha_n^4]}{c\ \alpha_n^2}\ , \tag{50a}$$

where

$$EI = E^f_{11} f^3/12\ ; \quad \alpha_n = n\pi/a\ . \tag{50b}$$

In the case of antisymmetric wrinkling, the critical load from the HSAPT is:

$$P_{cr,HSAPT,antisymm} = P_e \left\{ \frac{1 + \left[1 + \frac{(2c)^2 G^c_{31} n^2\pi^2}{12 E^c_3 a^2}\right] \left(\frac{P_{ef}}{P_c} - \frac{P^2_{ef}}{P_c P_e}\right)}{1 + \left[1 + \frac{(2c)^2 G^c_{31} n^2\pi^2}{12 E^c_3 a^2}\right] \frac{(P_e - P_{ef})}{P_c}} \right\}\ , \tag{51a}$$

where

$$P_e = E^f_{11} \frac{n^2\pi^2}{a^2} \left[\frac{f^3}{6} + \frac{f(2c+f)^2}{2}\right]\ , \tag{51b}$$

$$P_{ef} = E_{11}^{f} \frac{n^2\pi^2}{a^2} \frac{f^3}{6} \; ; \qquad P_c = G_{c31} \frac{(2c+f)^2}{2c} \; , \tag{51c}$$

Among the other simple wrinkling formulas, which are outlined in Carlsson and Kardomateas [6], Hoff and Mautner's formula is mostly known and used in the form:

$$\sigma_{cr,HoffMautner} = 0.5(E_{11}^{f} E_{33}^{c} G_{31}^{c})^{(1/3)} \; , \tag{52}$$

where the critical stress refers to the face sheets. The cubic root form of the Hoff-Mautner equation was derived using an energy approach for the problem of symmetric wrinkling of a sandwich (with isotropic material and neglible axial rigidity in the core). The theoretical approach led to a coefficient of 0.91 in front of the cubic root of the Hoff-Mautner formulation Hoff and Mautner (1945) [18]. However, a conservative version of the formula with a coefficient of 0.5 instead of 0.91 is commonly used. The formula is independent of the sandwich geometry and mode of wrinkling, and has been used as a wrinkling failure approximation for sandwich design. As can be seen in Hoff-Mautner's simple formula the transverse stiffness of the core in particular is critical in improving the susceptibility of a sandwich material to wrinkling failure.

For the case of uniform strain loading on a sandwich with a symmetric configuration, the Hoff-Mautner critical load can also be expressed as

$$P_{cr,HoffMautner} = \sigma_{cr,HoffMautner}(2fb) \tag{53}$$

i.e., the entire load is assumed to be carried by the face sheets.

5.3 Comparison of Theories with elasticity

An elasticity solution to the wrinkling phenomenon of a simply supported sandwich beam was presented by Kardomateas [23]. This elasticity solution can serve as a benchmark to determine the accuracy of the different sandwich beam/ wide panel theories and simple wrinkling formulas.

Tables 5 through 8 give the critical loads (normalized with the Euler load) for sandwich beams with length ratio $a/h_{tot} = 5$ and varying thickness ratios f/h_{tot},

where $h_{tot} = 2(f + c)$ is the total beam thickness. The four tables correspond to the following material configurations: Isotropic face and core with E_f/E_c=1,000, Isotropic face and core with E_f/E_c=500, E-glass/polyester faces with PVC/R75 foam core, and graphite/epoxy faces with glass/phenolic honeycomb core, respectively. These tables compare the elasticity results to the wrinkling predictions from the two methods of EHSAPT (PFLC and USNLC), the HSAPT, and the Hoff-Mautner (semi-empirical constant=0.5). The tables also show the mode and percent Error with respect to elasticity.

Table 5: Critical loads for E_f/E_c=1,000; normalized with the Euler load (w/o shear). Superscripts a and b are for method PFLC and USNLC, respectively. A and S in the wave numbers stand for Anti-symmetric and Symmetric, respectively

f/h_{tot}	elasticity (n)	Hoff (n) (Error%)	HSAPT (n) (Error%)	EHSAPT^a (n) (Error%)	EHSAPT^b (n) (Error%)
0.01	0.07381 (A24)	0.04038 (27) (-45.3%)	0.02654 (S20) (-64.0%)	0.07909 (A22) (+7.2%)	0.08228 (A22) (+11.5%)
0.02	0.07393 (A12)	0.04154 (13) (-43.8%)	0.03902 (S12) (-47.2%)	0.07080 (A12) (-4.2%)	0.07212 (A12) (-2.5%)
0.03	0.07288 (A7)	0.04251 (9) (-41.7%)	0.04945 (S9) (-32.2%)	0.06967 (A8) (-4.4%)	0.07040 (A8) (-3.4%)
0.04	0.06489 (A1)	0.04345 (7) -(33.0%)	0.05900 (S7) (-9.1%)	0.06389 (A1) (-1.5%)	0.06391 (A1) (-1.5%)
0.05	0.05411 (A1)	0.04439 (5) (-18.0%)	0.05336 (A1) (-1.4%)	0.05336 (A1) (-1.4%)	0.05337 (A1) (-1.4%)

For Tables 5 and 6, results are produced for the following configuration: isotropic faces and core with E_f/E_c=1,000 and 500, $\nu_f = 0.35$ and $\nu_c = 0$. Table 7 gives results for E-glass/polyester unidirectional facings and R75 cross-linked PVC foam core with the facings moduli (in GPa): $E_1^f = 40$, $E_2^f = E_3^f = 10$, $G_{23}^f = 3.5$, $G_{12}^f = G_{31}^f = 4.5$; and the facings Poisson's ratios: $\nu_{12}^f = 0.26$, $\nu_{23}^f = 0.40$, $\nu_{31}^f = 0.065$. The PVC core

Table 6: Critical loads for E_f/E_c=500; normalized with the Euler load (w/o shear). Superscripts a and b are for method PFLC and USNLC, respectively. A and S in the wave numbers stand for Anti-symmetric and Symmetric, respectively

f/h_{tot}	elasticity (n)	Hoff (n) (Error%)	HSAPT (n) (Error%)	$EHSAPT^a$ (n) (Error%)	$EHSAPT^b$ (n) (Error%)
0.01	0.1222 (A30)	0.0631 (34) (-48.4%)	0.0370 (S24) (-69.8%)	0.1370 (A26) (+12.1%)	0.1479 (A26) (+21.1%)
0.02	0.1210 (A15)	0.0654 (17) (-45.9%)	0.0548 (S14) (-54.7%)	0.1162 (A15) (-4.0%)	0.1207 (A15) (-0.3%)
0.03	0.1211 (A10)	0.0672 (11) (-44.5%)	0.0698 (S11) (-42.3%)	0.1143 (A10) (-5.6%)	0.1169 (A10) (-3.4%)
0.04	0.1188 (A6)	0.0687 (9) (-42.1%)	0.0836 (S9) (-29.6%)	0.1128 (A7) (-5.0%)	0.1144 (A7) (-3.7%)
0.05	0.1027 (A1)	0.0703 (7) (-31.6%)	0.0962 (S7) (-6.3%)	0.1003 (A1) (-2.3%)	0.1003 (A1) (-2.3%)

is isotropic with modulus $E^c = 0.075$ GPa and Posson's ratio $\nu^c = 0.3$. The axial modulus ratio of the facings and the core is close to 500. In general, we can make the following conclusions for the isotropic core case:

(1) Sandwich structures will exhibit local wrinkling as f/h_{tot} becomes small (i.e. sandwiches with relatively thin faces), and global buckling as f/h_{tot} becomes bigger (i.e. sandwiches with relatively thick faces).

(2) The semi-emprical Hoff-Mautner formula is always very conservative between 18% to 50% under that of elasticity.

(3) The HSAPT is inaccurate in predicting wrinkling loads for sandwiches with very thin faces, underpredicting the critical load by as much as 70% for the more moderately stiffer core configuration with $E_f/E_c = 500$ and $f/h_{tot} = 0.01$.

(4) The EHSAPT is the more accurate with the USNLC approach (Uniform Strain, Nonlinear Core) predicting slightly higher critical loads than the PFLC approach

Table 7: Critical loads for E-glass/polyester faces and PVC/R75 foam core; normalized with the Euler load (w/o shear). Superscripts a and b are for method PFLC and USNLC, respectively. A and S in the wave numbers stand for Anti-symmetric and Symmetric, respectively

f/h_{tot}	elasticity (n)	Hoff (n) (Error%)	HSAPT (n) (Error%)	$EHSAPT^a$ (n) (Error%)	$EHSAPT^b$ (n) (Error%)
0.01	0.10230 (A30)	0.05549 (32) (-45.8%)	0.03586 (S23) (-65.0%)	0.10775 (A25) (+5.3%)	0.11583 (A25) (+13.2%)
0.02	0.10120 (A15)	0.05749 (16) (-43.2%)	0.05307 (S14) (-47.6%)	0.09593 (A14) (-5.2%)	0.09932 (A14) (-1.9%)
0.03	0.10080 (A9)	0.05898 (11) (-41.5%)	0.06751 (S10) (-33.0%)	0.09533 (A9) (-5.4%)	0.09720 (A9) (-3.6%)
0.04	0.09096 (A1)	0.06035 (8) (-33.6%)	0.08080 (S8) (-11.2%)	0.08953 (A1) (-1.6%)	0.08957 (A1) (-1.5%)
0.05	0.07596 (A1)	0.06170 (6) (-18.8%)	0.07486 (A1) (-1.4%)	0.07495 (A1) (-1.3%)	0.07497 (A1) (-1.3%)

(Loading on Faces, Linear Core). In general, USNLC is more accurate the PFLC when the beam wrinkles for all f/h_{tot} other than 0.01. The deviation from elasticity for the USNLC is no more than about 4%. (7) The EHSAPT PFLC approach has good accuracy for the range of thickness ratios with at most 12% Error for the extreme case of $f/h_{tot} = 0.01$ for isotropic face and core with E_f/E_c=500 (Table 6). (8) The HSAPT predicts symmetric wrinkling modes, while the EHSAPT predicts antisymmetric wrinkling modes, similar to elasticity.

Table 8 gives results for graphite/epoxy unidirectional facings and hexagonal glass/phenolic honeycomb core with the facings moduli (in GPa): $E_1^f = 181$, $E_2^f = E_3^f = 10.3$, $G_{23}^f = 5.96$, $G_{12}^f = G_{31}^f = 7.17$; and the facings Poisson's ratios: $\nu_{12}^f = 0.28$, $\nu_{23}^f = 0.49$, $\nu_{31}^f = 0.0159$. The honeycomb core moduli are in (GPa):

Table 8: Critical loads for graphite/epoxy faces and glass/phenolic honeycomb core; normalized with the Euler load (w/o shear). Superscripts a and b are for method PFLC and USNLC, respectively. A and S in the wave numbers stand for Anti-symmetric and Symmetric, respectively

f/h_{tot}	elasticity (n)	Hoff (n) (Error%)	HSAPT (n) (Error%)	$EHSAPT^a$ (n) (Error%)	$EHSAPT^b$ (n) (Error%)
0.01	0.07037 (A26)	0.04277 (15) (-39.2%)	0.03947 (S24) (-43.9%)	0.07099 (A25) (+0.9%)	0.07147 (A25) (+1.6%)
0.02	0.06552 (A1)	0.04371 (7) (-33.3%)	0.05773 (S14) (-11.9%)	0.06506 (A9) (-0.7%)	0.06517 (A9) (-0.5%)
0.03	0.04576 (A1)	0.04463 (5) (-2.5%)	0.04558 (A1) (-0.4%)	0.04559 (A1) (-0.4%)	0.04559 (A1) (-0.4%)
0.04	0.03577 (A1)	0.04556 (4) (+27.4%)	0.03564 (A1) (-0.4%)	0.03564 (A1) (-0.4%)	0.03564 (A1) (-0.4%)
0.05	0.02988 (A1)	0.04652 (3) (+55.7%)	0.02978 (A1) (-0.3%)	0.02978 (A1) (-0.3%)	0.02978 (A1) (-0.3%)

$E_1^c = E_2^c = 0.032$, $E_3^c = 0.390$, $G_{23}^c = G_{31}^c = 0.048$, $G_{12}^c = 0.013$; and the core Posson's ratio $\nu_{31}^c = \nu_{32}^c = \nu_{21}^c = 0.25$. For this orthotropic core case, the following observations are made:

(9) According to elasticity, the beam wrinkles only at $f/h_{tot} = 0.01$ and globally buckles for the relatively thicker faces.

(10) The semi-empirical Hoff-Mautner formula is always very conservative with respect to elasticity when the beam wrinkles, but can be nonconservative when the beam globally buckles (it would not be expected to be applicable for global buckling, anyway).

(11) The HSAPT is very conservative when the beam wrinkles, but becomes more accurate for thicker faces.

(12) The EHSAPT (both PFLC and USNLC approaches) is very accurate even at the extreme case of $f/h_{tot} = 0.01$.

The wrinkling results display some trends that were seen when studying the global buckling phenomenon in Phan et al [32], such as that the HSAPT tends to become less accurate and underpredicts critical loads for very thin faces, and that both the HSAPT and the EHSAPT (PFLC and USNLC) converge for thicker faces (bigger f/h_{tot}). The discrepancy between HSAPT and EHSAPT for very low f/h_{tot} (when the beam is most susceptible to wrinkling), but convergence for higher f/h_{tot} (when the beam tends to globally buckle), indicates that including the axial rigidity of the core is important during wrinkling. Though both high order theories have the same order of displacements in z in the core, the theories differ in shear stress distribution through the core. The HSAPT ignores the axial rigidity of the core, which makes the shear stress through the thickness constant. The EHSAPT accounts for the axial rigidity in the core and the shear stress is parabolic. In Kardomateas [23], the most accurate formula for wrinkling of isotropic faces and cores was that of Goodier and

Neou [17], which accounts for the compressive axial stress in the core. However the Goodier and Neou formula no longer exhibited good accuracy when the phases were orthotropic. The EHSAPT, however, can show good accuracy in these cases.

5.3.1 Experimental Study

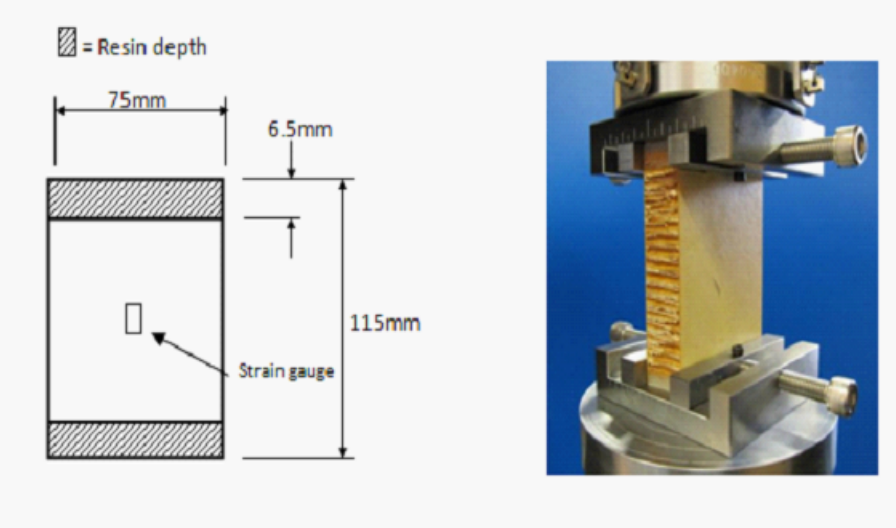

Figure 16: Details of the Test setup.

Sandwich construction consisting of a Nomex honeycomb core with a glass fiber and phenolic resin face sheet are common in aerospace applications. The material for this study is a beam/ wide panel consisting of 0.5 mm thick glass-phenolic face sheets (L528-7781) and a 24.4 mm Nomex honeycomb core (HRH 10-3.0). Sandwich beams/ wide panels were manufactured using layers of honeycomb core, adhesive and pre-impregnated face sheets, which are consolidated in a heated press. Due to the nature of honeycomb the core properties are anisotropic with a large transverse stiffness compared to the in-plane properties. The stiffer ribbon direction of the core was aligned with the loading or compression direction for all tests. Specimen geometry is shown in Figure 16 and illustrates the area of core removed and replaced with epoxy resin. This region of potting was required to prevent edge failure of the structure during loading whereby the face sheet delaminates from the core at the

Table 9: Material and Geometry Data for Glass-Phenolic Face sheet and Nomex Honeycomb Core Sandwich

	Face sheet Glass-Phenolic	Core Nomex Honeycomb 1/8-3.0
Thickness, mm	0.5	24.4
Width, mm	75	75
Length, mm	115	115
E_1, MPa	22000	0.44
E_2, MPa	22000	0.29
E_3, MPa	-	138
G_{13}, MPa	-	40
G_{23}, MPa	-	25
ν_{13}	-	0.01
ν_{31}	-	3.136
Longitudinal Tensile Strength σ_1, MPa	300	-
In-Plane Transverse Tensile Strength σ_2, MPa	300	-
Compressive Out-of-plane Strength σ_3, MPa	-	2.3

boundary due to the contact with the loading platen at this point. Premature edge failure occurs at a significantly lower load than the anticipated failure mode of skin wrinkling. After the edges were plotted they were post machined to ensure the ends were parallel and square. The data for the materials used are in Table 9.

The residual strength testing was carried out using an edgewise compression test method ASTM C364-07. The test fixture shown in Figure 16 was made of two identical loading plates with bars to lightly clamp the specimen to assist in preventing end failures. A spherical head was used to evenly distribute the load over the top plate. The load was applied at a displacement rate of 0.5 mm/min and wrinkling failure occurred within three to six minutes.

Seven specimens were instrumented with strain gauges to measure longitudinal or compressive strain in the center of the face sheets during edgewise loading. The purpose of the direct strain measurement was to ensure even distribution of the load between the face sheets. Strain was recorded to the data acquisition program in real-time. Prior to testing, a 50 N compressive pre-load was applied and the strain

Table 10: Wrinkling Experiments on Glass Face/ Nomex Honeycomb Core Sandwich specimens and comparison with theories. Superscripts a and b are for method PFLC and USNLC, respectively. A and S in the wave numbers stand for Anti-symmetric and Symmetric, respectively

Sample	Wrinkling Load (kN)
1	17.161
2	17.006
3	18.659
4	17.278
5	18.644
6	18.072
7	17.489

Average Experimental (Standard Deviation)	Hoff-Mautner	HSAPT	EHSAPT (PFLC)	EHSAPT (USNLC)
17.758 (0.646)	18.57 (4.6%)	15.281 (-13.9%) (S17)	17.158 (-3.4%) (S16)	17.164 (-3.3%) (S16)

in each face sheet was measured. The spherical head was then adjusted until the strain distribution between the face sheets was within 5%. This pre-load ensured that a more even loading distribution of the face sheets was achieved. Without this pre-loading alignment, and adjustment of the spherical head, the average critical load reduced by 12%.

Table 10 shows the measured critical loads P for the 7 specimens tested. The average compressive critical load was 17.8 kN with a standard deviation of 0.646 kN. The onset of wrinkling failure was catastrophic. The specimens were examined after failure and the face sheets were observed to have failed between the loading platens with a crack propagating from one edge of the specimen. It is believed that wrinkling was the cause of failure and not face crushing because the compressive stress in the face at the time of failure was 22% below the yield strength of the virgin face sheet material. The variation in critical load was also very good with only a 3.6% coefficient of variation from the seven tests (attributed to the careful alignment of the loading platens via strain measurement). Though the variation in critical load among the

seven specimens was small, scatter in the experimental results may be due to the slight waviness of the face sheets that occur during manufacturing process of the sandwich specimens.

In Table 10, the experimental results are compared with the predictions from the various approaches. It should be noted that the theories do not take into account initial imperfections such as waviness of the faces that can occur during manufacturing. Therefore perfect agreement between experiment and theory is not to be expected. Yet, both EHSAPT approaches are remarkably close to the experimental data and provide the most accurate predictions compared to all other available approaches. In particular, the Hoff-Mautner's conservative formula predicts a nonconservative critical stress in the face sheets, and is within 4.6% error. Both the HSAPT and the EHSAPT predict the wrinkling mode to be symmetric and conservative loads. However, the EHSAPT is closest to experiments (within 3.4% error for both approaches), while the HSAPT is more conservative (underpredicting by about 14%).

5.3.2 Comparison with Wrinkling Tests in the Literature

Experimental wrinkling stresses of sandwich beams/ wide panels with 24ST clad aluminum face sheets and granulated-cork core (with 0.35 specific gravity) are reported in Norris et al [29] for three different geometric core-to-facesheet thickness ratios of $2c/f = \{3.63, 2.87, 3.85\}$. The aluminum face sheets had a modulus $E^f = 10^7$ psi, and the granulated-cork core had the following mechanical properties: $E_1^c = 1.18$ ksi, $E_3^c = 0.52$ ksi, $G_{31}^c = 0.33$ ksi and $\nu_{31}^c = 0.06$. The widths of all the specimens were 2 inches. For a given sandwich configuration, only specimens that had the same exact lengths were considered for comparison. Only 3 specimens had a length of 3.63 inches for the $2c/f$ ratio of 3.63, while there were 5 specimens each for configurations with $2c/f$ of 2.87 and 3.85. This set of experimental data was chosen for comparison because it is known that wrinkling was the cause of failure and the tests

Table 11: Comparison of the Theories with the Wrinkling Experiments of Norris et al (1961) [32]. Aluminum Face/Granulated-Cork Core

face f, in.	core $2c$, in.	Ratio $2c/f$	Length a, in.	Exper. Avg. σ_{cr}, ksi	Hoff-Mautner σ_{cr}, ksi (% Error)	HSAPT σ_{cr}, ksi (% Error) (n)	EHSAPT (PFLC) σ_{cr}, ksi (% Error) (n)	EHSAPT (USNLC) σ_{cr}, ksi (% Error) (n)
0.0196	1	51.0	3.63	9.817	5.986 (-39.0%)	8.264 (-15.8%) (S4)	8.51 (-13.3%) (A2)	8.491 (-13.5%) (A2)
0.0120	0.75	62.5	2.87	10.422	5.986 (-42.6%)	7.452 (-28.5%) (S5)	9.19 (-11.8%) (A4)	9.175 (-12.0%) (A4)
0.0120	1	83.3	3.85	10.418	5.986 (-42.5%)	6.492 (-37.7%) (S6)	9.61 (-7.8%) (A6)	9.597 (-7.9%) (A6)

had good repeatability; the standard deviation is no greater than 0.78 ksi for all 3 configurations.

Table 11 shows the average wrinkling stress in the faces from the experiments as well as those predicted from Hoff-Mautner, HSAPT, and EHSAPT (both PFLC and USNLC methods). The Hoff-Mautner is very conservative (generally about 40% lower) and is the same for the three configurations because the formula is independent of the geometry. The EHSAPT is in best agreement with the experimental data, staying within 14% of the experimental results for the three configurations and is always conservative. Moreover, both EHSAPT approaches are close to each other for all three configurations. The HSAPT is less accurate, being as much as 38% below the experimental data and becomes less accurate as the ratio of $2c/f$ increases. The predicted mode of the high-order theories are also shown in parenthesis. S and A stand for symmetric and antisymmetric, respectively, and is followed the by the semi-wave number. The HSAPT predicts symmetric wrinkling mode, unlike the EHSAPT, which predicts antisymmetric wrinkling.

5.3.3 Conclusions

The wrinkling predictions of the EHSAPT, the earlier High Order Sandwich Panel theory (HSAPT), and the Hoff-Mautner's semi-empirical formula are compared with (a) predictions from elasticity and (b) wrinkling experiments. Two experimental sets are chosen for comparison: one set is experiments conducted by the authors on Glass face/Nomex Honeycomb core sandwich specimens and the other set is experiments from the literature on Aluminum faces/granulated-cork core system.

In all cases the EHSAPT was the closest to both the elasticity predictions and the experimental data. There was little difference between the two formulations of the EHSAPT, which argues for the much simpler PFLC (Loading on Faces, Linear Core) approach. The earlier HSAPT was in significant error for the relatively thinner faces. The large discrepancy between HSAPT and EHSAPT for very low f/h_{tot} (when the beam is most susceptible to wrinkling), and the associated smaller discrepancy for higher f/h_{tot} (when the beam tends to buckle globally), indicates that including the axial rigidity of the core is very important during wrinkling.

The comparison of the different wrinkling formulations with elasticity show that in general the semi-empirical Hoff-Mautner formula is quite conservative, yet less so than the HSAPT. The good agreement of the EHSAPT with the experiments on honeycomb core sandwich specimens show that although the EHSAPT models the core as a homogenous material with global properties, the theory can be used to predict critical loads of nonhomogeneous honeycomb cores just as well as for homogeneous solid cores.

CHAPTER VI

FREE VIBRATIONS

In this section we shall study the free vibrations of a sandwich beam that is simply supported throughout its thickness. First the solution procedure using the linear dynamic formulation of EHSAPT will be outlined followed by comments on finding the natural frequencies and mode shapes using HSAPT, and FOSDT used for comparison. Next numerical results for several sandwich configurations will demonstrate the predicted mode shapes that EHSAPT can capture. Also, comparison with experiments from literature and elasticity will be made.

6.0.4 Solution Procedure using EHSAPT

For free vibrations of a simply supported sandwich beam we consider the unforced linear problem, which means that the right hand side in the governing differential equations (11) to (17) are zero. Since the sandwich beam is simply supported throughout its height at both ends, the boundary conditions for $x = 0,\ a$ are the three kinematic conditions

$$w^t = w^b = w_0^c = 0 \ , \tag{54}$$

and the right hand side of the 6 natural boundary conditions in (20a), (22), (23), (24), (26a), and (28) are equal to zero.

The seven displacement functions are assumed to have the form:

$$u_0^t = U_{0n}^t \cos\frac{n\pi x}{a} e^{i\omega_n t} \ ; \qquad u_0^c = U_{0n}^c \cos\frac{n\pi x}{a} e^{i\omega_n t} \ ; \tag{55a}$$

$$\phi_0^c = \Phi_{0n}^c \cos\frac{n\pi x}{a} e^{i\omega_n t} \ ; \qquad u_0^b = U_{0n}^b \cos\frac{n\pi x}{a} e^{i\omega_n t} \ , \tag{55b}$$

$$w^t = W_n^t \sin\frac{n\pi x}{a} e^{i\omega_n t} \ ; \qquad w_0^c = W_{0n}^c \sin\frac{n\pi x}{a} e^{i\omega_n t} \ ; \qquad w^b = W_n^b \sin\frac{n\pi x}{a} e^{i\omega_n t} \ . \tag{55c}$$

which satisfy the governing equations and boundary conditions and are harmonic in time with natural frequency ω_n. The parameter n corresponds to the wave number and how many half wavelengths occur in the mode shapes. After substituting these displacement mode shapes into the linear governing equations (excluding the nonlinear terms) and rearranging the equations into matrix form, the natural frequencies can be found by solving the following eigenvalue problem:

$$(-\lambda_n[M_n] + [K_n])\{U_n\} = \{0\} \tag{56}$$

where the eigenvalue λ_n is related the natural frequency by $\lambda_n = \omega_n^2$. $[M_n]$ and $[K_n]$ (given in Appendix F) are the mass and stiffness matrices, respectively, for a given wave number n. The rows of the unforced equations of motion in (56) correspond to Eqns. (16a), (13), (14), (11), (17a), (15), (12a), respectively. The eigenvector holds the relative amplitude coefficients:

$$\{U_n\} = \{U_{0n}^b, U_{0n}^c, \Phi_{0n}^c, U_{0n}^t, W_n^b, W_{0n}^c, W_n^t\}^T \tag{57}$$

In EHSAPT, $[M_n]$ and $[K_n]$ are 7x7 matrices, therefore there are 7 eigenvalues/natural frequencies and 7 eigenvectors/modes shapes for a given wave number n.

6.0.5 Solution procedure for FOSDT and HSAPT

Classical FOSDT assumes that the sandwich composite is transversely incompressible, and assumes a constant average value of shear strain (through the height) in the core. In our solution procedure using FOSDT, in-plane stresses in the faces and the core are taken into account. HSAPT accounts for the transverse compressibility and the shear in the core, considers axial stresses in the faces but neglects axial stresses in the core.

In our solution procedure we consider rotary inertia in all of the theories. The solution to the eigenvalues and the modes shapes of FOSDT and HSAPT are very

similar to that outlined in Section 6.0.4 for EHSAPT in that they result in the same eigenvalue problem of the form shown in Eqn. (56). However, the size of matrices $[M_n]$ and $[K_n]$ and eigenvector $\{U_n\}$ depend on each theory. In the appendix the details of the mass and stiffness matrices and eigenvectors for the FOSDT and HSAPT are given in Appendix F.1 and F.2, respectively. Once the mass and stiffness matrices and the eigenvector are defined, the eigenvalue problem is ready to be solved.

It should be noted that $[M_n]$ and $[K_n]$ are the size N x N, where N is the number of generalized coordinates of the theory, and n is the wave number. Therefore, for FOSDT the matrices are size 3x3 because there are 3 generalized coordinates: u_0, w_0, and ϕ_0. Notice there are no superscripts because FOSDT is an equivalent single layer theory. For HSAPT the matrices are 5x5 because there are 5 generalized coordinates: u_0^t, u_0^b, w^t, w_0^c, and w^b. For the simply supported sandwich case, these generalized coordinates have the same form as those in Eqn. (55) (i.e. axial displacements u and rotation ϕ have Cosine mode shapes and transverse displacements w have Sine mode shapes).

6.0.6 Comparison with Experimental Results

The first comparison is made with the TV-holograph measurements of Jensen and Irgens[22]. They measured and identified antisymmetric and symmetric modes of a simply supported sandwich beam. The antisymmetric mode is characterized by displacements that are antisymmetric with respect to the beam mid-height, that is, the face sheets move in phase with each other. The symmetric mode has a displacement pattern that is symmetric with respect to the mid-height, that is, the face sheets move 180 deg out of phase with respect to each other. The beam was assembled by two steel face sheets and an H60 Divinycell plastic foam core. The face sheets were identical with $f_t = f_b = f = 2\ mm$, while the core had a height of $2c = 30$ mm. The beam had a span $a = 300$ mm with a 10 mm free end (overhang) at each side,

and width $b = 50$ mm. The face and core material are assumed to be isotropic, and the material parameters from [22] are given in Table 12. Some ratios of interests are: $E^c/E^f = 0.00026$ therefore the sandwich has a very soft core compared to the face sheets, $a/H_{tot} = a/(2f + 2c) = 8.8$ so the beam is short, and $f/H_{tot} = 0.06$ so the faces are thin compared to the total height of the beam.

Table 12: Material parameters of the sandwich beam from [22]

Material	Young's Modulus E, Pa	Shear Modulus G, Pa	Poisson's Ratio, ν	Density $\rho\ kg/m^3$
Steel	210 x 10^9	81 x 10^9	0.30	7900
Divinycell H60	56 x 10^6	22 x 10^6	0.27	60

Table 13: Comparison of Experiment, High Order and Classical Theories for Antisymmetric modal natural frequencies

Mode	Experiments [22]	EHSAPT	HSAPT	FOSDT (k=5/6)	FOSDT (k=1)
1	263	251	251	211	231
2	——	535	535	427	467
3	889	868	868	641	702
4	1289	1269	1269	855	936
5	1774	1749	1749	1069	1171
6	——	2318	2318	1283	1405
7	——	2979	2979	1497	1640
8	3806	3737	3737	1711	1874
9	4621	4594	4593	1925	2108

Table 13 shows the first 9 antisymmetric frequencies from experiment, and the predictions of EHSAPT, HSAPT, and FOSDT (when the shear correction factor k=5/6 and k=1). It can be seen that EHSAPT and HSAPT predict practically the same antisymmetric natural frequencies for the first 9 frequencies. The high-order theories are within -5% of the experimentally found fundamental mode, and are within -2% for the higher modes. Jensen and Irgens reported that they had to slightly clamp the specimen at the supports to prevent it from sliding and this would effect the fundamental mode more than higher modes, due to the number of nodal

Table 14: Comparison of natural frequencies of a sandwich beam with a soft core, Symmetric Modes

Mode	Experiments [22]	EHSAPT	HSAPT
1	——	2492	2424
2	——	2499	2431
3	——	2508	2464
4	——	2569	2554
5	——	2744	2734
6	3358	3056	3035
7	——	3517	3473
8	——	4127	4052
9	——	4878	4767

points they affect (see [22]). Therefore, we believe that the slightly lower accuracy at fundamental mode is due to the slightly clamped supports. The superiority of the high-order theories is apparent when comparing the classical FOSDT with the experimental results. FOSDT (k=5/6) and FOSDT (k=1) predict -20% and -12% error, respectively, for the fundamental modes, and even greater error for the higher modes, whereas EHSAPT and HSAPT improve in accuracy for higher modes.

Table 14 shows the comparison between the measured and predicted symmetric vibrational modes. Only one symmetric mode was found in their experiments. Note FOSDT is not shown for comparison because they treat the sandwich as transversely incompressible. EHSAPT and HSAPT's 6th symmetric natural frequency is within -9% and -10% of the one experimentally found symmetric mode, respectively, whereas EHSAPT and HSAPT's 7th symmetric mode are within +5% and +3% of the experimentally found symmetric mode, respectively. Jenesn and Irgens did not report the exact number of wavelength, therefore the exact mode is not known. It should be noted that the first 4 symmetric natural frequencies predicted by EHSAPT and HSAPT are relatively close to each other in the spectrum. When the modes are close, they can mix and make it difficult for the TV-holograph instrument to identify the mode. Jensen and Irgens gave this explanation for not being able to identify the missing modes in the tables.

It should be noted that the results were obtained from the solution procedure in the previous section, in which the overhang was not modeled. Despite using a more simplified model (without the overhang), the high-order theories give good results.

6.0.7 Mode shapes of EHSAPT

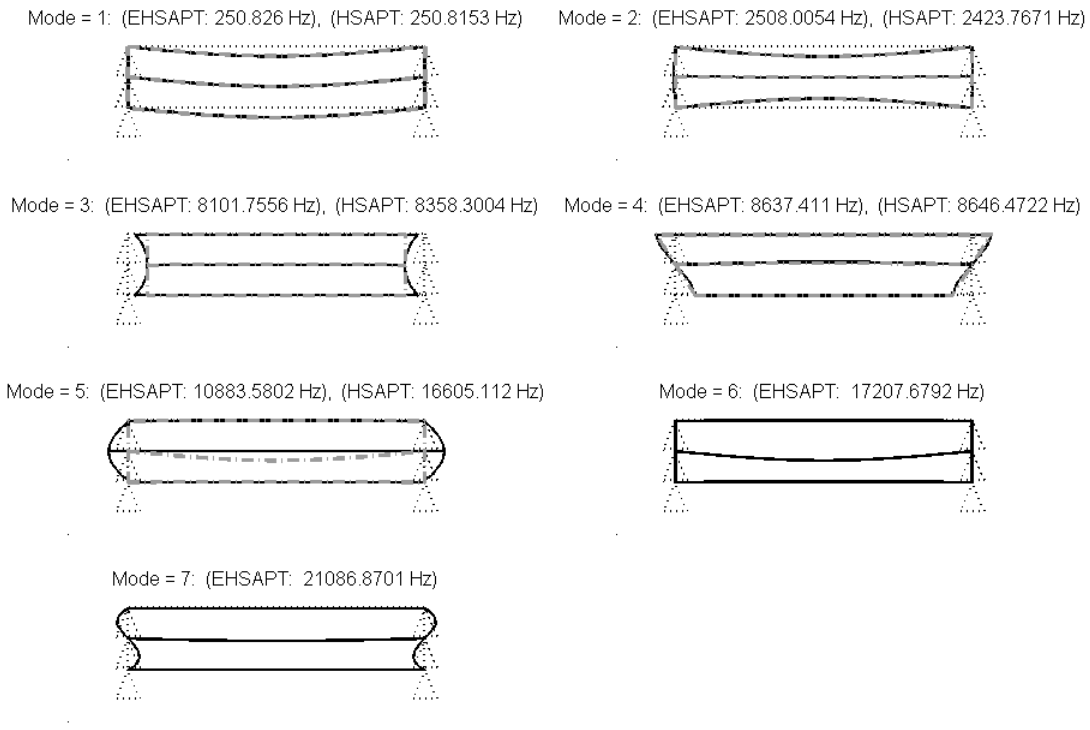

Figure 17: Predicted mode shapes and natural frequencies of EHSAPT (solid black line) and HSAPT (II) (gray dash dotted line) when wave number is n=1.

In this section we shall show the predicted mode shapes of EHSAPT. We used the same material and geometric parameters in the previous section and only consider when the wave number $n = 1$. Figure 17 shows the seven predicted mode shapes of the present theory EHSAPT (solid black lines) and the 5 predicted mode shapes of the earlier HSAPT (dashed dotted gray lines). The mid-surface of the core is also drawn because it is independent of the top and bottom face sheets. The un-deformed shape and the simple supports at the edges are shown with dotted black lines.

The first mode is antisymmetric, whereas the second mode is symmetric with respect to the mid-height. EHSAPT and HSAPT predict an axial compressive mode for mode 3, but differ in the mode shape. EHSAPT predicts that the shape is parabolic through the height, while HSAPT compresses practically uniformly through the height. For mode 4, EHSAPT and HSAPT predict that the top and bottom face sheets stretch axially in opposite directions. For mode 5, EHSAPT predicts that the mid-core axially stretches while the face sheets do not, and HSAPT predicts a very different mode shape where the mid-core is vibrating transversely independent of the faces. This last mode of HSAPT is actually the 6th mode of EHSAPT. Lastly, EHSAPT's 7th mode is one in which a cubic axial wave is vibrating though the height of the beam.

6.0.8 Comparison with elasticity

Comparison of the fundamental mode between the different theories and elasticity is made for several typical sandwich configurations. In the following study 12 symmetric sandwich configurations are considered which result from considering two different face-core material combinations, two different face to height ratios, and 3 different length to height ratios. Since the sandwich is symmetric then $E_1^t = E_1^b = E_1^f$ and $f_t = f_b = f$. The first material combination is graphite-epoxy faces with a glass phenolic honeycomb core which results in a modulus ratio of $E_1^c/E_1^f \sim 0.0002$. Since the core is very soft compared to the faces this material combination is designated as (SC) for soft-core. The second material combination is E-glass faces with a balsa wood core and has a modulus ratio of $E_1^c/E_1^f \sim 0.02$. Since the core is moderately stiff compared to the faces this material combination is designated as (MC) for moderate-core. All the sandwich configurations in this study have a total thickness $H_{tot} = (2f + 2c) = 25.4$ mm. The two different face thickness to total height ratios are $foh = f/Ht = 0.02$ or 0.2. These two ratios are considered as thin and thick face

sheet configurations, respectively. Details of the geometric parameters and material properties that were used can be found in Table 15 and Table 18, respectively. A configuration with a soft core lay-up and thick face geometry is designated "SCthick", and the other configurations follow this nomenclature. Three different length ratios of $a/H_{tot} = \{4, 10, 100\}$ are also considered in our comparison study.

Table 15: Geometry parameters for Thinner and Thicker faces.

	Thinner faces (foh=0.02)	Thicker Faces (foh=0.2)
Ht = b (mm)	25.4	25.4
ft=fb=f (mm)	0.508	5.08
2*c (mm)	24.384	24.384
a = 30*Ht (mm)	762	762

Table 16: Material properties. Moduli data are in GPa. Densities are in kg/m^3.

	Graphite Epoxy FACE	E-Glass Polyester FACE	Balsa Wood CORE	Glass-Phenolic Honeycomb CORE
E_1	181.0	40.0	0.671	0.032
E_2	10.3	10.0	0.158	0.032
E_3	10.3	10.0	7.72	0.300
G_{23}	5.96	3.5	0.312	0.048
G_{31}	7.17	4.5	0.312	0.048
G_{12}	7.17	4.5	0.200	0.013
ν_{32}	0.40	0.40	0.49	0.25
ν_{31}	0.016	0.26	0.23	0.25
ν_{12}	0.277	0.065	0.66	0.25
ρ	1632	2000	250	64

Table 17 shows the comparison of fundamental frequency for the 12 different configurations. The natural frequency given by elasticity is given in Hz, and the percent error with respect to elasticity are given for the different theories.

For SCthin, EHSAPT and HSAPT are less than 0.1% in error from elasticity for even a short sandwich with $a/H_{tot} = 4$. For the longer SCthin beams, EHSAPT is slightly more accurate than HSAPT. The SCthick configuration is most demanding when it is short ($a/H_{tot} = 4$). Here the high-order theories are within 2.4% error, and

Table 17: Comparison of fundamental mode for several configurations. elasticity in (Hz) and theories given as % Error with respect to elasticity

Config.	a/h_{tot}	4	10	100
SCthin	elasticity	2965.98	1071.62	22.57
	EHSAPT	$< 0.1\%$	$< 0.1\%$	-0.2%
	HSAPT(II)	$< 0.1\%$	-0.1%	-0.3%
	FOSDT(k=5/6)	-10.3%	-8.6%	-0.6%
	FOSDT(k=1)	-2.0%	-1.7%	-0.3%
SCthick	elasticity	2579.27	637.06	23.23
	EHSAPT	2.4%	0.3%	-0.2%
	HSAPT(II)	2.4%	0.3%	-0.2%
	FOSDT(k=5/6)	-64.5%	-43.0%	-9.7%
	FOSDT(k=1)	-61.1%	-37.7%	-7.1%
MCthin	elasticity	3276.42	676.03	7.27
	EHSAPT	-0.4%	-0.6%	-1.0%
	HSAPT(II)	-3.7%	-5.8%	-6.9%
	FOSDT(k=5/6)	-5.4%	-2.0%	-1.1%
	FOSDT(k=1)	-1.2%	-0.8%	-1.0%
MCthick	elasticity	2770.19	776.42	10.31
	EHSAPT	0.9%	0.2%	-0.7%
	HSAPT(II)	0.9%	0.1%	-0.9%
	FOSDT(k=5/6)	-31.3%	-18.9%	-1.1%
	FOSDT(k=1)	-25.4%	-14.4%	-1.0%

the first order shear theories have more than -60% error. For this demanding case the length of the beam to the total thickness of the facesheets $a/(2f)$ approaches 10. Shear of the faces would become important as the beam becomes shorter.

For MCthin and different lengths, EHSAPT is the most accurate theory with error between -1% to -0.4%. FOSDT (k=1) is slightly less accurate than EHSAPT. FOSDT (k=5/6) and HSAPT are up to -5% and -7% in error, respectively. For MCthick and different lengths, EHSAPT and HSAPT have error less than 1% error. FOSDT (k=5/6) and (k=1) have up to -30% and -25% error, respectively, when the length is short, but improve in accuracy up to about -1% error when the length is the longest.

In general FOSDT with k=5/6 is more inaccurate than when k=1 for all the 12

configurations studied. For one of the more demanding configurations of SCthick and $a/H_{tot} = 100$, FOSDT was up to -10% in error, while the high-order theories were -0.2% in error. Table 17 shows that EHSAPT can give accurate fundamental frequencies for a wide range of material and geometry configurations.

6.0.9 Conclusions

The dynamic formulation of EHSAPT is derived via Hamilton's principle for a general asymmetric sandwich configuration, and nonlinear axial strains of the face sheets are taken into account. The solution procedure for using linear EHSAPT formulation to determine the free vibrations of a sandwich beam/ wide panel that is simply supported throughout its edges is explained. Comparison is made with experimental results reported in literature for a nearly simply supported sandwich specimen. Results show that EHSAPT give accurate results up to 2% error for higher frequencies. The seven predicted mode shapes of EHSAPT were shown for wave number $n = 1$, and revealed similar mode shapes of HSAPT plus two additional modes. Comparison is also made with elasticity solution for the fundamental mode of 12 different sandwich configurations that results from considering two face-core material combinations, thin or thick faces, and three different length ratios. EHSAPT has been shown to have good accuracy for the wide range of sandwich configurations, while FOSDT was shown to have poor accuracy when the beam was not very long. EHSAPT was shown to have better accuracy than HSAPT for the demanding case of sandwich beam/ wide panel with a moderately stiff core and thin faces.

CHAPTER VII

DYNAMIC LOADING PROBLEM

In this section we consider a simply supported sandwich beam/ wide panel that is initially at rest, and then subjected to a load on the top face sheet of the form:

$$\widetilde{q}^t(x,t) = T(t)\sum_{n=1}^{\infty} Q_n \ \sin(\alpha_n x)\,; \quad \alpha_n = \frac{n\pi}{a}. \tag{58}$$

The loading profile is symmetric about the mid-span yet takes a general form via a Fourier series. The next section explains the solution approach using the EHSAPT formulation, but with the nonlinear terms excluded. Afterwards, a particular case study of a blast load with a half-sine profile (only $n = 1$) is investigated. The case study is used to assess the accuracy of EHSAPT, and HSAPT with the elastodynamic solution used as the benchmark.

7.0.10 Solution Approach

In this approach, the nonlinear strains of the face sheets are neglected so comparison can be made with the linear elastodynamic benchmark. Therefore, the nonlinear terms in the equations of motion and the boundary conditions are ignored. The boundary conditions are simply supported at both ends and throughout the entire beam/ wide panel thickness. Therefore the solution must satisfy at $x = 0$ and a, the three kinematic boundary conditions:

$$w_0^t = w_0^b = w_0^c = 0 \tag{59}$$

and the right hand sides of the six natural boundary conditions in (20), (22), (23), (24), (26a), and (28) are equal to zero.

The following displacement shape functions satisfy these boundary conditions:

$$u_0^t = \sum_{n=1}^{\infty} U_n^t(t) \cos\frac{\pi x}{a} \; ; \qquad u_0^c = \sum_{n=1}^{\infty} U_n^c(t) \cos\frac{\pi x}{a} \; ;$$

$$\phi_0^c = \sum_{n=1}^{\infty} \Phi_n^c(t) \cos\frac{\pi x}{a} \; ; \qquad u_0^b = \sum_{n=1}^{\infty} U_n^b(t) \cos\frac{\pi x}{a} \; ,$$

$$w^t = \sum_{n=1}^{\infty} W_n^t(t) \sin\frac{\pi x}{a} \; ; \qquad w_0^c = \sum_{n=1}^{\infty} W_n^c(t) \sin\frac{\pi x}{a} \; ; \qquad w_=^b \sum_{n=1}^{\infty} W_n^b(t) \sin\frac{\pi x}{a} \; . \tag{60}$$

Substituting (7.0.10) into (11) to (17) (neglecting the nonlinear terms), turns the governing partial differential equations into linear ordinary differential equations in time, and can be cast in the following matrix form:

$$[M_n]\{\ddot{U}_n(t)\} + [K_n]\{U_n(t)\} = \{F_n(t)\} \tag{61}$$

where $[M_n]$ and $[K_n]$ are the mass and the stiffness matrices, respectively, of the nth Fourier term, and are each 7x7 and symmetric. The elements of the mass and stiffness matrix are given in Appendix F. The mass and stiffness matrices were arranged such that the rows of the system of equations in (61) correspond to Eqns. (16a), (13), (14), (11), (17a), (15), (12a), respectively, and the vector of the unknown generalized coordinates are

$$\{U_n(t)\} = \{U_n^b(t), U_n^c(t), \Phi_n^c(t), U_n^t(t), W_n^b(t), W_n^c(t), W_n^t(t)\}^T \tag{62}$$

and the load vector $\{F_n(t)\} = T(t)\{0, 0, 0, 0, 0, 0, Q_n\}^T$. Eqn. (61) can be solved by rearranging the equations into state space form (1st order differential equations in time with the generalized coordinates and their first time derivatives as the states) and using standard numerical integration methods to give the response in time.

In the next section we will use a particular blast loading case study to assess the accuracy of EHSAPT as well as the earlier HSAPT that does not take into account the in-plane stresses in the core. The solution procedure using displacements based formulation of HSAPT[34] is outlined in Appendix F.2.

7.0.11 Numerical Case Study of Blast

In this section the dynamic response of a simply supported sandwich panel, initially at rest, then subjected to a temporal blast load that exponentially decays in time and has a half-sine spatial profile along the beam/ wide panel is studied. Only the first term in the Fourier series is needed. The applied load is:

$$\widetilde{q}^t(x,t) = e^{-(t*1.25)ms} 510 \; sin\,(\alpha_1 x) \; \frac{kN}{m}; \quad \alpha_1 = \frac{\pi}{a} \tag{63}$$

which decays to less than 0.1% of its original magnitude after 5.5 ms. The above blast load parameters, as well as the material and geometry data were taken from the experimental investigations of [16]. The faces are E-glass vinyl-ester composite: Young's modulus $E_1^c = 13,600 \; MPa$, density $\rho^f = 1800 \; kg/m^3$. The isotropic core is Corecell A300 styrene acrylonitrile (SAN) foam: Young's modulus $E^c = 32 \; MPa$, $\rho^c = 58.5 \; kg/m^3$, Poisson's ratio $\nu^c = 0.3$, and shear modulus $G^c = E^c/(2(1+\nu^c))$. The geometry of the sandwich configuration is: face thickness $f_t = f_b = 5 \; mm$, core thickness $2c = 38 \; mm$, width $b = 102 \; mm$, and span of beam/ wide panel $a = 152.4 \; mm$.

The equations of motion of the form in Eqn. (61) for EHSAPT and HSAPT were numerically integrated using ode45 function in the the commercial software Matlab. The built-in function is based on an explict Runge-Kutta(4,5) formula which adapts the time step until error tolerances are met. Default error tolerances were used: relative error tolerance of 1e-3 and absolute error tolerance of 1e-6.

The transverse displacements w^t, w_0^c, and w^b at the mid-span location $x = a/2$ versus time are shown in Figure 18. In this figure we show the results from elasticity, EHSAPT, and HSAPT. The two high-order sandwich beam/ wide panel theories are practically on top of each other and display the same trend in behavior of the top, core, and bottom displacements as elasticity, i.e. that the top face travels down first, followed by the core, then the bottom face sheet. Differences between the high-order

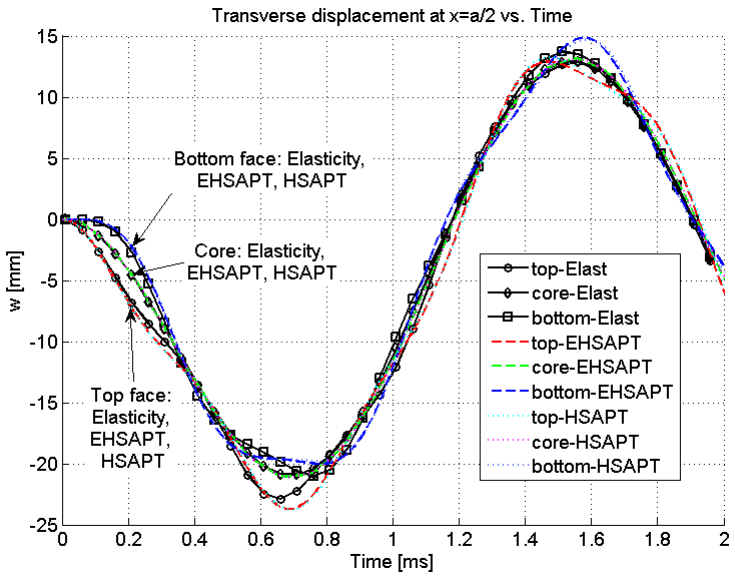

Figure 18: Transverse displacement of the top face, middle of the core, and bottom face at the mid-span location for elasticity, EHSAPT,and HSAPT between t=0 to 2 ms (E-glass Vinyl-Ester faces/A300 Core)

theories and elasticity can be distinguished by focusing on the time between 0.4 and 1 ms when the different phases first reach their maximum values as shown in Figure 19. EHSAPT and HSAPT match the mid-height transverse displacement of elasticity. The high-order theories over estimate the maximum displacement of the top face by 4%. The bottom face transverse displacements from EHSAPT and HSAPT do not exactly follow elasticity, but give values within less than 6% error over the time range in Figure 19.

Figure 20 shows the axial displacements u_0^t, u_0^c, and u_0^b at the edge $x = 0$ versus time. EHSAPT and HSAPT capture the high cyclic behavior of u_0^c that elasticity displays, with EHSAPT being closer in value to elasticity than HSAPT. The first minimum in u_0^c of EHSAPT is 10% under elasticity, while the first minimum in u_0^c of HSAPT is 32% under elasticity. Both high-order theories and elasticity predict very similar behavior of u_0^t and u_0^b with time.

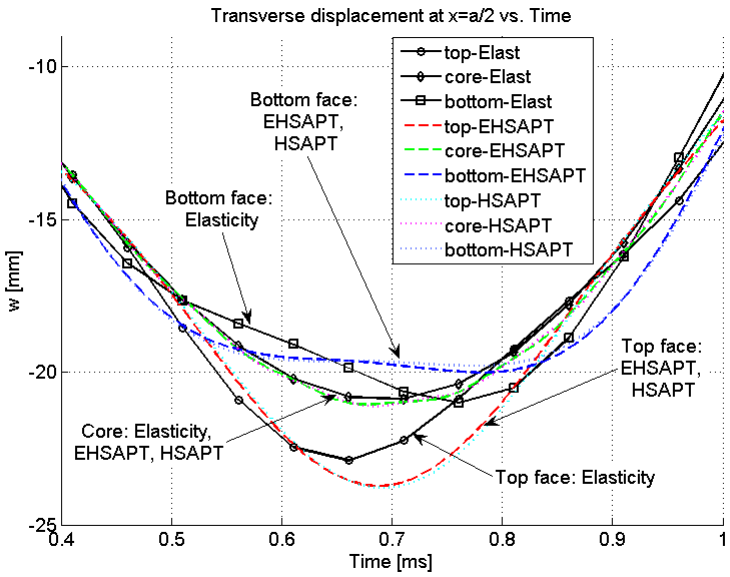

Figure 19: Transverse displacement of the top face, middle of the core, and bottom face at the mid-span location for elasticity, EHSAPT,and HSAPT between t=0.4 to 1 ms (E-glass Vinyl-Ester faces/A300 Core)

The transverse stress at the top and bottom face/core interfaces at the mid-span are shown in Figure 21. EHSAPT and HSAPT predict similar behavior in transverse stresses versus time. The high-order theories show that a tensile stress wave occurs in the bottom face/core interface just after the blast (within the first 50 microseconds). Afterwards the compressive stress wave reaches the bottom face. This is similar to the cavitation zone in water that occurs behind a shock wave front. The numerical solution of elasticity could not recover this behavior so soon after the initial blast due to numerical instabilities at very small time steps. This cavitation phenomenon is further detailed in Figure 22 by showing that the core moves upwards before moving downwards microseconds just after the initial blast. The maximum compressive transverse stress at the top face/core interface predicted by the high-order theories (at around 0.23 ms) overpredicts the elasticity value by 5%. The maximum compressive transverse stress at the bottom face/core interface predicted by the high-order theories (at around 0.2 ms) overpredicts the elasticity

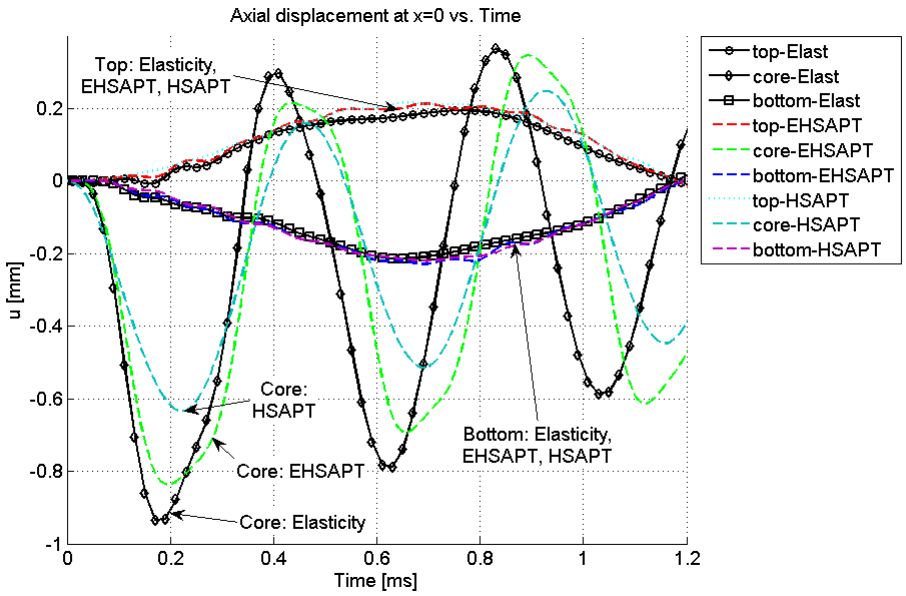

Figure 20: Axial displacement of the top face, middle of the core, and bottom face at the edge x=0 for elasticity, EHSAPT,and HSAPT between t=0 to 1.2 ms (E-glass Vinyl-Ester faces/A300 Core)

value by 6%. The high-order theories correctly predict that the bottom face/core interface undergoes a tensile stress at the bottom/face core interface over time. The first maximum tensile transverse stress at the bottom face/core interface (after the cavitation phenomenon) predicted by the high-order theories (at around 0.44 ms) overpredicts the elasticity value by 14%.

The shear stress at the top and bottom face/core interfaces at $x = 0$ is shown in Figure 23. EHSAPT is the only theory that can show the differences in the shear stresses at the top and bottom face/core interfaces like elasticity, while HSAPT predicts that the shear stress is constant throughout the thickness and is the average value of EHSAPT and elasticity. EHSAPT gives a minimum shear stress (most negative shear stress) at the top and bottom face/core interface under the minimum elasticity values by -0.5%. HSAPT is within 3% and -6% of elasticity's predictions of minimum $\tau^c(z = c)$ and $\tau^c(z = -c)$, respectively.

It was shown in the author's previous work on static stability using high-order

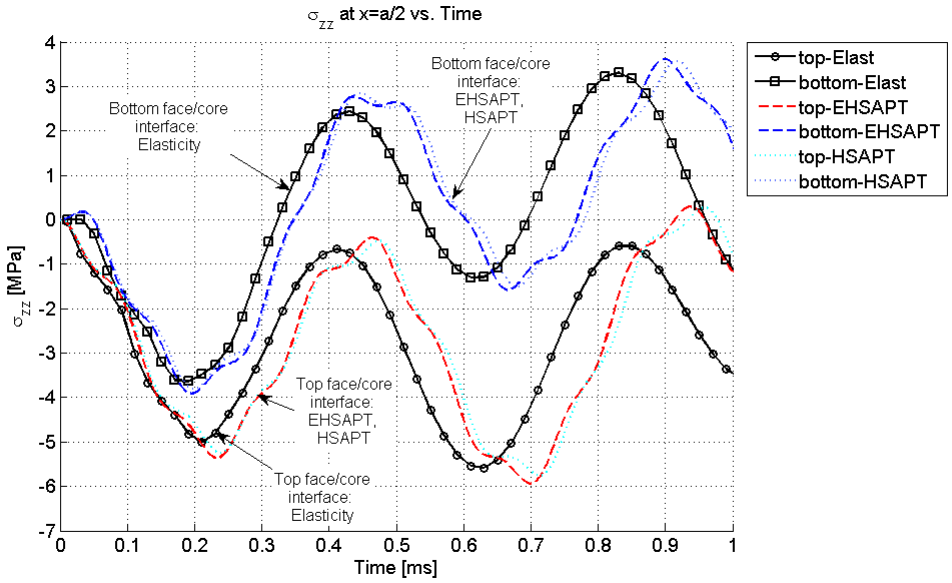

Figure 21: Transverse stress of the top face, middle of the core, and bottom face at the mid-span location for elasticity, EHSAPT,and HSAPT between t=0 to 1 ms (E-glass Vinyl-Ester faces/A300 Core)

sandwich beam/ wide panel theories that HSAPT can be inaccurate for very thin face configurations of face thickness to total height $f/H_{tot} = 0.02$. Plotted in Figures 24 and 25 are the transverse shear stresses at the top and bottom face/core interfaces for a soft core and moderate core configuration with thin face sheet ratios $f/H_{tot} = 0.02$. The soft core configuration is graphite epoxy faces with a glass phenolic honeycomb core ($E_1^f/E_1^c < 0.001$) and the moderate core configuration is E-glass faces with a Balsa wood core ($E_1^f/E_1^c \sim 0.02$). See Table 18 for the material data for the soft core and moderate core configurations. Both configurations have the same $H_{tot} = 48\ mm$ as before and all other geometric parameters kept the same except f/H_{tot} is now 0.02. It can be seen from Figure 24 that for soft cores and thin faces the shear stresses at the top and bottom face/core interfaces can be very different, as predicted by EHSAPT. Though HSAPT predicts an average value of the shear stress at the top and bottom face core interface for the E-glass vinyl face/A300 foam core and graphite epoxy face/glass phenolic honeycomb core, HSAPT overpredicts the negative shear

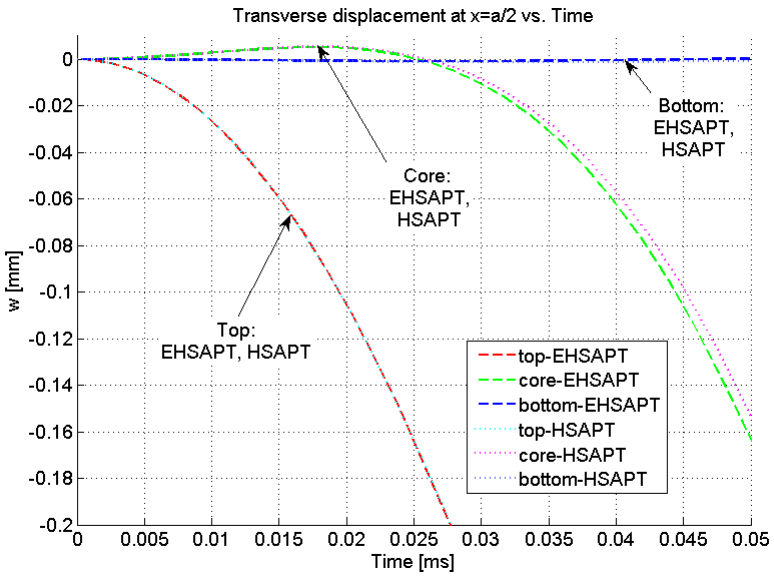

Figure 22: Transverse displacement of the top face, middle of the core, and bottom face at the mid-span location for EHSAPT and HSAPT between t=0 to 50 microseconds (E-glass Vinyl-Ester faces/A300 Core)

stress of the top and bottom face/core interfaces for the E-glass face/Balsa wood core configuration by as must as 10%.

7.0.12 Discussion

In the previous numerical study it was shown that EHSAPT and HSAPT can give reasonably close results to elasticity in the prediction of transverse displacements of the top face, middle of the core, and the bottom face in time. Also, the high-order theories give accurate results for the axial displacements of the top and bottom face sheets. EHSAPT and HSAPT show different predictions for the mid-core axial displacement with time, with EHSAPT being closer in value to elasticity. The high-order theories were able to predict the cavitation phenomenon in the transverse stresses and transverse displacements while the numerical method of the elasticity solution could not capture this behavior so close to the initial blast. There also was a phase shift between elasticity and the high-order theories for the prediction of the transverse stresses. EHSAPT showed that it can capture the nonequal shear stresses at the top

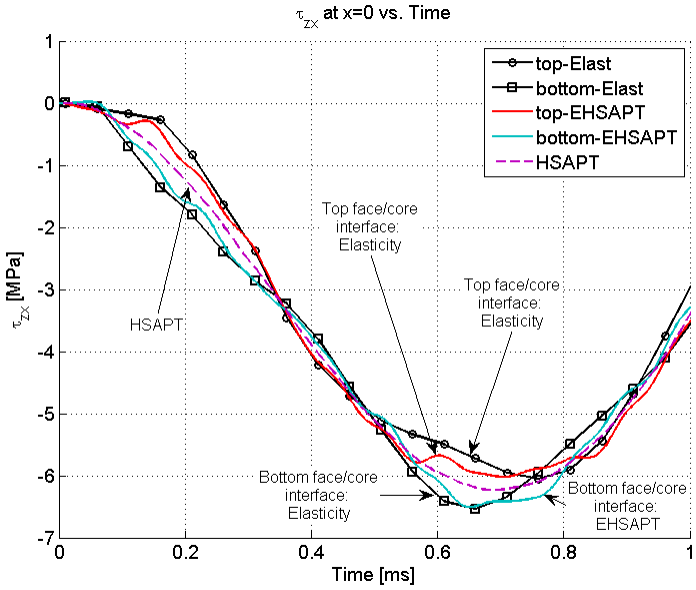

Figure 23: Shear stress at the top face and bottom face/core interfaces at the x=0 for elasticity, EHSAPT,and HSAPT between t=0 to 1 ms (E-glass Vinyl-Ester faces/A300 Core)

and bottom face/core interface with time, while HSAPT predicts a constant value through the height of the core. It was also shown that for sandwich beams/ wide panels with very thin faces and very soft cores ($E_1^f/E_1^c < 0.001$) that the difference between the shear stress at the top and bottom face/core interface can be much different. For sandwich beams/ wide panels with very thin faces and moderate cores ($E_1^f/E_1^c \sim 0.02$) HSAPT does not give the average value of the top and bottom face/core interface shear stress.

7.0.13 Conclusions

The dynamic formulation of EHSAPT is presented for a general sandwich configuration. The solution procedure for using EHSAPT to determine the linear dynamic response of a sandwich beams/ wide panels that is simply supported throughout its edges and loaded just on the top face sheet is explained. A numerical case study involving the blast load with a temporal exponential decay and a spatial half-sine profile across the top of the beam/ wide panel is used to compare EHSAPT, and HSAPT

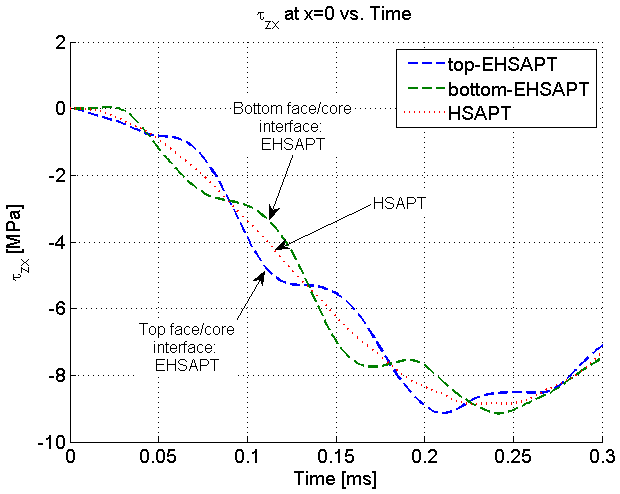

Figure 24: Shear stress at the top face and bottom face/core interfaces at the x=0 for EHSAPT,and HSAPT between t=0 to 0.3 ms (SCthin configuration)

to an elasticity benchmark. HSAPT predicts well the transverse displacements of the top sheet, middle of the core, and the bottom face sheet, as well as the in-plane displacements of the top and bottom face sheets. EHSAPT does this as well, but is also able to capture the non uniform shear stresses by showing that the shear stress at the top and bottom face/core interfaces can be different, while HSAPT cannot.

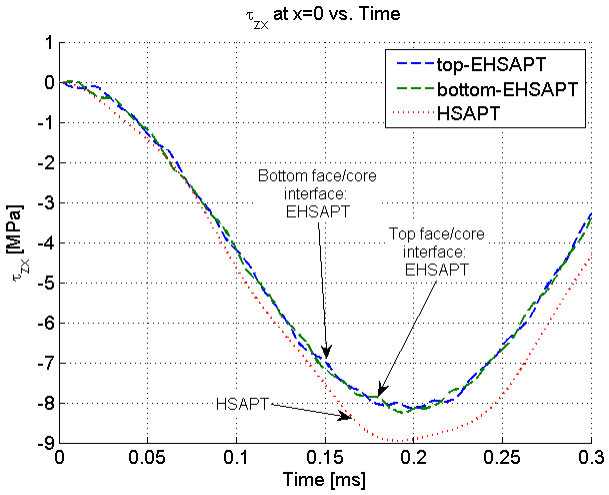

Figure 25: Shear stress at the top face and bottom face/core interfaces at the x=0 for EHSAPT,and HSAPT between t=0 to 0.3 ms (MCthin configuration)

Table 18: Material properties. Moduli data are in GPa. Densities are in kg/m^3.

	Graphite Epoxy FACE	E-Glass Polyester FACE	Balsa Wood CORE	Glass-Phenolic Honeycomb CORE
E_1	181.0	40.0	0.671	0.032
E_2	10.3	10.0	0.158	0.032
E_3	10.3	10.0	7.72	0.300
G_{23}	5.96	3.5	0.312	0.048
G_{31}	7.17	4.5	0.312	0.048
G_{12}	7.17	4.5	0.200	0.013
ν_{32}	0.40	0.40	0.49	0.25
ν_{31}	0.016	0.26	0.23	0.25
ν_{12}	0.277	0.065	0.66	0.25
ρ	1632	2000	250	64

CHAPTER VIII

IMPACT LOADING PROBLEM

Impact upon sandwich beams/ wide panels can occur during their manufacturing process from dropped tools, or in service depending on the application; possible bird strike upon a wind turbine, or debris hitting an armored tank during a nearby explosion. An impact experiment was conducted upon a sandwich beam/ wide panel to experimentally validate the dynamic formulation of EHSAPT. The three-point bending impact experiment was conducted upon a symmetric sandwich beam/ wide panel that consisted of Glass CSM faces and Airex T90.320 PET foam core. The mechanical properties of the top and bottom faces were: Young's modulus of the faces $E_1^f = 13.9\ GPa$ and $\rho^f = 1801.082\ kg/m^3$. The mechanical properties of the isotropic core were: $E^c = 270\ MPa$ and Poisson's ratio $\nu = 0.3$, and density $\rho^c = 320\ kg/m^3$. The sandwich beam/ wide panel rested on two supports on the bottom face sheets as depicted in Figure 26.

The beam had a total length of 451 mm, a width $b = 60.85\ mm$, face thickness $f_b = f_t = f = 2.24\ mm$, and core thickness $2c = 18.5\ mm$. The beam was placed on supports that were 400 mm apart, and the beam overhung 25.5 mm on both sides of the supports (i.e. the supports were symmetric about the beam's mid-span). A composite tab of length 32 mm was glued to the top face sheet to distribute the impact load, and prevent local damage from occurring at low impact energies. A number of tests were conducted to ensure that the tab did not significantly effect the stiffness of the beam.

Some ratios of interest are the face thickness to total height of the sandwich beam/ wide panel $f/H_{tot} = f/(2f + 2c) = 0.0975$, so the beam had thin faces, and Young's

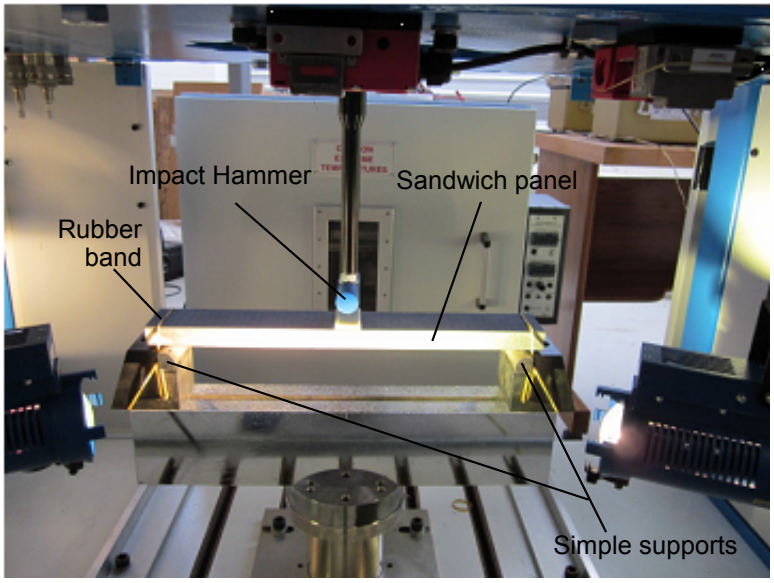

Figure 26: Experimental setup of Three point impact experiment

modulus ratio $E^c/E_1^f = 0.02$, therefore the core did not have a negligible in-plane rigidity compared to the faces.

The experiment was conducted using a Drop Weight Impact Tester from Imatek Impact Test Systems (owned by the Centre for Advanced Composites Materials, Auckland University, Auckland, NZ). The system includes the capability to record transient force, displacement, velocity, energy and strains during the impact event. The impact hammer spanned the entire width of the beam, so the loading was symmetric about the $x-z$ plane of the beam. An impact mass of 10.494 kg was dropped on the center of the beam with 1.005 m/s impact velocity, for a set impact energy of 6 Joules. The mass was allowed to hit the beam under its own weight and bounce upwards. The test system automatically prevented it from striking the beam a second time.

8.1 Results

A load cell recorded the force time history of the impact, shown in Figure 27. During the 20 ms shown in the plot, the impact hammer was in contact with the specimen.

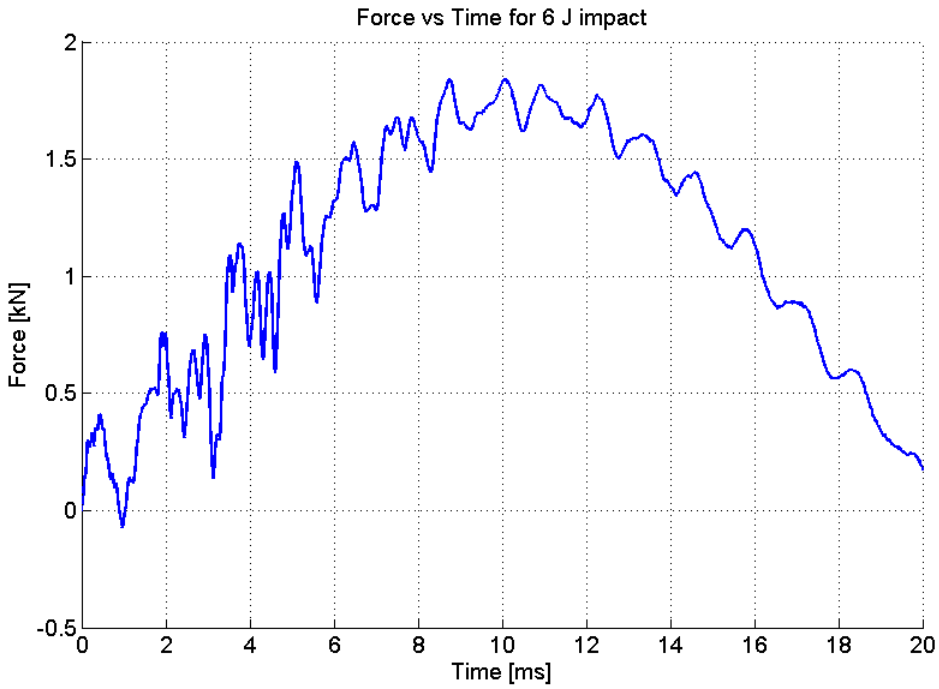

Figure 27: Force versus time

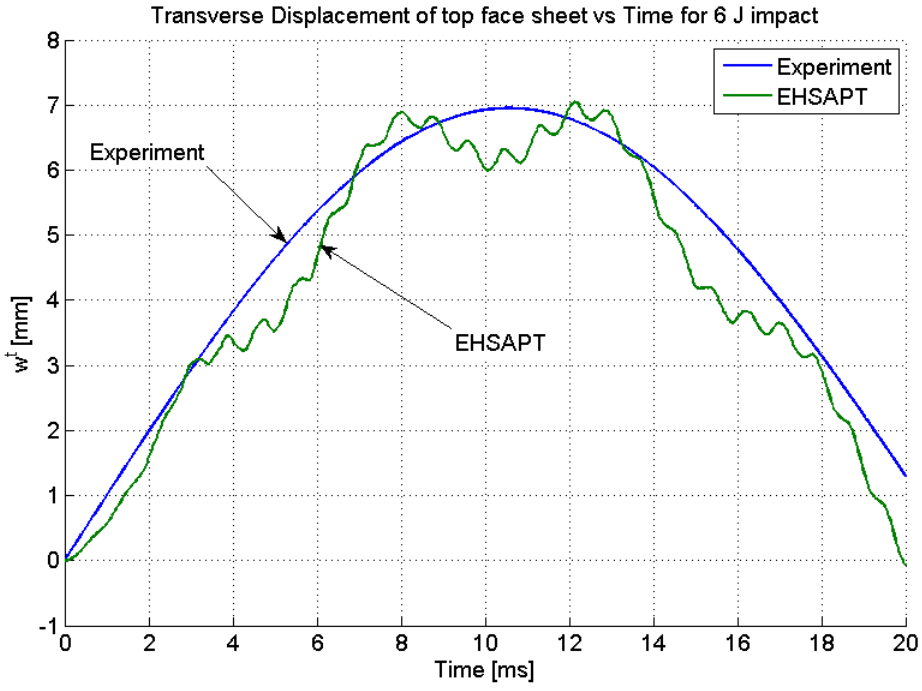

Figure 28: Transverse displacement of impact hammer versus time, shown as positive, though transverse displacement is downwards.

The load profile shows oscillations in time due to the interaction of the mass with the elastic structure. At around 10 ms, the load is maximum and afterwards the load decreases. From looking at the transverse displacement of the hammer with time, shown in Figure 28, the maximum load occurs around the same time as the maximum displacement. Also shown in Figure 28 is the prediction from EHSAPT, which follow the experimental value quite well. However oscillations are observed from the theory, whereas the experimental values look quite smooth with time. It is believed that the resolution of the Imatek system might be too coarse, or perhaps it smooths the displacement data readout. It should be noted that the maximum measured displacement is around 7 mm which has allowed us to use the linear formulation of EHSAPT, since displacements are small.

Three strain gauges were placed on the top face sheet and two strain gauges were placed on the bottom face sheet of the specimen at locations detailed in Figure 29. Comparison between measured and predicted (from EHSAPT) strain for these five locations are shown in Figures 30 to 34. It can be observed in all comparisons that EHSAPT follows the measured data quite well for the first 2 ms. Beyond 2 ms high frequency oscillation in EHSAPT are more apparent (have higher amplitudes) than the experimental data. This is believed to be due to structural damping being neglected in the model of EHSAPT. The fundamental period of the sandwich panel,

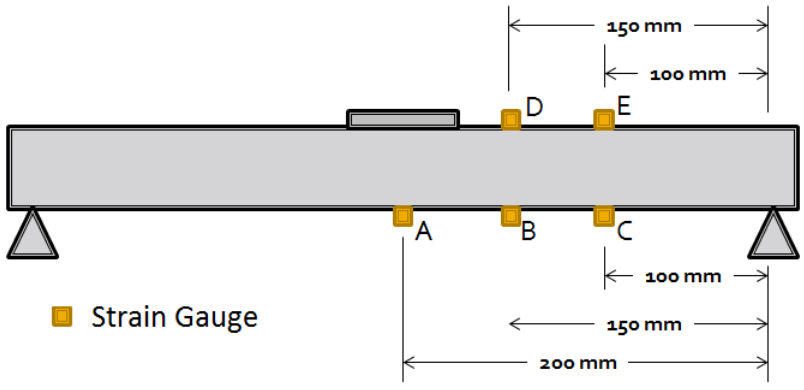

Figure 29: Locations of strain gauges A, B, C, D, and E

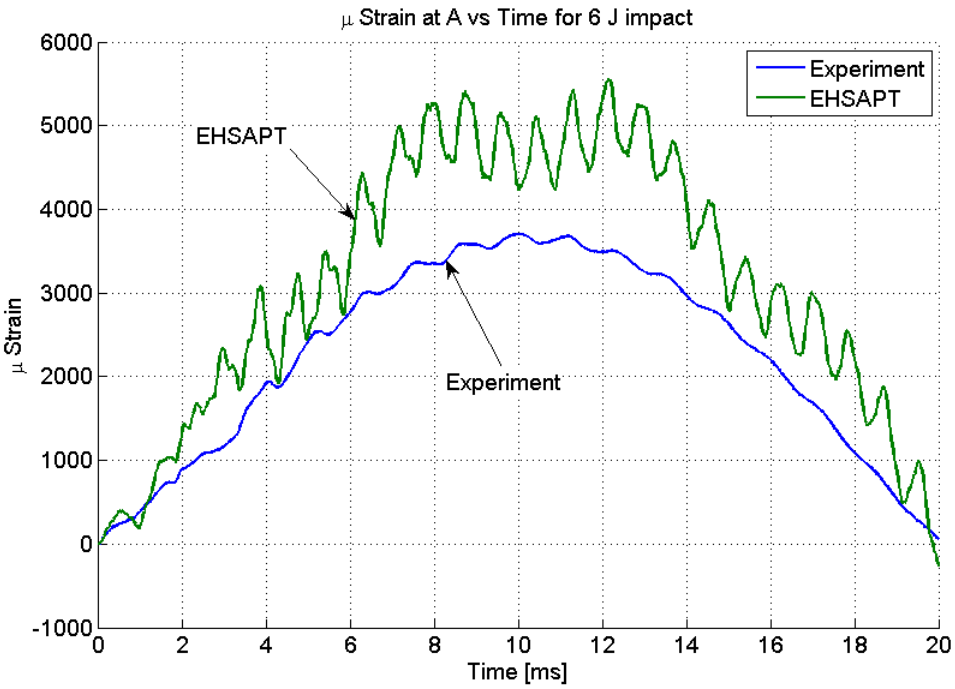

Figure 30: Microstrain at location A

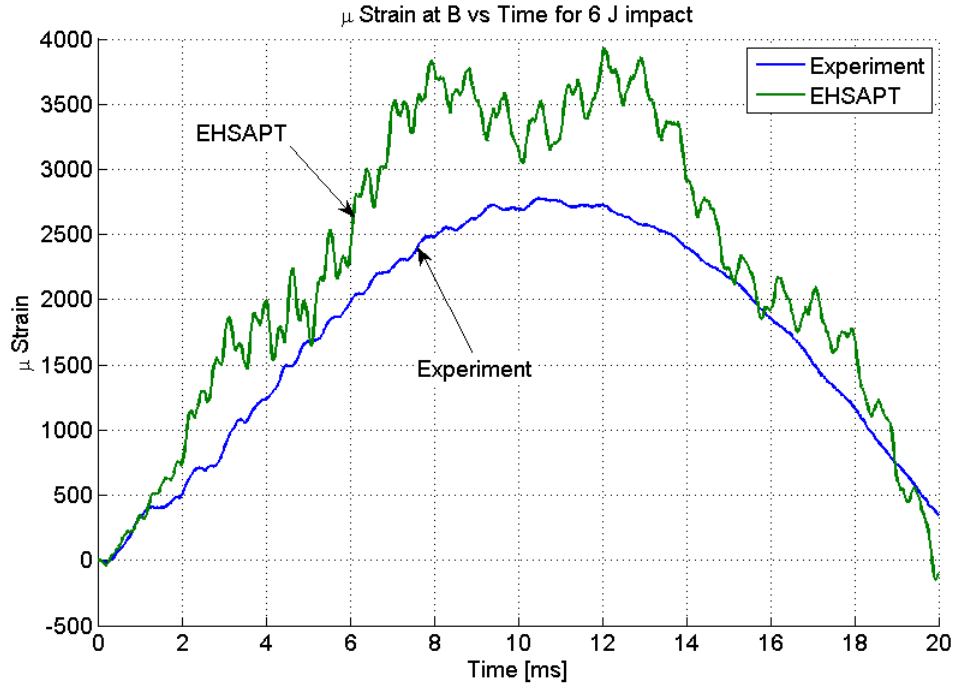

Figure 31: Microstrain at location B

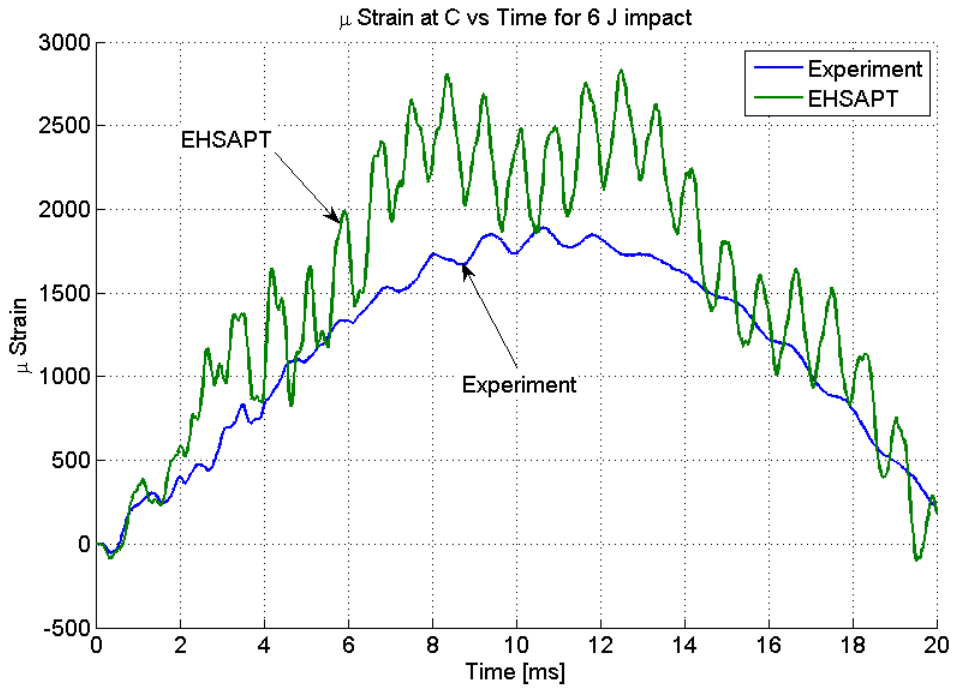

Figure 32: Microstrain at location C

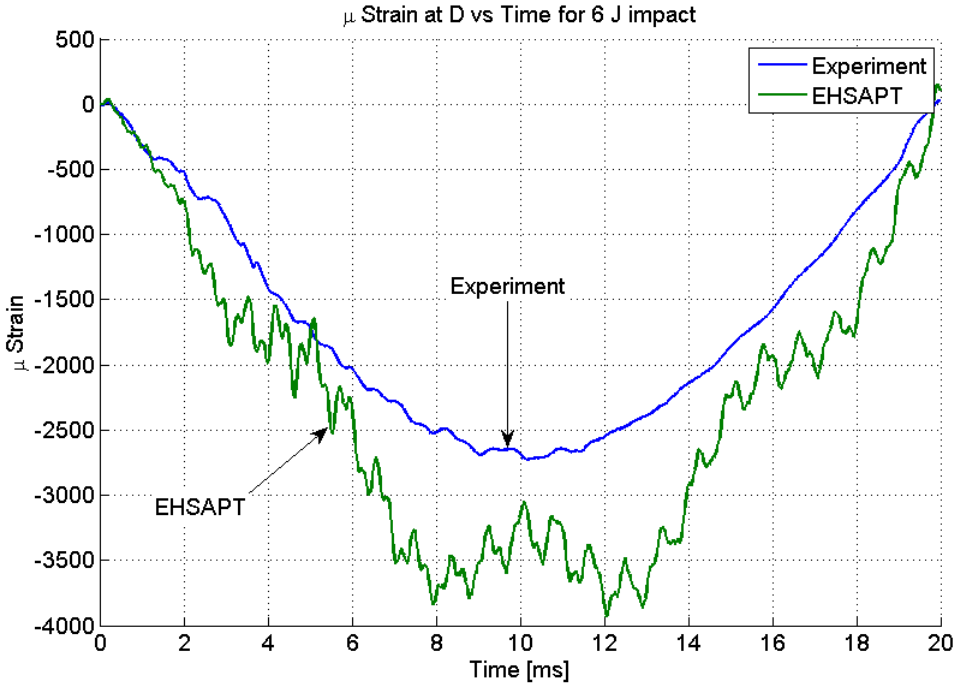

Figure 33: Microstrain at location D

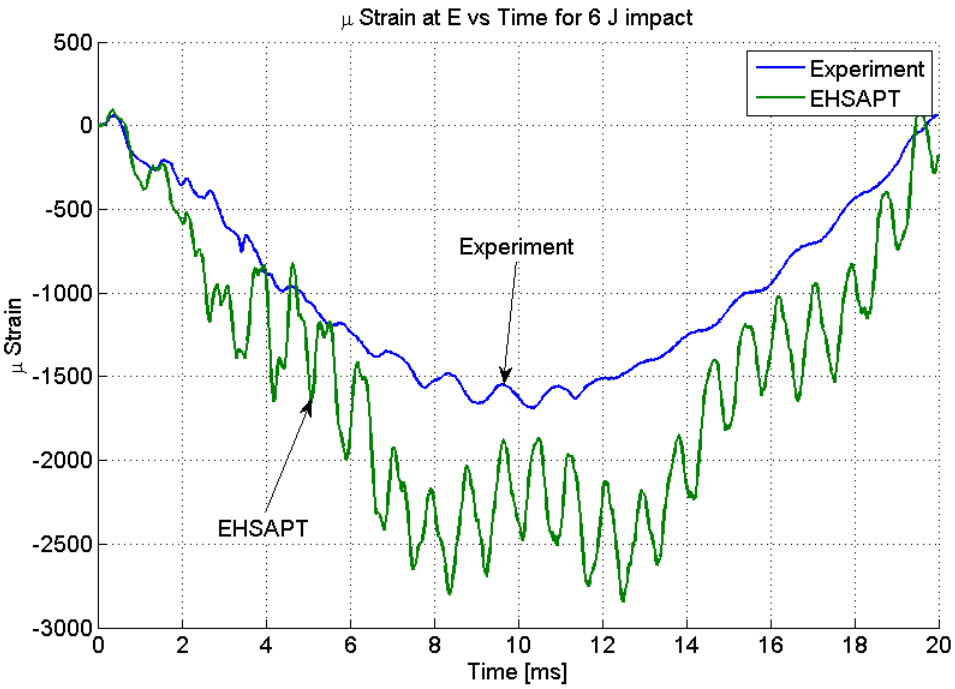

Figure 34: Microstrain at location E

predicted from EHSAPT if it were assumed to be simply supported throughout at the support locations, would be $T_1 = 2.3\ ms$. Therefore, the impact experiment spanned about nine fundamental periods, and structural damping must have played a role for the fundamental as well as higher frequencies in the beam. The predicted peak strain values overestimate the measure peak strain values, which would can also be explained by the lack of structural damping in the model.

One validation of the theory occurs in the first couple of ms just after impact. Figure 35, shows that EHSAPT correctly predicts that the measured strain at location C on the bottom "tensile" side of the beam the face sheet undergoes a compressive strain before becoming tensile. Also a similar observation is made at location E on the top "compressive" side of the beam, that the top face sheet undergoes a tensile strain before becoming compressive. After about 2 ms EHSAPT seems to show similar oscillations as experiment but with bigger amplitudes due to no structural damping.

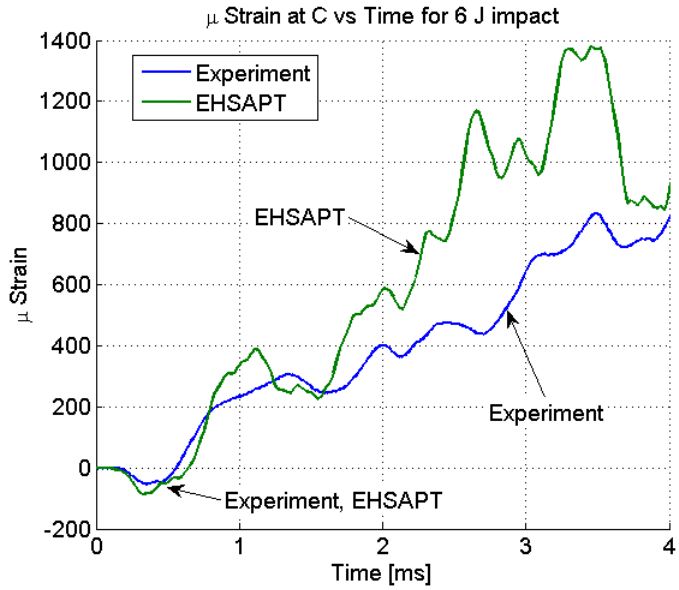

Figure 35: Microstrain at location C just after impact

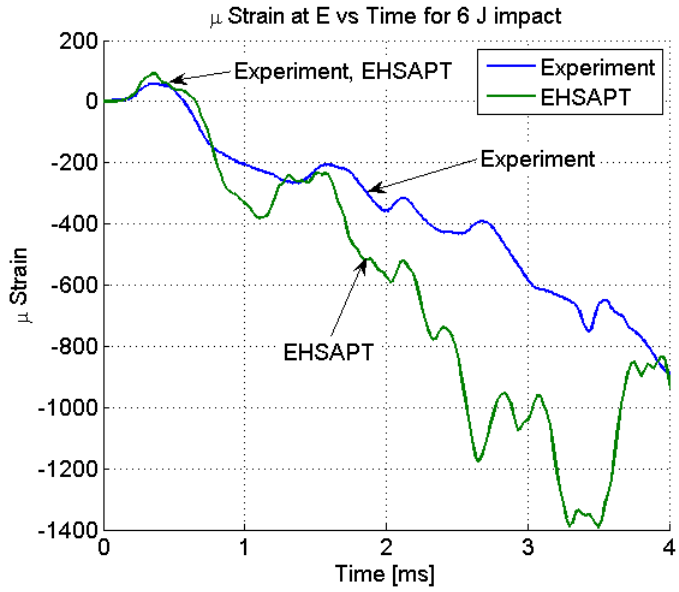

Figure 36: Microstrain at location E just after impact

8.2 Conclusions

The impact experiment in some way validated EHSAPT in the first fundamental period of the impact. EHSAPT was able to capture very detailed features such as compressive strain on the "tensile" side of the beam, and tensile strain on the

"compressive" side of the beam. After about 2 ms, it is believed that neglecting structural damping in the EHSAPT model caused high oscillation in the predicted strains to never dissipate. Also since the beam was still being loaded during that time, the total of energy of the beam continued to increase and in a sense kept "feeding" these higher modes of vibration of the beam. Therefore, it is recommended that a structural damping model be included with comparison with real dynamic loading experiments involving sandwich panels.

CHAPTER IX

CONCLUSIONS

The Extended High-order SAndwich Panel Theory (EHSAPT) was presented for a sandwich beam/wide panel that allows for the transverse shear distribution in the core to acquire the proper distribution as the core stiffness increases as a result of non-negligible axial stresses in the core. Thus, this theory is valid for weak or stiff cores. The theory assumes a transverse displacement in the core that varies as a second-order equation in z, and an axial displacement that is of third order in z, following the displacement distributions of the High-order SAndwich Panel Theory (HSAPT) model, see Frostig et al. [15]. The novelty of EHSAPT is that it allows for three generalized displacement variables in the core (the axial and transverse displacements at the centroid of the core, and the rotation at the centroid of the core) instead of just one (mid-point transverse displacement) commonly adopted in other available theories [19, 27]. The theory is formulated for a sandwich panel with a general layout. The major assumptions of the theory are as follows:

(1) The face sheets satisfy the Euler-Bernoulli assumptions, and their thicknesses are small compared with the overall thickness of the sandwich section. The face sheets can be made of different materials and can have different thicknesses, and they can undergo large displacements with moderate rotations.

(2) The core is compressible in the transverse and axial directions (transverse displacement is 2nd order in z and axial displacement is 3rd order in z), following the displacement distributions of the HSAPT model, see Frostig et al. [15]. The core has in-plane, transverse and shear rigidities, and it undergoes large displacements while maintating the kinematic relations of small deformations

due to its low in-plane rigidity as compared with that of the face sheets.

(3) The face sheets and core are perfectly bonded at their interfaces.

(4) The face sheets and core material do not exhibit bend-twist coupling.

(5) Only loads that do not cause displacements in the y-direction are considered.

Validation of the present theory was performed using several structural analysis problems including static loading, static instability (global buckling and wrinkling), free vibrations, and dynamic loading. The accuracy of the theory was assessed by comparison with the elasticity solutions and with experimental data.

In the study of a static half-sine load applied to the top face sheet of a simply supported sandwich beam/wide panel, the present extended-high order theory is very close to the elasticity solution in terms of both the displacements and the transverse stress or strain, as well as axial stress through the core, and, in addition, the shear stress distributions in the core for core materials ranging from very soft to almost half the stiffness of the face sheets. In particular, it captures the very large range of core shear stress and the nearly parabolic profile in the cases of cores that are not "soft". Results also show that the First-Order Shear Deformable Theory (FOSDT) can yield very inaccurate results in terms of the transverse displacements and shear stress for the range of material and geometry combinations considered.

In the study of global buckling of a simply supported sandwich panel undergoing a static edgewise load, the nonlinear EHSAPT formulation was solved using a perturbation approach, and the elasticity solution was used as the benchmark. The results from three different solution approaches (in conjunction with the perturbation approach) using EHSAPT revealed that accurate global buckling critical loads can only be obtained by either applying the load to just the face sheets and only considering nonlinear deformations in the face sheets (Case(a)), or applying a more realistic distributed load to the faces and the core and considering nonlinear deformations

in the faces and the core (Case(c)). A third solution approach (Case(b)) in which the load is applied to the faces and the core but large deformations in the core are neglected give inaccurate critical loads. The accuracy of these solution approaches using EHSAPT was examined for sandwich panels with a range of face sheet thickness. HSAPT and FOSDT were shown to give less accurate critical loads as the face sheets become thinner with respect to the total height of the sandwich panel.

PFLC (loading on the faces and linear strains in the core) and USNLC (uniform strain loading and nonlinear strains in the core) solution approaches, referred to above as Case (a) and Case (c), respectively, are used to study wrinkling instability of thin face sandwich panels. Predictions of critical wrinkling modes using these two approaches with EHSAPT are compared to elasticity, experiments in literature, and recent experiments that involve sandwich panels with homogeneous and honeycomb type core material. In all sandwich panel configurations considered, including ones with very soft and moderately soft cores, EHSAPT was closest to elasticity. The large discrepancy between HSAPT and elasticity for configurations with very thin face sheets indicate that the in-plane rigidity can play a significant role during wrinkling. Good agreement was found between EHSAPT and wrinkling experiments for sandwich panels with solid and honeycomb cores.

The accuracy of EHSAPT for predicting antisymmetric and symmetric modal frequencies is assessed by comparison with experimental results reported in literature. The predicted modes shapes of EHSAPT are drawn and compared to HSAPT. Further validation of the new theory is conducted by comparing the predicted fundamental frequency with an elasticity solution. Twelve different sandwich configurations ranging from soft to moderate core, thin to thick faces, and short to long beams/wide panels are used as test cases. The classical FOSDT and HSAPT are also shown for comparison. It is shown that EHSAPT yields accurate results for the wide range of test cases.

A numerical case study involving a blast load with a temporal exponential decay and a spatial half-sine profile across the top of the panel is used to compare EHSAPT and HSAPT to a dynamic elasticity benchmark. HSAPT accurately predicts the transverse displacements of the top sheet, middle of the core, and the bottom face sheet, as well as the in-plane displacements of the top and bottom face sheets. EHSAPT does this as well but is also able to capture the non-uniform shear stresses by showing that the shear stress at the top and bottom face/core interfaces can be different.

A three-point bending impact experiment was conducted on a sandwich panel in order to validate the dynamic formulation of EHSAPT. The new sandwich panel theory was able to accurately capture features of the collected strain gauge data on the top and bottom face sheets within the first couple milliseconds of the impact. Beyond this time, but still during impact, structural damping (not taken into account) was believed to play a role.

EHSAPT has been formulated for sandwich beams/wide panel that only undergo loads which make it deform only in the $x - z$ plane. Future work can take the displacement formulation of EHSAPT and extend it to account for deformation out of the $x - z$ plane, i.e., allow for bend-twist coupling, or loading in the $y - z$ plane. Also EHSAPT can be further formulated for plates and shells. EHSAPT in its current or further extended form can be used to solve a number of other structural analysis problems such as: thermal loading, effect of delamination, dynamic stability, to name a few. EHSAPT can be turned into a finite element for use in commercial structural analysis tools.

APPENDIX A

CLASSICAL AND FOSDT

A.1 Classical Sandwich Beam Theory (without shear)

The Classical sandwich theory assumes that the core is transversely incompressible and the displacement of the top and bottom face sheets and core are the same. The governing differential equation is:

$$D_{11}\frac{\partial^4 w(x)}{\partial x^4} = \widetilde{q}^t(x) \ , \tag{64}$$

where D_{11} is the bending stiffness per unit width of the beam.

In the general asymmetric case, the neutral axis of the sandwich section is defined at a distance e from the x-axis (Figure 1):

$$e\left(E_1^t f_t + E_1^b f_b\right) = E_1^t f_t\left(\frac{f_t}{2} + c\right) - E_1^b f_b\left(\frac{f_b}{2} + c\right) \ . \tag{65}$$

Therefore, the bending stiffness per unit width, D_{11}, is:

$$D_{11} = E_1^t\frac{f_t^3}{12} + E_1^t f_t\left(\frac{f_t}{2} + c - e\right)^2 + E_1^b\frac{f_b^3}{12} + E_1^t f_b\left(\frac{f_b}{2} + c + e\right)^2 \ . \tag{66}$$

For the load of (23) the displacement is expressed as:

$$w(x) = W_0 \sin\frac{\pi x}{a} \ . \tag{67}$$

Substituting into Eqn (A1) leads to:

$$W_0 = \frac{q_0 a^4}{D_{11}\pi^4} \ . \tag{68}$$

A.2 First-Order Shear Sandwich Panel Theory

For the First Order Shear model, if we let ψ be the shear deformation then the governing equations with shear effects can be written as:

$$D_{11}\psi_{,xx}(x) - \kappa D_{55}\left[\psi(x) + w_{,x}(x)\right] = 0 \ , \tag{69}$$

$$\kappa D_{55}\left[\psi_{,x}(x) + w_{,xx}(x)\right] + \widetilde{q}^{t}(x) = 0 \ , \tag{70}$$

where $\kappa = 5/6$ is the shear correction factor and

$$D_{55} = G^{c}_{13}(2c) \ . \tag{71a}$$

In some versions of the First Order Shear model, the shear of the face sheets is included, i.e.

$$D_{55} = G^{c}_{13}(2c) + G^{t}_{13}f_t + G^{b}_{13}f_b \ . \tag{71b}$$

Setting

$$w(x) = W_0 \sin\frac{\pi x}{a} \ ; \qquad \psi(x) = \Psi_0 \cos\frac{\pi x}{a} \ . \tag{72}$$

with the load in the same manner as Eqn (23), and substituting in (A5-6) leads to:

$$\Psi_0 = -\frac{L_{13}}{L_{11}L_{33} - L^2_{13}}q_0 \ ; \qquad W_0 = \frac{L_{11}}{L_{11}L_{33} - L^2_{13}}q_0 \ , \tag{73}$$

where

$$L_{11} = D_{11}\frac{\pi^2}{a^2} + \kappa D_{55} \ ; \qquad L_{13} = \kappa D_{55}\frac{\pi}{a} \ ; \qquad L_{33} = \kappa D_{55}\frac{\pi^2}{a^2} \ . \tag{74}$$

APPENDIX B

HSAPT

This theory was first presented in [15] is expressed in terms of five unknown displacement variables, the $u_0^t(x)$, $w_0^t(x)$, $u_0^b(x)$, $w_0^b(x)$ and $\tau^c(x)$. The five differential equations, adapted from Frostig et al (1992) for the present sandwich geometric and coordinate configuration, are as follows:

Top Face Sheet:

$$C_{11}^t f_t u_{0,xx}^t(x) - \tau^c(x) = 0 \ , \tag{75}$$

$$-\frac{C_{33}^c}{2c} w_0^b(x) + C_{11}^t \frac{f_t^3}{12} w_{0,xxxx}^t(x) + \frac{C_{33}^c}{2c} w_0^t(x) - \frac{2c+f_t}{2} \tau_{,x}^c(x) = \widetilde{q}^t(x) \ . \tag{76}$$

Core:

$$u_0^b(x) - u_0^t(x) - \frac{2c+f_b}{2} w_{0,x}^b(x) - \frac{2c+f_t}{2} w_{0,x}^t(x) - \frac{(2c)^3}{12 C_{33}^c} \tau_{,xx}^c(x) + \frac{2c}{C_{55}^c} \tau^c(x) = 0 \ . \tag{77}$$

Bottom Face Sheet:

$$C_{11}^b f_b u_{0,xx}^b(x) + \tau^c(x) = 0 \ , \tag{78}$$

$$C_{11}^b \frac{f_b^3}{12} w_{0,xxxx}^b(x) + \frac{C_{33}^c}{2c} w_0^b(x) - \frac{C_{33}^c}{2c} w_0^t(x) - \frac{2c+f_b}{2} \tau_{,x}^c(x) = 0 \ . \tag{79}$$

By setting the unknown displacement variable profiles in the form

$$u_0^{t,b} = U_0^{t,b} \cos\left(\frac{\pi x}{a}\right) \ ; \quad w_0^{t,b} = W_0^{t,b} \sin\left(\frac{\pi x}{a}\right) \ ; \quad \tau^c = T^c \cos\left(\frac{\pi x}{a}\right) \ , \tag{80}$$

which satisfy the simply supported boundary conditions, and substituting $\widetilde{q}^t(x)$ from Eqn (23), we obtain a system of five linear equations for the $U_0^{t,b}$, $W_0^{t,b}$ and T^c.

In this theory, the displacement field of the core depends on the unknown displacement variables in the following way:

$$w^c(x,z) = w_0^b(x) + \frac{z+c}{2c}\left[w_0^t(x) - w_0^b(x)\right] - \frac{z^2-c^2}{2C_{33}^c}\tau_{,x}^c(x)\ , \tag{81}$$

and

$$u^c(x,z) = u_0^b(x) + \frac{z+c}{C_{55}^c}\tau^c(x) - \frac{1}{2C_{33}^c}\left[(z+c)^2 c - \frac{(z+c)^3}{3}\right]\tau_{,xx}^c(x) -$$
$$-\frac{(z+c)^2}{4c}w_{0,x}^t(x) - \left[\frac{f_t}{2} - \frac{(z+c)^2}{4c} + (z+c)\right]w_{0,x}^b(x)\ . \tag{82}$$

APPENDIX C

EHSAPT WITH STRESS RESULTANTS

C.1 Governing differential equations of EHSAPT

Top face sheet:

$$\begin{aligned}\delta u_0^t: \quad & -N_{,x}^t - \left(\frac{4}{5}C_{55}^c + \frac{2c^2}{35}C_{11}^c\frac{\partial^2}{\partial x^2}\right)\phi_0^c - \left(\frac{7}{30c}C_{55}^c + \frac{c}{35}C_{11}^c\frac{\partial^2}{\partial x^2}\right)u_0^b \\ & - \left(\frac{4}{3c}C_{55}^c + \frac{2c}{15}C_{11}^c\frac{\partial^2}{\partial x^2}\right)u_0^c + \left(\frac{47}{30c}C_{55}^c - \frac{6c}{35}C_{11}^c\frac{\partial^2}{\partial x^2}\right)u_0^t \\ & - \left(\eta_2^b\frac{\partial}{\partial x} - \frac{cf_b}{70}C_{11}^c\frac{\partial^3}{\partial x^3}\right)w_0^b + \beta_1\frac{\partial w_0^c}{\partial x} + \left(\eta_3^t\frac{\partial}{\partial x} - \frac{3cf_t}{35}C_{11}^c\frac{\partial^3}{\partial x^3}\right)w_0^t = 0\ , \end{aligned} \tag{83a}$$

and

$$\begin{aligned}\delta w_0^t: \quad & -N_{,x}^t w_{0,x}^t + M_{,xx}^t - N^t w_{0,xx}^t + \left(\eta_4^t\frac{\partial}{\partial x} + \frac{c^2 f_t}{35}C_{11}^c\frac{\partial^3}{\partial x^3}\right)\phi_0^c + \left(-\eta_2^t\frac{\partial}{\partial x} + \frac{cf_t}{70}C_{11}^c\frac{\partial^3}{\partial x^3}\right)u_0^b \\ & + \left(\eta_6^t\frac{\partial}{\partial x} + \frac{cf_t}{15}C_{11}^c\frac{\partial^3}{\partial x^3}\right)u_0^c + \left(-\eta_3^t\frac{\partial}{\partial x} + \frac{3cf_t}{35}C_{11}^c\frac{\partial^3}{\partial x^3}\right)u_0^t \\ & + \left(\frac{1}{6c}C_{33}^c + \beta_2\frac{\partial^2}{\partial x^2} - \frac{cf_b f_t}{140}C_{11}^c\frac{\partial^4}{\partial x^4}\right)w_0^b + \left(-\frac{4}{3c}C_{33}^c + \eta_7^t\frac{\partial^2}{\partial x^2}\right)w_0^c \\ & + \left(\frac{7}{6c}C_{33}^c + \eta_8^t\frac{\partial^2}{\partial x^2} + \frac{3cf_t^2}{70}C_{11}^c\frac{\partial^4}{\partial x^4}\right)w_0^t = 0\ . \end{aligned} \tag{83b}$$

Core:

$$\begin{aligned}\delta u_0^c: \quad & -N_{,x}^c + \left(-\frac{4}{3c}C_{55}^c + \frac{c}{5}C_{11}^c\frac{\partial^2}{\partial x^2}\right)u_0^b + \left(\frac{8}{3c}C_{55}^c + \frac{4c}{15}C_{11}^c\frac{\partial^2}{\partial x^2}\right)u_0^c \\ & + \left(-\frac{4}{3c}C_{55}^c + \frac{c}{5}C_{11}^c\frac{\partial^2}{\partial x^2}\right)u_0^t - \left(\eta_{6a}^b\frac{\partial}{\partial x} + \frac{cf_b}{10}C_{11}^c\frac{\partial^3}{\partial x^3}\right)w_0^b \\ & + \left(\eta_{6a}^t\frac{\partial}{\partial x} + \frac{cf_t}{10}C_{11}^c\frac{\partial^3}{\partial x^3}\right)w_0^t = 0\ , \end{aligned} \tag{84a}$$

$$\delta\phi_0^c: \quad V^c + M^c_{,x} + \left(\frac{8c}{5}C^c_{55} + \frac{4c^3}{35}C^c_{11}\frac{\partial^2}{\partial x^2}\right)\phi_0^c + \left(\frac{9}{5}C^c_{55} - \frac{c^2}{7}C^c_{11}\frac{\partial^2}{\partial x^2}\right)u_0^b$$
$$+\left(-\frac{9}{5}C^c_{55} + \frac{c^2}{7}C^c_{11}\frac{\partial^2}{\partial x^2}\right)u_0^t + \left(\frac{3}{2}\eta^b_{4a}\frac{\partial}{\partial x} + \frac{c^2 f_b}{14}C^c_{11}\frac{\partial^3}{\partial x^3}\right)w_0^b$$
$$-2c\beta_1\frac{\partial w_0^c}{\partial x} + \left(\frac{3}{2}\eta^t_{4a}\frac{\partial}{\partial x} + \frac{c^2 f_t}{14}C^c_{11}\frac{\partial^3}{\partial x^3}\right)w_0^t = 0\ , \tag{84b}$$

and

$$\delta w_0^c: \quad -V^c_{,x} - \frac{4c}{3}\beta_1\frac{\partial\phi_0^c}{\partial x} + (\beta_1 - C^c_{55})\left(\frac{\partial u_0^b}{\partial x} - \frac{\partial u_0^t}{\partial x}\right) - \left(\frac{4}{3c}C^c_{33} - \eta^b_{7a}\frac{\partial^2}{\partial x^2}\right)w_0^b$$
$$+\left(\frac{8}{3c}C^c_{33} + \frac{4c}{15}C^c_{55}\frac{\partial^2}{\partial x^2}\right)w_0^c - \left(\frac{4}{3c}C^c_{33} - \eta^t_{7a}\frac{\partial^2}{\partial x^2}\right)w_0^t = 0\ . \tag{84c}$$

Bottom face sheet:

$$\delta u_0^b: \quad -N^b_{,x} + \left(\frac{4}{5}C^c_{55} + \frac{2c^2}{35}C^c_{11}\frac{\partial^2}{\partial x^2}\right)\phi_0^c + \left(\frac{47}{30c}C^c_{55} - \frac{6c}{35}C^c_{11}\frac{\partial^2}{\partial x^2}\right)u_0^b$$
$$-\left(\frac{4}{3c}C^c_{55} + \frac{2c}{15}C^c_{11}\frac{\partial^2}{\partial x^2}\right)u_0^c - \left(\frac{7}{30c}C^c_{55} + \frac{c}{35}C^c_{11}\frac{\partial^2}{\partial x^2}\right)u_0^t$$
$$+\left(-\eta^b_3\frac{\partial}{\partial x} + \frac{3cf_b}{35}C^c_{11}\frac{\partial^3}{\partial x^3}\right)w_0^b - \beta_1\frac{\partial w_0^c}{\partial x} + \left(\eta^t_2\frac{\partial}{\partial x} - \frac{cf_t}{70}C^c_{11}\frac{\partial^3}{\partial x^3}\right)w_0^t = 0, \tag{85a}$$

and

$$\delta w_0^b: \quad -N^b_{,x}w^b_{0,x} + M^b_{,xx} - N^b w^b_{0,xx} + \left(\eta^b_4\frac{\partial}{\partial x} + \frac{c^2 f_b}{35}C^c_{11}\frac{\partial^3}{\partial x^3}\right)\phi_0^c + \left(\eta^b_3\frac{\partial}{\partial x} - \frac{3cf_b}{35}C^c_{11}\frac{\partial^3}{\partial x^3}\right)u_0^b$$
$$-\left(\eta^b_6\frac{\partial}{\partial x} + \frac{cf_b}{15}C^c_{11}\frac{\partial^3}{\partial x^3}\right)u_0^c + \left(\eta^b_2\frac{\partial}{\partial x} - \frac{cf_b}{70}C^c_{11}\frac{\partial^3}{\partial x^3}\right)u_0^t$$
$$+\left(\frac{7}{6c}C^c_{33} + \eta^b_8\frac{\partial^2}{\partial x^2} + \frac{3cf_b^2}{70}C^c_{11}\frac{\partial^4}{\partial x^4}\right)w_0^b + \left(-\frac{4}{3c}C^c_{33} + \eta^b_7\frac{\partial^2}{\partial x^2}\right)w_0^c$$
$$+\left(\frac{1}{6c}C^c_{33} + \beta_2\frac{\partial^2}{\partial x^2} - \frac{cf_bf_t}{140}C^c_{11}\frac{\partial^4}{\partial x^4}\right)w_0^t = 0, \tag{85b}$$

The following constants, which were used in the governing equations, are defined ($i = t, b$):

$$\eta_2^i = \frac{1}{30}C_{13}^c + \left(\frac{1}{30} - \frac{7f_i}{60c}\right)C_{55}^c \ , \tag{86a}$$

$$\eta_3^i = -\frac{11}{30}C_{13}^c + \left(\frac{19}{30} + \frac{47f_i}{60c}\right)C_{55}^c \ , \quad \eta_4^i = \frac{4c}{15}C_{13}^c + \left(\frac{4c}{15} + \frac{2f_i}{5}\right)C_{55}^c \ , \tag{86b}$$

$$\eta_6^i = \frac{2}{3}C_{13}^c + \left(\frac{2}{3} + \frac{2f_i}{3c}\right)C_{55}^c \ , \quad \eta_7^i = -\frac{f_i}{5}C_{13}^c - \left(\frac{2c}{15} + \frac{f_i}{5}\right)C_{55}^c \tag{86c}$$

$$\eta_8^i = \frac{11f_i}{30}C_{13}^c - \left(\frac{4c}{15} + \frac{19f_i}{30} + \frac{47{f_i}^2}{120c}\right)C_{55}^c \ , \quad \eta_{4a}^i = \eta_4^i - \left(\frac{2c}{3} + f_i\right)C_{55}^c \tag{86d}$$

$$\eta_{6a}^i = C_{13}^c - \eta_6^i \ , \quad \eta_{7a}^i = \frac{2c + 3f_i}{6}C_{55}^c + \eta_7^i \ , \quad \eta_{8a}^i = \frac{11f_i}{60}C_{13}^c - \eta_8^i \ , \tag{86e}$$

and

$$\beta_1 = \frac{2}{5}(C_{13}^c + C_{55}^c) \ , \tag{86f}$$

$$\beta_2 = \frac{f_b + f_t}{60}C_{13}^c + \left(\frac{c}{15} + \frac{f_b + f_t}{60} - \frac{7f_b f_t}{120c}\right)C_{55}^c \ , \tag{86g}$$

C.2 Boundary conditions of EHSAPT

At each end there are nine boundary conditions, three for each face sheet and three for the core. The corresponding boundary conditions at $x = 0$ and $x = a$, read as follows:

For the top face sheet:

(i) *Either* $\delta u_0^t = 0$ *or,*

$$N^t + \left(\frac{2c^2}{35}C_{11}^c\right)\phi_{0,x}^c + \left(\frac{c}{35}C_{11}^c\right)u_{0,x}^b + \left(\frac{2c}{15}C_{11}^c\right)u_{0,x}^c + \left(\frac{6c}{35}C_{11}^c\right)u_{0,x}^t +$$

$$+ \left(\frac{1}{30}C_{13}^c - \frac{cf_b}{70}C_{11}^c\frac{\partial^2}{\partial x^2}\right)w_0^b - \frac{2}{5}C_{13}^c w_0^c + \left(\frac{11}{30}C_{13}^c + \frac{3cf_t}{35}C_{11}^c\frac{\partial^2}{\partial x^2}\right)w_0^t = \widetilde{N}^t + \frac{\widetilde{n}^c c}{3}, \tag{87a}$$

where $\widetilde{N}^t$ is the end axial force per unit width at the top face.

(ii) *Either* $\delta w_0^t = 0$ *or,*

$$N^t w_{0,x}^t - M_{,x}^t - \left[\frac{2(2c+3f_t)}{15}C_{55}^c + \frac{c^2 f_t}{35}C_{11}^c\frac{\partial^2}{\partial x^2}\right]\phi_0^c + \left[\frac{(2c-7f_t)}{60c}C_{55}^c - \frac{cf_t}{70}C_{11}^c\frac{\partial^2}{\partial x^2}\right]u_0^b$$
$$- \left[\frac{2(c+f_t)}{3c}C_{55}^c + \frac{cf_t}{15}C_{11}^c\frac{\partial^2}{\partial x^2}\right]u_0^c + \left[\frac{(38c+47f_t)}{60c}C_{55}^c - \frac{3cf_t}{35}C_{11}^c\frac{\partial^2}{\partial x^2}\right]u_0^t$$
$$+ \left[\left(\frac{f_b}{60}C_{13}^c - \beta_2\right)\frac{\partial}{\partial x} + \frac{cf_b f_t}{140}C_{11}^c\frac{\partial^3}{\partial x^3}\right]w_0^b$$
$$-\eta_7^t\frac{\partial w_0^c}{\partial x} + \left[\eta_{8a}^t\frac{\partial}{\partial x} - \frac{3cf_t^2}{70}C_{11}^c\frac{\partial^3}{\partial x^3}\right]w_0^t = 0\ , \tag{87b}$$

(iii) Either: $\delta w_{0,x}^t = 0$ or,

$$M^t + \left(\frac{c^2 f_t}{35}C_{11}^c\right)\phi_{0,x}^c + \left(\frac{cf_t}{70}C_{11}^c\right)u_{0,x}^b + \left(\frac{cf_t}{15}C_{11}^c\right)u_{0,x}^c + \left(\frac{3cf_t}{35}C_{11}^c\right)u_{0,x}^t$$
$$+\left(\frac{f_t}{60}C_{13}^c - \frac{cf_b f_t}{140}C_{11}^c\frac{\partial^2}{\partial x^2}\right)w_0^b - \left(\frac{f_t}{5}C_{13}^c\right)w_0^c + \left(\frac{11f_t}{60}C_{13}^c + \frac{3cf_t^2}{70}C_{11}^c\frac{\partial^2}{\partial x^2}\right)w_0^t = \frac{\widetilde{n}^c c f_t}{6}\ , \tag{87c}$$

where $\widetilde{M}^t$ is the end moment per unit width at the top face (at the end $x = 0$ or $x = a$).

For the core:

(i) *Either* $\delta u_0^c = 0$ *or,*

$$N^c - \left(\frac{c}{5}C_{11}^c\right)u_{0,x}^b - \left(\frac{4c}{15}C_{11}^c\right)u_{0,x}^c - \left(\frac{c}{5}C_{11}^c\right)u_{0,x}^t$$
$$+\left(\frac{1}{3}C_{13}^c + \frac{cf_b}{10}C_{11}^c\frac{\partial^2}{\partial x^2}\right)w_0^b - \left(\frac{1}{3}C_{13}^c + \frac{cf_t}{10}C_{11}^c\frac{\partial^2}{\partial x^2}\right)w_0^t = \frac{4\widetilde{n}^c c}{3}\ . \tag{88a}$$

(ii) *Either* $\delta\phi_0^c = 0$ *or,*

$$-M^c - \left(\frac{4c^3}{35}C_{11}^c\right)\phi_{0,x}^c + \left(\frac{c^2}{7}C_{11}^c\right)u_{0,x}^b - \left(\frac{c^2}{7}C_{11}^c\right)u_{0,x}^t - \left(\frac{2c}{5}C_{13}^c + \frac{c^2 f_b}{14}C_{11}^c\frac{\partial^2}{\partial x^2}\right)w_0^b$$
$$+\frac{4c}{5}C_{13}^c w_0^c - \left(\frac{2c}{5}C_{13}^c + \frac{c^2 f_t}{14}C_{11}^c\frac{\partial^2}{\partial x^2}\right)w_0^t = 0\ . \tag{88b}$$

(iii) *Either* $\delta w_0^c = 0$ *or*,

$$V^c + \left[\frac{8c}{15}\phi_0^c + \frac{3}{5}u_0^b - \frac{3}{5}u_0^t - \frac{(2c+3f_b)}{10}w_{0,x}^b - \frac{4c}{15}w_{0,x}^c - \frac{(2c+3f_t)}{10}w_{0,x}^t\right] C_{55}^c = 0 \ . \tag{88c}$$

For the bottom face sheet:

(i) *Either* $\delta u_0^b = 0$ *or*,

$$N^b - \left(\frac{2c^2}{35}C_{11}^c\right)\phi_{0,x}^c + \left(\frac{6c}{35}C_{11}^c\right)u_{0,x}^b + \left(\frac{2c}{15}C_{11}^c\right)u_{0,x}^c + \left(\frac{c}{35}C_{11}^c\right)u_{0,x}^t$$
$$-\left(\frac{11}{30}C_{13}^c + \frac{3cf_b}{35}C_{11}^c\frac{\partial^2}{\partial x^2}\right)w_0^b + \frac{2}{5}C_{13}^c w_0^c + \left(-\frac{1}{30}C_{13}^c + \frac{cf_t}{70}C_{11}^c\frac{\partial^2}{\partial x^2}\right)w_0^t = \widetilde{N}^b + \frac{\widetilde{n}^c c}{3} \ , \tag{89a}$$

where $\widetilde{N}^b$ is the end axial force per unit width at the bottom face

(ii) *Either* $\delta w_0^b = 0$ *or*,

$$N^b w_{0,x}^b - M_{,x}^b - \left[\frac{2(2c+3f_b)}{15}C_{55}^c + \frac{c^2 f_b}{35}C_{11}^c\frac{\partial^2}{\partial x^2}\right]\phi_0^c + \left[-\frac{(38c+47f_b)}{60c}C_{55}^c + \frac{3cf_b}{35}C_{11}^c\frac{\partial^2}{\partial x^2}\right]u_0^b$$
$$+\left[\frac{2(c+f_b)}{3c}C_{55}^c + \frac{cf_b}{15}C_{11}^c\frac{\partial^2}{\partial x^2}\right]u_0^c + \left[\frac{(-2c+7f_b)}{60c}C_{55}^c + \frac{cf_b}{70}C_{11}^c\frac{\partial^2}{\partial x^2}\right]u_0^t$$
$$+\left(\eta_{8a}^b\frac{\partial}{\partial x} - \frac{3cf_b^2}{70}C_{11}^c\frac{\partial^3}{\partial x^3}\right)w_0^b - \left(\eta_7^b\frac{\partial}{\partial x}\right)w_0^c$$
$$+\left[\left(\frac{f_t}{60}C_{13}^c - \beta_2\right)\frac{\partial}{\partial x} + \frac{cf_b f_t}{140}C_{11}^c\frac{\partial^3}{\partial x^3}\right]w_0^t = 0 \ , \tag{89b}$$

(iii) *Either* $\delta w_{0,x}^b = 0$ *or*,

$$M^b + \left(\frac{c^2 f_b}{35}C_{11}^c\right)\phi_{0,x}^c - \left(\frac{3cf_b}{35}C_{11}^c\right)u_{0,x}^b - \left(\frac{cf_b}{15}C_{11}^c\right)u_{0,x}^c - \left(\frac{cf_b}{70}C_{11}^c\right)u_{0,x}^t$$
$$+\left(\frac{11f_b}{60}C_{13}^c + \frac{3cf_b^2}{70}C_{11}^c\frac{\partial^2}{\partial x^2}\right)w_0^b - \frac{f_b}{5}C_{13}^c w_0^c + \left(\frac{f_b}{60}C_{13}^c - \frac{cf_b f_t}{140}C_{11}^c\frac{\partial^2}{\partial x^2}\right)w_0^t = -\frac{\widetilde{n}^c c f_b}{6} \ . \tag{89c}$$

In the above equations, the superscript $\widetilde{}$ denotes the known external boundary values.

APPENDIX D

K_{LC} MATRIX OF EHSAPT

The $[K_{LC}]$ matrix of EHSAPT is symmetric and has the following elements, k_{ij}, $i, j = 1, \ldots 7$:

$$k_{11} = \frac{47}{30c}C_{55}^c + \frac{6c\pi^2}{35a^2}C_{11}^c + C_{11}^b f_b \frac{\pi^2}{a^2} \; ; \quad k_{12} = -\frac{4}{3c}C_{55}^c + \frac{2c\pi^2}{15a^2}C_{11}^c \; , \tag{90a}$$

$$k_{13} = \frac{4}{5}C_{55}^c - \frac{2c^2\pi^2}{35a^2}C_{11}^c \; ; \quad k_{14} = -\frac{7}{30c}C_{55}^c + \frac{c\pi^2}{35a^2}C_{11}^c \; , \tag{90b}$$

$$k_{15} = -\frac{3cf_b\pi^3}{35a^3}C_{11}^c - \eta_3^b\frac{\pi}{a} \; ; \quad k_{16} = -\frac{\pi}{a}\beta_1 \; ; \quad k_{17} = \frac{cf_t\pi^3}{70a^3}C_{11}^c + \eta_2^t\frac{\pi}{a} \; . \tag{90c}$$

$$k_{22} = \frac{8}{3c}C_{55}^c + \frac{16c\pi^2}{15a^2}C_{11}^c \; ; \quad k_{23} = 0 \; ; \quad k_{24} = k_{12} \; , \tag{91a}$$

$$k_{25} = -\frac{cf_b\pi^3}{15a^3}C_{11}^c + \eta_6^b\frac{\pi}{a} \; ; \quad k_{26} = 0 \; ; \quad k_{27} = \frac{cf_t\pi^3}{15a^3}C_{11}^c - \eta_6^t\frac{\pi}{a} \; . \tag{91b}$$

$$k_{33} = \frac{8c}{5}C_{55}^c + \frac{16c^3\pi^2}{105a^2}C_{11}^c \; ; \quad k_{34} = -\frac{4}{5}C_{55}^c + \frac{2c^2\pi^2}{35a^2}C_{11}^c \; , \tag{92a}$$

$$k_{35} = \frac{c^2f_b\pi^3}{35a^3}C_{11}^c - \eta_4^b\frac{\pi}{a} \; ; \quad k_{36} = \frac{4c\beta_1\pi}{3a} \; ; \quad k_{37} = \frac{c^2f_t\pi^3}{35a^3}C_{11}^c - \eta_4^t\frac{\pi}{a} \; . \tag{92b}$$

$$k_{44} = \frac{47}{30c}C_{55}^c + \frac{6c\pi^2}{35a^2}C_{11}^c + C_{11}^t f_t \frac{\pi^2}{a^2} \; ; \quad k_{45} = -\frac{cf_b\pi^3}{70a^3}C_{11}^c - \eta_2^b\frac{\pi}{a} \; , \tag{93a}$$

$$k_{46} = \beta_1\frac{\pi}{a} \; ; \quad k_{47} = \frac{3cf_t\pi^3}{35a^3}C_{11}^c + \eta_3^t\frac{\pi}{a} \; . \tag{93b}$$

$$k_{55} = \frac{7}{6c}C_{33}^c + \frac{3cf_b^2\pi^4}{70a^4}C_{11}^c + \frac{f_b^3\pi^4}{12a^4}C_{11}^b - \eta_8^b\frac{\pi^2}{a^2} \; ; \quad k_{56} = -\frac{4}{3c}C_{33}^c - \eta_7^b\frac{\pi^2}{a^2} \; , \tag{94a}$$

$$k_{57} = \frac{1}{6c} C_{33}^c - \frac{c f_b f_t \pi^4}{140 a^4} C_{11}^c - \beta_2 \frac{\pi^2}{a^2} \ . \tag{94b}$$

$$k_{66} = \frac{8}{3c} C_{33}^c + \frac{16 c \pi^2}{15 a^2} C_{55}^c \ ; \quad k_{67} = -\frac{4}{3c} C_{33}^c - \eta_7^t \frac{\pi^2}{a^2} \ . \tag{95}$$

$$k_{77} = \frac{7}{6c} C_{33}^c + \frac{3 c f_t^2 \pi^4}{70 a^4} C_{11}^c + \frac{f_t^3 \pi^4}{12 a^4} C_{11}^t - \eta_8^t \frac{\pi^2}{a^2} \ . \tag{96}$$

D.1 Elements of the K_{LC} Matrix

The $[K_{LC}]$ matrix is 7×7 symmetric matrix and has the following elements, k_{ij}, $i, j = 1, \ldots 7$:

$$k_{11} = \frac{47}{30c} C_{55}^c + \frac{6 c \alpha_n^2}{35} C_{11}^c + C_{11}^b f_b \alpha_n^2 \ ; \quad k_{12} = -\frac{4}{3c} C_{55}^c + \frac{2 c \alpha_n^2}{15} C_{11}^c \ , \tag{97a}$$

$$k_{13} = \frac{4}{5} C_{55}^c - \frac{2 c^2 \alpha_n^2}{35} C_{11}^c \ ; \quad k_{14} = -\frac{7}{30c} C_{55}^c + \frac{c \alpha_n^2}{35} C_{11}^c \ , \tag{97b}$$

$$k_{15} = -\frac{3 c f_b \alpha_n^3}{35} C_{11}^c - \eta_3^b \alpha_n \ ; \quad k_{16} = -\alpha_n \beta_1 \ ; \quad k_{17} = \frac{c f_t \alpha_n^3}{70} C_{11}^c + \eta_2^t \alpha_n \ . \tag{97c}$$

$$k_{22} = \frac{8}{3c} C_{55}^c + \frac{16 c \alpha_n^2}{15} C_{11}^c \ ; \quad k_{23} = 0 \ ; \quad k_{24} = k_{12} \ , \tag{98a}$$

$$k_{25} = -\frac{c f_b \alpha_n^3}{15} C_{11}^c + \eta_6^b \alpha_n \ ; \quad k_{26} = 0 \ ; \quad k_{27} = \frac{c f_t \alpha_n^3}{15} C_{11}^c - \eta_6^t \alpha_n \ . \tag{98b}$$

$$k_{33} = \frac{8c}{5} C_{55}^c + \frac{16 c^3 \alpha_n^2}{105} C_{11}^c \ ; \quad k_{34} = -\frac{4}{5} C_{55}^c + \frac{2 c^2 \alpha_n^2}{35} C_{11}^c \ , \tag{99a}$$

$$k_{35} = \frac{c^2 f_b \alpha_n^3}{35} C_{11}^c - \eta_4^b \alpha_n \ ; \quad k_{36} = \frac{4 c \beta_1 \alpha_n}{3} \ ; \quad k_{37} = \frac{c^2 f_t \alpha_n^3}{35} C_{11}^c - \eta_4^t \alpha_n \ . \tag{99b}$$

$$k_{44} = \frac{47}{30c} C_{55}^c + \frac{6 c \alpha_n^2}{35} C_{11}^c + C_{11}^t f_t \alpha_n^2 \ ; \quad k_{45} = -\frac{c f_b \alpha_n^3}{70} C_{11}^c - \eta_2^b \alpha_n \ , \tag{100a}$$

$$k_{46} = \beta_1 \alpha_n \ ; \quad k_{47} = \frac{3cf_t\alpha_n^3}{35} C_{11}^c + \eta_3^t \alpha_n \ . \tag{100b}$$

$$k_{55} = \frac{7}{6c} C_{33}^c + \frac{3cf_b^2\alpha_n^4}{70} C_{11}^c + \frac{f_b^3\alpha_n^4}{12} C_{11}^b - \eta_8^b \alpha_n^2 \ ; \quad k_{56} = -\frac{4}{3c} C_{33}^c - \eta_7^b \alpha_n^2 \ , \tag{101a}$$

$$k_{57} = \frac{1}{6c} C_{33}^c - \frac{cf_b f_t \alpha_n^4}{140} C_{11}^c - \beta_2 \alpha_n^2 \ . \tag{101b}$$

$$k_{66} = \frac{8}{3c} C_{33}^c + \frac{16c\alpha_n^2}{15} C_{55}^c \ ; \quad k_{67} = -\frac{4}{3c} C_{33}^c - \eta_7^t \alpha_n^2 \ . \tag{102}$$

$$k_{77} = \frac{7}{6c} C_{33}^c + \frac{3cf_t^2\alpha_n^4}{70} C_{11}^c + \frac{f_t^3\alpha_n^4}{12} C_{11}^t - \eta_8^t \alpha_n^2 \ . \tag{103}$$

where

$$\alpha_n = \frac{n\pi}{a}, \quad \eta_2^i = \frac{1}{30} C_{13}^c + \left(\frac{1}{30} - \frac{7f_i}{60c} \right) C_{55}^c \ , \tag{104a}$$

$$\eta_3^i = -\frac{11}{30} C_{13}^c + \left(\frac{19}{30} + \frac{47f_i}{60c} \right) C_{55}^c \ , \quad \eta_4^i = \frac{4c}{15} C_{13}^c + \left(\frac{4c}{15} + \frac{2f_i}{5} \right) C_{55}^c \ , \tag{104b}$$

$$\eta_6^i = \frac{2}{3} C_{13}^c + \left(\frac{2}{3} + \frac{2f_i}{3c} \right) C_{55}^c \ , \quad \eta_7^i = -\frac{f_i}{5} C_{13}^c - \left(\frac{2c}{15} + \frac{f_i}{5} \right) C_{55}^c \tag{104c}$$

$$\eta_8^i = \frac{11f_i}{30} C_{13}^c - \left(\frac{4c}{15} + \frac{19f_i}{30} + \frac{47{f_i}^2}{120c} \right) C_{55}^c \ , \quad \eta_{4a}^i = \eta_4^i - \left(\frac{2c}{3} + f_i \right) C_{55}^c \tag{104d}$$

$$\eta_{6a}^i = C_{13}^c - \eta_6^i, \quad \eta_{7a}^i = \frac{2c + 3f_i}{6} C_{55}^c + \eta_7^i$$

$$\eta_{8a}^i = \frac{11f_i}{60} C_{13}^c - \eta_8^i \ , \tag{104e}$$

and

$$\beta_1 = \frac{2}{5} (C_{13}^c + C_{55}^c) \ , \tag{105a}$$

$$\beta_2 = \frac{f_b + f_t}{60} C_{13}^c + \left(\frac{c}{15} + \frac{f_b + f_t}{60} - \frac{7f_b f_t}{120c} \right) C_{55}^c \ , \tag{105b}$$

APPENDIX E

HSAPT & ALLEN'S BUCKLING FORMULA

The sandwich buckling formula of Allen (thick faces version) considers the shear stress in the core, and neglects the axial and transverse stiffnesses of the core. The critical load for global buckling from this formula is given in Allen (1969) [2] for a symmetric configuration as:

$$P_{cr,Allen} = P_{E2}\left[\frac{1+\frac{P_{Ef}}{P_c}-\frac{P_{Ef}^2}{P_cP_{E2}}}{1+\frac{P_{E2}}{P_c}-\frac{P_{Ef}}{P_c}}\right] , \tag{106a}$$

where

$$P_{E2} = E_{f1}\frac{\pi^2}{a^2}\left[\frac{f^3}{6}+\frac{f(2c+f)^2}{2}\right] , \tag{106b}$$

$$P_{Ef} = E_{f1}\frac{\pi^2}{a^2}\frac{f^3}{6} ; \quad P_c = G_{c31}\frac{(2c+f)^2}{2c} , \tag{106c}$$

i.e., P_{E2} respresents the Euler load of the sandwich column in the absence of core shear strain with the bending stiffness of the core ignored, but with local bending stiffness of the faces included; P_{Ef} represents the sum of the Euler loads of the two faces when they buckle as independent struts (i.e., when the core is absent) and P_c is the contribution to the buckling load due to shear.

The critical load from the High Order Sandwich Panel theory (HSAPT) is found from solving for the load P in the governing equation for the nontrivial solution (Frostig and Baruch, 1993) [13]:

$$P_{cr,HSAPT} = \frac{2\pi^2\left[(EA)(EI)(2c)g_1\pi^2+6E_3^cG_{31}^cg_2a^2\right]}{(EA)G_{31}^c(2c)^3\pi^4+12(EA)E_3^c(2c)\pi^2a^2+24E_3^cG_{31}^ca^4} , \tag{107a}$$

where EA and EI are respectively, the axial and bending stiffnesses per unit width

of a sandwich beam that is geometrically uniform along the span, i.e.,

$$EA = E_1^f f, \qquad EI = \frac{E_1^f f^3}{12} \ , \tag{107b}$$

and we have defined

$$g_1 = G_{31}^c (2c)^2 \frac{\pi^2}{a^2} + 12 E_3^c \ ; \quad g_2 = (EA) f^2 + 2(EA)(2c) f + (EA)(2c)^2 + 4(EI) \ , \tag{107c}$$

This original formulation of the critical global buckling load of HSAPT can be algebraically manipulated by making use of the Allen thick parameters above to appear in the following form:

$$P_{cr,HSAPT} = P_{E2} \left\{ \frac{1 + \left[1 + \frac{(2c)^2 G_{31}^c \pi^2}{12 E_3^c a^2} \right] \left(\frac{P_{Ef}}{P_c} - \frac{P_{Ef}^2}{P_c P_{E2}} \right)}{1 + \left[1 + \frac{(2c)^2 G_{31}^c \pi^2}{12 E_3^c a^2} \right] \frac{(P_{E2} - P_{Ef})}{P_c}} \right\} \ . \tag{108}$$

Thus, when E_3^c goes to infinity (an incompressible core) the $P_{cr,HSAPT}$ approaches the $P_{cr,Allen}$ formula.

APPENDIX F

M & K MATRICES OF EHSAPT

The mass matrix matrix $[M_n]$ of EHSAPT is symmetric and contains elements $m_{ij} = m_{ji}$ and $\alpha_n = \frac{n\pi}{a}$:

$$m_{11} = b\left(f_b\rho^b + \frac{6c\rho^c}{35}\right) \;; \quad m_{12} = \frac{2bc\rho^c}{15} \;, \tag{109a}$$

$$m_{13} = -\frac{2bc^2\rho^c}{35} \;; \quad m_{14} = \frac{bc\rho^c}{35} \;, \tag{109b}$$

$$m_{15} = -\frac{3bcf_b\rho^c\alpha_n}{35} \;; \quad m_{16} = 0 \;; \quad m_{17} = \frac{bcf_t\rho^c\alpha_n}{70} \;. \tag{109c}$$

$$m_{22} = \frac{16bc\rho^c}{15} \;; \quad m_{23} = 0 \;; \quad m_{24} = m_{12} \;, \tag{109d}$$

$$m_{25} = -\frac{bcf_b\rho^c\alpha_n}{15} \;; \quad m_{26} = 0 \;; \quad m_{27} = \frac{bcf_t\rho^c\alpha_n}{15} \;. \tag{109e}$$

$$m_{33} = \frac{16bc^3\rho^c}{105} \;; \quad m_{34} = \frac{2bc^2\rho^c}{35} \;, \tag{109f}$$

$$m_{35} = \frac{bc^2f_b\rho^c\alpha_n}{35} \;; \quad m_{36} = 0 \;; \quad m_{37} = \frac{bc^2f_t\rho^c\alpha_n}{35} \;. \tag{109g}$$

$$m_{44} = b\left(\frac{6c\rho^c}{35} + f_t\rho^t\right) \;; \quad m_{45} = -\frac{bcf_b\rho^c\alpha_n}{70} \;, \tag{109h}$$

$$m_{46} = 0 \;; \quad m_{47} = \frac{3bcf_t\rho^c\alpha_n}{35} \;. \tag{109i}$$

$$m_{55} = b\left(f_b\rho_b + \frac{4c\rho^c}{15} + \left(\frac{f_b^3\rho_b}{12} + \frac{3cf_b^2\rho^c}{70}\right)\alpha_n^2\right) \;; \quad m_{56} = m_{12} \;, \tag{109j}$$

$$m_{57} = b\left(-\frac{c\rho^c}{15} - \frac{cf_bf_t\rho^c\alpha_n^2}{140}\right) \;. \tag{109k}$$

$$m_{66} = \frac{16bc\rho^c}{15} \;; \quad m_{67} = m_{12} \;. \tag{109l}$$

$$m_{77} = b\left(\frac{4c\rho_c}{15} + f_t\rho^t + \left(\frac{3cf_t^2\rho^c}{70} + \frac{f_t^3\rho^t}{12}\right)\alpha_n^2\right) \;. \tag{109m}$$

The stiffness matrix $[K_n]$ of EHSAPT is also symmetric and contains elements $k_{ij} = k_{ji}$:

$$k_{11} = b\left(\frac{47}{30c}C^c_{55} + \alpha^b_1\alpha^2_n\right) \;; \quad k_{12} = b\left(-\frac{4}{3c}C^c_{55} + \frac{2c\alpha^2_n}{15}C^c_{11}\right) \;, \tag{110a}$$

$$k_{13} = b\left(\frac{4}{5}C^c_{55} - \frac{2c^2\alpha^2_n}{35}C^c_{11}\right) \;; \quad k_{14} = b\left(-\frac{7}{30c}C^c_{55} + \frac{c\alpha^2_n}{35}C^c_{11}\right) \;, \tag{110b}$$

$$k_{15} = -b\left(\frac{3cf_b\alpha^3_n}{35}C^c_{11} + \eta^b_3\alpha_n\right) \;; \quad k_{16} = -b\beta_1\alpha_n \;; \quad k_{17} = b\left(\frac{cf_t\alpha^3_n}{70}C^c_{11} + \eta^t_2\alpha_n\right) \;. \tag{110c}$$

$$k_{22} = b\left(\frac{8}{3c}C^c_{55} + \frac{16c\alpha^2_n}{15}C^c_{11}\right) \;; \quad k_{23} = 0 \;; \quad k_{24} = k_{12} \;, \tag{110d}$$

$$k_{25} = b\left(-\frac{cf_b\alpha^3_n}{15}C^c_{11} + \eta^b_6\alpha_n\right) \;; \quad k_{26} = 0 \;; \quad k_{27} = b\left(\frac{cf_t\alpha^3_n}{15}C^c_{11} - \eta^t_6\alpha_n\right) \;. \tag{110e}$$

$$k_{33} = b\left(\frac{8c}{5}C^c_{55} + \frac{16c^3\alpha^2_n}{105}C^c_{11}\right) \;; \quad k_{34} = b\left(-\frac{4}{5}C^c_{55} + \frac{2c^2\alpha^2_n}{35}C^c_{11}\right) \;, \tag{110f}$$

$$k_{35} = b\left(\frac{c^2f_b\alpha^3_n}{35}C^c_{11} - \eta^b_4\alpha_n\right) \;; \quad k_{36} = \frac{4bc\beta_1\alpha_n}{3} \;; \quad k_{37} = b\left(\frac{c^2f_t\alpha^3_n}{35}C^c_{11} - \eta^t_4\alpha_n\right) \;. \tag{110g}$$

$$k_{44} = b\left(\frac{47}{30c}C^c_{55} + \alpha^t_1\alpha^2_n\right) \;; \quad k_{45} = -b\left(\frac{cf_b\alpha^3_n}{70}C^c_{11} + \eta^b_2\alpha_n\right) \;, \tag{110h}$$

$$k_{46} = b\beta_1\alpha_n \;; \quad k_{47} = b\left(\frac{3cf_t\alpha^3_n}{35}C^c_{11} + \eta^t_3\alpha_n\right) \;. \tag{110i}$$

$$k_{55} = b\left(\frac{7}{6c}C^c_{33} - \eta^b_8\alpha^2_n + \eta^b_9\alpha^4_n\right) \;; \quad k_{56} = -b\left(\frac{4}{3c}C^c_{33} + \eta^b_7\alpha^2_n\right) \;, \tag{110j}$$

$$k_{57} = b\left(\frac{1}{6c}C^c_{33} - \frac{cf_bf_t\alpha^4_n}{140}C^c_{11} - \beta_2\alpha^2_n\right) \;. \tag{110k}$$

$$k_{66} = b\left(\frac{8}{3c}C^c_{33} + \frac{16c\alpha^2_n}{15}C^c_{55}\right) \;; \quad k_{67} = -b\left(\frac{4}{3c}C^c_{33} + \eta^t_7\alpha^2_n\right) \;. \tag{110l}$$

$$k_{77} = b\left(\frac{7}{6c}C^c_{33} - \eta^t_8\alpha^2_n + \eta^t_9\alpha^4_n\right) \;. \tag{110m}$$

F.1 First Order Shear Deformable Theory (FOSDT)

For the First Order Shear model, the transverse and axial displacement field are, respectively:

$$w(x,z,t) = w(x,t); \quad u(x,z,t) = u_0 - z\phi(x,t) \tag{111}$$

The 3x3 symmetric mass matrix of FOSDT contains $m_{ij} = m_{ji}$ and $\alpha_n = \frac{n\pi}{a}$:

$$m_{11} = b(f_b\rho^b + 2c\rho^c + f_t\rho^t); \tag{112a}$$

$$m_{12} = \frac{b}{2}\left(2cf_b\rho^b + f_b^2\rho^b - 2cf_t\rho^t - f_t^2\rho_t\right); \quad m_{13} = 0; \tag{112b}$$

$$m_{22} = \frac{b}{3}\left(f_b^3\rho^b + 2c^3\rho^c + f_t^3\rho^t + 3c^2\left(f_b\rho^b + f_t\rho^t\right) + 3c\left(f_b^2\rho^b + f_t^2\rho^t\right)\right) \tag{112c}$$

$$m_{23} = 0; \quad m_{33} = b(f_b\rho^b + 2c\rho^c + f_t\rho^t) \tag{112d}$$

and the 3x3 symmetric stiffness matrix of FOSDT with $k_{ij} = k_{ji}$ contain:

$$k_{11} = b\alpha_n^2\left(2cE_1^c + E_1^b f_b + E_1^t f_t\right); \tag{113a}$$

$$k_{12} = \frac{b\alpha_n^2}{2}\left(2cE_1^b f_b + E_1^b f_b^2 - 2cE_1^t f_t - E_1^t f_t^2\right); \quad k_{13} = 0; \tag{113b}$$

$$\begin{aligned} k_{22} = \frac{b}{6}(2\alpha_n^2(2c^3E_1^c + E_1^b f_b^3 + E_1^t f_t^3 + 3c^2(E_1^b f_b + E_1^t f_t) \\ +3c(E_1^b f_b^2 + E_1^t f_t^2)) + 3(4c + f_b + f_t)kG_{31}^c) \end{aligned} \tag{113c}$$

$$k_{23} = -\frac{b\alpha_n}{2}(4c + f_b + f_t)kG_{31}^c; \quad k_{33} = -\alpha_n k_{23} \tag{113d}$$

where k with no subscript is the shear correction factor, taken as either $k = 5/6$ or $k = 1$.

The eigenvector of FOSDT is

$$\{U_n(t)\} = \{U_{0n}, \Phi_{0n}, W_{0n}\}^T \tag{114}$$

F.2 High-Order Sandwich Panel Theory (HSAPT)

The High-Order Sandwich Panel Theory accounts for the shear and transverse normal stresses in the core and assumes that the in-plane stresses in the core are null. The displacements based formulation of HSAPT has the following 5 unknown displacements variables: $u_0^t(x)$, $u_0^b(x)$, $w^t(x)$, $w^b(x)$, and $w_0^c(x)$.

The axial and transverse displacement fields of the top and bottom face sheet, as well as the transverse displacement field of the core are the same as ESHAPT shown in Eqns. (2a), (2b), and (4a). However, this model differs from EHSAPT in that the axial displacement field between $-c < z < c$ is defined as:

$$\begin{aligned} u^c(x,z,t) = &\left(\frac{1}{2}+\frac{z}{2c}\right)u_0^t(x,t) + \left(\frac{1}{2}-\frac{z}{2c}\right)u_0^b(x,t) + \left(-\frac{z}{3}+\frac{z^3}{3c^2}\right)w_{0,x}^c(x,t) \\ &+\left(-\left(\frac{f_b}{4}+\frac{c}{4}\right)+\left(\frac{1}{6}+\frac{f_b}{4c}\right)z+\frac{1}{4c}z^2-\frac{1}{6c^2}z^3\right)w_{,x}^b(x,t) \\ &+\left(\left(\frac{f_t}{4}+\frac{c}{4}\right)+\left(\frac{1}{6}+\frac{f_t}{4c}\right)z-\frac{1}{4c}z^2-\frac{1}{6c^2}z^3\right)w_{,x}^t(x,t) \end{aligned} \tag{115}$$

It should be noted that the the accelerations in the core are allowed to be nonlinear throughout the height of the core. This distinguishes it from an earlier model of HSAPT in which the accelerations were assumed to be linear through the height of the core in [14].

The 5×5 symmetric mass matrix of HSAPT has $m_{ij} = m_{ji}$ and $\alpha_n = \frac{n\pi}{a}$:

$$m_{11} = \frac{b}{3}\left(3f_b\rho^b + 2c\rho^c\right); \quad m_{12} = \frac{1}{3}bc\rho^c; \tag{116a}$$

$$m_{13} = -\frac{1}{90}bc\rho^c\alpha_n\left(30f_b+17c\right); \quad m_{14}\frac{2}{45}bc^2\rho^c\alpha_n; \tag{116b}$$

$$m_{15} = \frac{1}{90}bc\rho^c\alpha_n\left(13c+15f_t\right); \tag{116c}$$

$$m_{22} = \frac{1}{3}b\left(2c\rho^c+3f_t\rho^t\right); \quad m_{23} = -\frac{1}{90}bc\rho^c\alpha_n\left(15f_b+13c\right); \tag{116d}$$

$$m_{24} = -\frac{2}{45}bc^2\rho^c\alpha_n; \quad m_{25} = \frac{1}{90}bc\rho^c\alpha_n\left(17c+30f_t\right); \tag{116e}$$

$$\begin{aligned} m_{33} = \frac{1}{72}b\Bigg(&\frac{2\alpha_n^2}{105}\left(714c^2f_b\rho^c+630cf_b^2\rho^c+315f_b^3\rho^b+268c^3\rho^c\right) \\ &+\frac{24}{5}\left(15f_b\rho^b+4c\rho^c\right)\Bigg); \end{aligned} \tag{116f}$$

$$m_{34} = \frac{1}{72}b\left(\frac{2}{105}\left(-84c^2 f_b \rho^c \alpha_n^2 - 32c^3 \rho^c \alpha_n^2\right) + \frac{48c\rho^c}{5}\right); \tag{116g}$$

$$m_{35} = \frac{1}{72}b\left(-\frac{2}{105}c\rho^c \alpha_n^2\left(273c\left(f_b + f_t\right) + 315 f_b f_t + 236c^2\right) - \frac{24c\rho^c}{5}\right); \tag{116h}$$

$$m_{44} = \frac{1}{36}b\left(\frac{64}{105}c^3 \rho^c \alpha_n^2 + \frac{192c\rho^c}{5}\right); \tag{116i}$$

$$m_{45} = \frac{1}{36}b\left(\frac{24c\rho^c}{5} - \frac{4}{105}c^2 \rho^c \alpha_n^2\left(8c + 21 f_t\right)\right); \tag{116j}$$

$$m_{55} = \frac{b\alpha_n^2\left(2c\rho^c\left(134c^2 + 357c f_t + 315 f_t^2\right) + 315 f_t^3 \rho^t\right)}{3780} + \frac{1}{15}b\left(4c\rho^c + 15 f_t \rho^t\right); \tag{116k}$$

and the 5×5 symmetric stiffness matrix of HSAPT with $k_{ij} = k_{ji}$ contain:

$$k_{11} = \frac{bG_{31}^c}{2c} + b f_b E_1^b \alpha_n^2; \tag{117a}$$

$$k_{12} = -\frac{bG_{31}^c}{2c}; \quad k_{13} = -\frac{bG_{31}^c \alpha_n\left(3 f_b + 2c\right)}{12c}; \tag{117b}$$

$$k_{14} = -\frac{2}{3}bG_{31}^c \alpha_n; \quad k_{15} = -\frac{bG_{31}^c \alpha_n\left(2c + 3 f_t\right)}{12c}; \tag{117c}$$

$$k_{22} = \frac{bG_{31}^c}{2c} + b f_t \alpha_n^2 E_1^t; \tag{117d}$$

$$k_{23} = \frac{bG_{31}^c \alpha_n\left(3 f_b + 2c\right)}{12c}; \quad k_{24} = \frac{2}{3}bG_{31}^c \alpha_n; \tag{117e}$$

$$k_{25} = \frac{bG_{31}^c \alpha_n\left(2c + 3 f_t\right)}{12c}; \tag{117f}$$

$$k_{33} = \frac{1}{72}b\left(\frac{G_{31}^c \alpha_n^2\left(3 f_b + 2c\right)^2}{c} + 6 f_b^3 E_1^b \alpha_n^4 + \frac{84E_3^c}{c}\right); \tag{117g}$$

$$k_{34} = \frac{1}{72}b\left(8G_{31}^c \alpha_n^2\left(3 f_b + 2c\right) - \frac{96E_3^c}{c}\right); \tag{117h}$$

$$k_{35} = \frac{1}{72}b\left(\frac{G_{31}^c \alpha_n^2\left(3 f_b + 2c\right)\left(2c + 3 f_t\right)}{c} + \frac{12E_3^c}{c}\right); \tag{117i}$$

$$k_{44} = \frac{1}{36}b\left(32cG_{31}^c \alpha_n^2 + \frac{96E_3^c}{c}\right); \quad k_{45} = \frac{1}{36}b\left(4G_{31}^c \alpha_n^2\left(2c + 3 f_t\right) - \frac{48E_3^c}{c}\right); \tag{117j}$$

$$k_{55} = \frac{bG_{31}^c \alpha_n^2\left(2c + 3 f_t\right)^2}{72c} + \frac{7bE_3^c}{6c} + \frac{1}{12}b f_t^3 \alpha_n^4 E_1^t; \tag{117k}$$

The eigenvector of HSAPT is

$$\{U_n\} = \{U_{0n}^b, U_{0n}^t, W_n^b, W_{0n}^c, W_n^t\}^T \tag{118}$$

F.3 Mass and stiffness matrices for EHSAPT

The mass matrix matrix $[M_n]$ is symmetric and contains elements $m_{ij} = m_{ji}$ and $\alpha_n = \frac{n\pi}{a}$:

$$m_{11} = b\left(f_b\rho^b + \frac{6c\rho^c}{35}\right) \;; \quad m_{12} = \frac{2bc\rho^c}{15} \;, \tag{119a}$$

$$m_{13} = -\frac{2bc^2\rho^c}{35} \;; \quad m_{14} = \frac{bc\rho^c}{35} \;, \tag{119b}$$

$$m_{15} = -\frac{3bcf_b\rho^c\alpha_n}{35} \;; \quad m_{16} = 0 \;; \quad m_{17} = \frac{bcf_t\rho^c\alpha_n}{70} \;. \tag{119c}$$

$$m_{22} = \frac{16bc\rho^c}{15} \;; \quad m_{23} = 0 \;; \quad m_{24} = k_{12} \;, \tag{119d}$$

$$m_{25} = -\frac{bcf_b\rho^c\alpha_n}{15} \;; \quad m_{26} = 0 \;; \quad m_{27} = \frac{bcf_t\rho^c\alpha_n}{15} \;. \tag{119e}$$

$$m_{33} = \frac{16bc^3\rho^c}{105} \;; \quad m_{34} = \frac{2bc^2\rho^c}{35} \;, \tag{119f}$$

$$m_{35} = \frac{bc^2f_b\rho^c\alpha_n}{35} \;; \quad m_{36} = 0 \;; \quad m_{37} = \frac{bc^2f_t\rho^c\alpha_n}{35} \;. \tag{119g}$$

$$m_{44} = b\left(\frac{6c\rho^c}{35} + f_t\rho^t\right) \;; \quad m_{45} = -\frac{bcf_b\rho^c\alpha_n}{70} \;, \tag{119h}$$

$$m_{46} = 0 \;; \quad m_{47} = \frac{3bcf_t\rho^c\alpha_n}{35} \;. \tag{119i}$$

$$m_{55} = b\left(f_b\rho_b + \frac{4c\rho^c}{15} + \left(\frac{f_b^3\rho_b}{12} + \frac{3cf_b^2\rho^c}{70}\right)\alpha_n^2\right) \;; \quad m_{56} = m_{12} \;, \tag{119j}$$

$$m_{57} = b\left(-\frac{c\rho^c}{15} - \frac{cf_bf_t\rho^c\alpha_n^2}{140}\right) \;. \tag{119k}$$

$$m_{66} = \frac{16bc\rho^c}{15} \;; \quad m_{67} = k_{12} \;. \tag{119l}$$

$$m_{77} = b\left(\frac{4c\rho_c}{15} + f_t\rho^t + \left(\frac{3cf_t^2\rho^c}{70} + \frac{f_t^3\rho^t}{12}\right)\alpha_n^2\right) \;. \tag{119m}$$

The stiffness matrix $[K_n]$ is also symmetric and contains elements $k_{ij} = k_{ji}$:

$$k_{11} = b\left(\frac{47}{30c}C_{55}^c + \alpha_1^b\alpha_n^2\right) \;; \quad k_{12} = b\left(-\frac{4}{3c}C_{55}^c + \frac{2c\alpha_n^2}{15}C_{11}^c\right) \;, \tag{120a}$$

$$k_{13} = b\left(\frac{4}{5}C_{55}^c - \frac{2c^2\alpha_n^2}{35}C_{11}^c\right) \;; \quad k_{14} = b\left(-\frac{7}{30c}C_{55}^c + \frac{c\alpha_n^2}{35}C_{11}^c\right) \;, \tag{120b}$$

$$k_{15} = -b\left(\frac{3cf_b\alpha_n^3}{35}C_{11}^c + \eta_3^b\alpha_n\right) \;; \quad k_{16} = -b\beta_1\alpha_n \;; \quad k_{17} = b\left(\frac{cf_t\alpha_n^3}{70}C_{11}^c + \eta_2^t\alpha_n\right) \;. \tag{120c}$$

$$k_{22} = b\left(\frac{8}{3c}C^c_{55} + \frac{16c\alpha_n^2}{15}C^c_{11}\right) \;; \quad k_{23} = 0 \;; \quad k_{24} = k_{12} \;, \tag{120d}$$

$$k_{25} = b\left(-\frac{cf_b\alpha_n^3}{15}C^c_{11} + \eta^b_6\alpha_n\right) \;; \quad k_{26} = 0 \;; \quad k_{27} = b\left(\frac{cf_t\alpha_n^3}{15}C^c_{11} - \eta^t_6\alpha_n\right) \;. \tag{120e}$$

$$k_{33} = b\left(\frac{8c}{5}C^c_{55} + \frac{16c^3\alpha_n^2}{105}C^c_{11}\right) \;; \quad k_{34} = b\left(-\frac{4}{5}C^c_{55} + \frac{2c^2\alpha_n^2}{35}C^c_{11}\right) \;, \tag{120f}$$

$$k_{35} = b\left(\frac{c^2f_b\alpha_n^3}{35}C^c_{11} - \eta^b_4\alpha_n\right) \;; \quad k_{36} = \frac{4bc\beta_1\alpha_n}{3} \;; \quad k_{37} = b\left(\frac{c^2f_t\alpha_n^3}{35}C^c_{11} - \eta^t_4\alpha_n\right) \;. \tag{120g}$$

$$k_{44} = b\left(\frac{47}{30c}C^c_{55} + \alpha^t_1\alpha_n^2\right) \;; \quad k_{45} = -b\left(\frac{cf_b\alpha_n^3}{70}C^c_{11} + \eta^b_2\alpha_n\right) \;, \tag{120h}$$

$$k_{46} = b\beta_1\alpha_n \;; \quad k_{47} = b\left(\frac{3cf_t\alpha_n^3}{35}C^c_{11} + \eta^t_3\alpha_n\right) \;. \tag{120i}$$

$$k_{55} = b\left(\frac{7}{6c}C^c_{33} - \eta^b_8\alpha_n^2 + \eta^b_9\alpha_n^4\right) \;; \quad k_{56} = -b\left(\frac{4}{3c}C^c_{33} + \eta^b_7\alpha_n^2\right) \;, \tag{120j}$$

$$k_{57} = b\left(\frac{1}{6c}C^c_{33} - \frac{cf_bf_t\alpha_n^4}{140}C^c_{11} - \beta_2\alpha_n^2\right) \;. \tag{120k}$$

$$k_{66} = b\left(\frac{8}{3c}C^c_{33} + \frac{16c\alpha_n^2}{15}C^c_{55}\right) \;; \quad k_{67} = -b\left(\frac{4}{3c}C^c_{33} + \eta^t_7\alpha_n^2\right) \;. \tag{120l}$$

$$k_{77} = b\left(\frac{7}{6c}C^c_{33} - \eta^t_8\alpha_n^2 + \eta^t_9\alpha_n^4\right) \;. \tag{120m}$$

F.4 High-Order Sandwich Panel Theory (HSAPT)

The High-Order Sandwich Panel Theory accounts for the shear and transverse normal stresses in the core and assumes that the in-plane stresses in the core are null. The displacements based formulation of HSAPT presented in [34] has the following 5 unknown displacements variables: $u^t_0(x)$, $u^b_0(x)$, $w^t(x)$, $w^b(x)$, and $w^c_0(x)$.

The in-plane and transverse displacement fields of the top and bottom face sheet, as well as the transverse displacement field of the core are the same as ESHAPT shown in Eqns. (2a), (2b), and (4a). However, this model differs from EHSAPT in

that the in-plane displacement field between $-c < z < c$ is defined as:

$$\begin{aligned} u^c(x,z,t) = &\left(\frac{1}{2}+\frac{z}{2c}\right)u_0^t(x,t) + \left(\frac{1}{2}-\frac{z}{2c}\right)u_0^b(x,t) + \left(-\frac{z}{3}+\frac{z^3}{3c^2}\right)w_{0,x}^c(x,t) \\ &+\left(-\left(\frac{f_b}{4}+\frac{c}{4}\right)+\left(\frac{1}{6}+\frac{f_b}{4c}\right)z+\frac{1}{4c}z^2-\frac{1}{6c^2}z^3\right)w_{,x}^b(x,t) \\ &+\left(\left(\frac{f_t}{4}+\frac{c}{4}\right)+\left(\frac{1}{6}+\frac{f_t}{4c}\right)z-\frac{1}{4c}z^2-\frac{1}{6c^2}z^3\right)w_{,x}^t(x,t) \end{aligned} \tag{121}$$

It should be noted that the the accelerations in the core are allowed to be nonlinear throughout the height of the core. This distinguishes it from an earlier model of HSAPT in which the accelerations were assumed to be linear through the height of the core in [14]. The transverse strain in the same as EHSAPT shown in Eqn. and shear strains in the core is given by the relation:

$$\gamma_{zx}^c = \frac{\partial u^c(x,z)}{\partial z} + \frac{\partial w^c(x,z)}{\partial x} \tag{122}$$

The transverse and shear stresses in the core are found from the constitutive relation:

$$\sigma_{zz}^c = E_3^c \epsilon_{zz}^c; \quad \tau_{zx}^c = G_{31}^c \gamma_{zx}^c \tag{123}$$

The governing equations of motion of a simply supported sandwich beam/ wide panel undergoing the load in Eqn. (58) using HSAPT can be cast in the following matrix form:

$$[M_n]\{\ddot{U_n}(t)\} + [K_n]\{U_n(t)\} = \{F_n(t)\} \tag{124}$$

where $[M_n]$ and $[K_n]$ are the mass and stiffness matrices of the nth Fourier term, respectively. The 5×5 symmetric mass matrix of HSAPT has $m_{ij} = m_{ji}$ and $\alpha_n = \frac{n\pi}{a}$:

$$m_{11} = \frac{b}{3}\left(3f_b\rho^b + 2c\rho^c\right); \quad m_{12} = \frac{1}{3}bc\rho^c; \tag{125a}$$

$$m_{13} = -\frac{1}{90}bc\rho^c\alpha_n\left(30f_b + 17c\right); \quad m_{14}\frac{2}{45}bc^2\rho^c\alpha_n; \tag{125b}$$

$$m_{15} = \frac{1}{90}bc\rho^c\alpha_n\left(13c + 15f_t\right); \tag{125c}$$

$$m_{22} = \frac{1}{3}b\left(2c\rho^c + 3f_t\rho^t\right); \quad m_{23} = -\frac{1}{90}bc\rho^c\alpha_n\left(15f_b + 13c\right); \tag{125d}$$

$$m_{24} = -\frac{2}{45} b c^2 \rho^c \alpha_n; \quad m_{25} = \frac{1}{90} b c \rho^c \alpha_n \left(17c + 30 f_t\right); \tag{125e}$$

$$m_{33} = \frac{1}{72} b \left(\frac{2\alpha_n^2}{105} \left(714 c^2 f_b \rho^c + 630 c f_b^2 \rho^c + 315 f_b^3 \rho^b + 268 c^3 \rho^c\right) + \frac{24}{5} \left(15 f_b \rho^b + 4 c \rho^c\right) \right); \tag{125f}$$

$$m_{34} = \frac{1}{72} b \left(\frac{2}{105} \left(-84 c^2 f_b \rho^c \alpha_n^2 - 32 c^3 \rho^c \alpha_n^2\right) + \frac{48 c \rho^c}{5} \right); \tag{125g}$$

$$m_{35} = \frac{1}{72} b \left(-\frac{2}{105} c \rho^c \alpha_n^2 \left(273 c \left(f_b + f_t\right) + 315 f_b f_t + 236 c^2\right) - \frac{24 c \rho^c}{5} \right); \tag{125h}$$

$$m_{44} = \frac{1}{36} b \left(\frac{64}{105} c^3 \rho^c \alpha_n^2 + \frac{192 c \rho^c}{5} \right); \tag{125i}$$

$$m_{45} = \frac{1}{36} b \left(\frac{24 c \rho^c}{5} - \frac{4}{105} c^2 \rho^c \alpha_n^2 \left(8c + 21 f_t\right) \right); \tag{125j}$$

$$m_{55} = \frac{b \alpha_n^2 \left(2 c \rho^c \left(134 c^2 + 357 c f_t + 315 f_t^2\right) + 315 f_t^3 \rho^t\right)}{3780} + \frac{1}{15} b \left(4 c \rho^c + 15 f_t \rho^t\right); \tag{125k}$$

and the 5×5 symmetric stiffness matrix of HSAPT with $k_{ij} = k_{ji}$ contain:

$$k_{11} = \frac{b G_{31}^c}{2c} + b f_b E_1^b \alpha_n^2; \tag{126a}$$

$$k_{12} = -\frac{b G_{31}^c}{2c}; \quad k_{13} = -\frac{b G_{31}^c \alpha_n \left(3 f_b + 2c\right)}{12c}; \tag{126b}$$

$$k_{14} = -\frac{2}{3} b G_{31}^c \alpha_n; \quad k_{15} = -\frac{b G_{31}^c \alpha_n \left(2c + 3 f_t\right)}{12c}; \tag{126c}$$

$$k_{22} = \frac{b G_{31}^c}{2c} + b f_t \alpha_n^2 E_1^t; \tag{126d}$$

$$k_{23} = \frac{b G_{31}^c \alpha_n \left(3 f_b + 2c\right)}{12c}; \quad k_{24} = \frac{2}{3} b G_{31}^c \alpha_n; \tag{126e}$$

$$k_{25} = \frac{b G_{31}^c \alpha_n \left(2c + 3 f_t\right)}{12c}; \tag{126f}$$

$$k_{33} = \frac{1}{72} b \left(\frac{G_{31}^c \alpha_n^2 \left(3 f_b + 2c\right)^2}{c} + 6 f_b^3 E_1^b \alpha_n^4 + \frac{84 E_3^c}{c} \right); \tag{126g}$$

$$k_{34} = \frac{1}{72} b \left(8 G_{31}^c \alpha_n^2 \left(3 f_b + 2c\right) - \frac{96 E_3^c}{c} \right); \tag{126h}$$

$$k_{35} = \frac{1}{72} b \left(\frac{G_{31}^c \alpha_n^2 \left(3 f_b + 2c\right) \left(2c + 3 f_t\right)}{c} + \frac{12 E_3^c}{c} \right); \tag{126i}$$

$$k_{44} = \frac{1}{36} b \left(32 c G_{31}^c \alpha_n^2 + \frac{96 E_3^c}{c} \right); \quad k_{45} = \frac{1}{36} b \left(4 G_{31}^c \alpha_n^2 \left(2c + 3 f_t\right) - \frac{48 E_3^c}{c} \right); \tag{126j}$$

$$k_{55} = \frac{bG_{31}^c \alpha_n^2 \left(2c + 3f_t\right)^2}{72c} + \frac{7bE_3^c}{6c} + \frac{1}{12} b f_t^3 \alpha_n^4 E_1^t; \tag{126k}$$

The vector of the unknown generalized coordinates in (124) are

$$\{U_n(t)\} = \{U_n^b(t), U_n^t(t), W_n^b(t), W_n^c(t), W_n^t(t)\}^T \tag{127}$$

and the load vector $\{F_n(t)\} = T(t)\{0, 0, 0, 0, Q_n\}^T$. The ordinary differential equations in time (Eqn. (124)) can be solved using standard numerical integration methods.

REFERENCES

[1] Aitharaju, V., "C0 zigzag kinematic displacement models for the analysis of laminated composites," *Mechanics of Composite Materials and Structures*, vol. 6, no. 1, pp. 31–56, 1999.

[2] Allen, H., *Analysis and design of structural sandwich panels*, vol. 51. Pergamon press Oxford, UK:, 1969.

[3] Berdichevsky, V., "An asymptotic theory of sandwich plates," *International Journal of Engineering Science*, vol. 48, no. 3, pp. 383–404, 2010.

[4] Berdichevsky, V., "Nonlinear theory of hard-skin plates and shells," *International Journal of Engineering Science*, vol. 48, no. 3, pp. 357–369, 2010.

[5] Bozhevolnaya, E. and Frostig, Y., "High-order modeling and experimental validation of local effects in sandwich beams," *Journal of aircraft*, vol. 43, no. 1, pp. 189–193, 2006.

[6] Carlsson, L. and Kardomateas, G., *Structural and failure mechanics of sandwich composites*, vol. 121. Kluwer Academic Pub, 2011.

[7] Carrera, E., "Theories and finite elements for multilayered plates and shells: a unified compact formulation with numerical assessment and benchmarking," *Archives of Computational Methods in Engineering*, vol. 10, no. 3, pp. 215–296, 2003.

[8] Carrera, E. and Brischetto, S., "A survey with numerical assessment of classical and refined theories for the analysis of sandwich plates," *Applied mechanics reviews*, vol. 62, p. 010803, 2009.

[9] Demasi, L., "Three-dimensional closed form solutions and ∞^3 theories for orthotropic plates," *Mechanics of Advanced Materials and Structures*, vol. 17, no. 1, pp. 20–39, 2009.

[10] Engesser, F., "Die knickfestigheit gerader stabe," *Zentralblatt der Bauverwaltung*, vol. 11, pp. 483–486, 1891.

[11] Frostig, Y., "Buckling of sandwich panels with a flexible core–high-order theory," *International Journal of Solids and Structures*, vol. 35, no. 3-4, pp. 183–204, 1998.

[12] Frostig, Y., "On wrinkling of a sandwich panel with a compliant core and self-equilibrated loads," June 2010 2010.

[13] Frostig, Y. and Baruch, M., "High-order buckling analysis of sandwich beams with transversely flexible core," *Journal of Engineering Mechanics*, vol. 119, p. 476, 1993.

[14] Frostig, Y. and Baruch, M., "Free vibrations of sandwich beams with a transversely flexible core: a high order approach," *Journal of sound and vibration*, vol. 176, no. 2, pp. 195–208, 1994.

[15] Frostig, Y., Baruch, M., Vilnay, O., and Sheinman, I., "Highorder theory for sandwichbeam behavior with transversely flexible core," *Journal of Engineering Mechanics*, vol. 118, p. 1026, 1992.

[16] Gardner, N., Wang, E., Kumar, P., and Shukla, A., "Blast mitigation in a sandwich composite using graded core and polyurea interlayer," *Experimental Mechanics*, pp. 1–15, 2011.

[17] Goodier, J. and Neou, I., "The evaluation of theoretical critical compression in sandwich plates," *Journal of the Aeronautical Sciences*, vol. 18, no. 10, p. 649, 1951.

[18] Hoff, N. and Mautner, S., "The buckling of sandwich-type panels," *Journal of the Aeronautical Sciences*, vol. 12, no. 3, pp. 285–297, 1945.

[19] Hohe, J., Librescu, L., and Yong Oh, S., "Dynamic buckling of flat and curved sandwich panels with transversely compressible core," *Composite structures*, vol. 74, no. 1, pp. 10–24, 2006.

[20] Huang, H. and Kardomateas, G., "Buckling and initial postbuckling behavior of sandwich beams including transverse shear," *AIAA journal*, vol. 40, no. 11, pp. 2331–2335, 2002.

[21] Jackson, M. and Shukla, A., "Performance of sandwich composites subjected to sequential impact and air blast loading," *Composites Part B: Engineering*, vol. 42, no. 2, pp. 155–166, 2011.

[22] Jensen, A. and Irgens, F., "Thickness vibrations of sandwich plates and beams and delamination detection," *Journal of intelligent material systems and structures*, vol. 10, no. 1, p. 46, 1999.

[23] Kardomateas, G., "Wrinkling of wide sandwich panels beams with orthotropic phases by an elasticity approach," *Journal of Applied Mechanics*, vol. 72, p. 818, 2005.

[24] Kardomateas, G., "An elasticity solution for the global buckling of sandwich beams/wide panels with orthotropic phases," *Journal of Applied Mechanics*, vol. 77, p. 021015, 2010.

[25] Kardomateas, G. and Phan, C., "Three-dimensional elasticity solution for sandwich beams/wide plates with orthotropic phases: The negative discriminant case," *Journal of Sandwich Structures and Materials*, vol. 13, no. 6, pp. 641–661, 2011.

[26] Ley, R. P., Weichuan, L., and Mbanefo, U., "Facesheet wrinkling in sandwich structures," 1999.

[27] Li, R. and Kardomateas, G., "Nonlinear high-order core theory for sandwich plates with orthotropic phases," *AIAA journal*, vol. 46, no. 11, pp. 2926–2934, 2008.

[28] Nemat-Nasser, S., Kang, W., McGee, J., Guo, W., and Isaacs, J., "Experimental investigation of energy-absorption characteristics of components of sandwich structures," *International journal of impact engineering*, vol. 34, no. 6, pp. 1119–1146, 2007.

[29] Norris, C., Ericksen, W., March, H., Smith, C., and Boller, K., "Wrinkling of the facings of sandwich construction subjected to edgewise compression," *FPL Report No. 1810*, 1961.

[30] Pagano, N., "Exact solutions for composite laminates in cylindrical bending," *Journal of Composite Materials*, vol. 3, no. 3, pp. 398–411, 1969.

[31] Phan, C., Frostig, Y., and Kardomateas, G., "Analysis of sandwich panels with a compliant core and with in-plane rigidity-extended high-order sandwich panel theory versus elasticity," *Journal of Applied Mechanics*, in press.

[32] Phan, C. and Kardomateas, G., "Global buckling of a sandwich wide panel/beam based on the extended high order theory," *AIAA Journal*, in press.

[33] Plantema, F., *Sandwich construction: the bending and buckling of sandwich beams, plates, and shells*. Wiley, 1966.

[34] Schwarts-Givli, H., Rabinovitch, O., and Frostig, Y., "Free vibration of delaminated unidirectional sandwich panels with a transversely flexible core and general boundary conditionsa high-order approach," *Journal of Sandwich Structures and Materials*, vol. 10, no. 2, pp. 99–131, 2008.

[35] Sokolinsky, V., Nutt, S., and Frostig, Y., "Boundary condition effects in free vibrations of higher-order soft sandwich beams," *AIAA journal*, vol. 40, no. 6, pp. 1220–1227, 2002.

[36] Swanson, S. and Kim, J., "Comparison of a higher order theory for sandwich beams with finite element and elasticity analyses," *Journal of Sandwich Structures and Materials*, vol. 2, no. 1, pp. 33–49, 2000.

[37] Tekalur, S., Bogdanovich, A., and Shukla, A., "Shock loading response of sandwich panels with 3-d woven e-glass composite skins and stitched foam core," *Composites Science and Technology*, vol. 69, no. 6, pp. 736–753, 2009.

[38] Vinson, J., *The behavior of sandwich structures of isotropic and composite materials*. CRC, 1999.

[39] Vonach, W. and Rammerstorfer, F., "The effects of in-plane core stiffness on the wrinkling behavior of thick sandwiches," *Acta mechanica*, vol. 141, no. 1, pp. 1–10, 2000.

[40] Wang, E., Gardner, N., and Shukla, A., "The blast resistance of sandwich composites with stepwise graded cores," *International Journal of Solids and Structures*, vol. 46, no. 18, pp. 3492–3502, 2009.

[41] Zenkour, A., "Three-dimensional elasticity solution for uniformly loaded cross-ply laminates and sandwich plates," *Journal of Sandwich Structures and Materials*, vol. 9, no. 3, p. 213, 2007.

REFERENCES

[1] Aitharaju, V., "C0 zigzag kinematic displacement models for the analysis of laminated composites," *Mechanics of Composite Materials and Structures*, vol. 6, no. 1, pp. 31–56, 1999.

[2] Allen, H., *Analysis and design of structural sandwich panels*, vol. 51. Pergamon press Oxford, UK:, 1969.

[3] Berdichevsky, V., "An asymptotic theory of sandwich plates," *International Journal of Engineering Science*, vol. 48, no. 3, pp. 383–404, 2010.

[4] Berdichevsky, V., "Nonlinear theory of hard-skin plates and shells," *International Journal of Engineering Science*, vol. 48, no. 3, pp. 357–369, 2010.

[5] Bozhevolnaya, E. and Frostig, Y., "High-order modeling and experimental validation of local effects in sandwich beams," *Journal of aircraft*, vol. 43, no. 1, pp. 189–193, 2006.

[6] Carlsson, L. and Kardomateas, G., *Structural and failure mechanics of sandwich composites*, vol. 121. Kluwer Academic Pub, 2011.

[7] Carrera, E., "Theories and finite elements for multilayered plates and shells: a unified compact formulation with numerical assessment and benchmarking," *Archives of Computational Methods in Engineering*, vol. 10, no. 3, pp. 215–296, 2003.

[8] Carrera, E. and Brischetto, S., "A survey with numerical assessment of classical and refined theories for the analysis of sandwich plates," *Applied mechanics reviews*, vol. 62, p. 010803, 2009.

[9] Demasi, L., "Three-dimensional closed form solutions and ∞^3 theories for orthotropic plates," *Mechanics of Advanced Materials and Structures*, vol. 17, no. 1, pp. 20–39, 2009.

[10] Engesser, F., "Die knickfestigheit gerader stabe," *Zentralblatt der Bauverwaltung*, vol. 11, pp. 483–486, 1891.

[11] Frostig, Y., "Buckling of sandwich panels with a flexible core–high-order theory," *International Journal of Solids and Structures*, vol. 35, no. 3-4, pp. 183–204, 1998.

[12] Frostig, Y., "On wrinkling of a sandwich panel with a compliant core and self-equilibrated loads," June 2010 2010.

[13] Frostig, Y. and Baruch, M., "High-order buckling analysis of sandwich beams with transversely flexible core," *Journal of Engineering Mechanics*, vol. 119, p. 476, 1993.

[14] Frostig, Y. and Baruch, M., "Free vibrations of sandwich beams with a transversely flexible core: a high order approach," *Journal of sound and vibration*, vol. 176, no. 2, pp. 195–208, 1994.

[15] Frostig, Y., Baruch, M., Vilnay, O., and Sheinman, I., "Highorder theory for sandwichbeam behavior with transversely flexible core," *Journal of Engineering Mechanics*, vol. 118, p. 1026, 1992.

[16] Gardner, N., Wang, E., Kumar, P., and Shukla, A., "Blast mitigation in a sandwich composite using graded core and polyurea interlayer," *Experimental Mechanics*, pp. 1–15, 2011.

[17] Goodier, J. and Neou, I., "The evaluation of theoretical critical compression in sandwich plates," *Journal of the Aeronautical Sciences*, vol. 18, no. 10, p. 649, 1951.

[18] Hoff, N. and Mautner, S., "The buckling of sandwich-type panels," *Journal of the Aeronautical Sciences*, vol. 12, no. 3, pp. 285–297, 1945.

[19] Hohe, J., Librescu, L., and Yong Oh, S., "Dynamic buckling of flat and curved sandwich panels with transversely compressible core," *Composite structures*, vol. 74, no. 1, pp. 10–24, 2006.

[20] Huang, H. and Kardomateas, G., "Buckling and initial postbuckling behavior of sandwich beams including transverse shear," *AIAA journal*, vol. 40, no. 11, pp. 2331–2335, 2002.

[21] Jackson, M. and Shukla, A., "Performance of sandwich composites subjected to sequential impact and air blast loading," *Composites Part B: Engineering*, vol. 42, no. 2, pp. 155–166, 2011.

[22] Jensen, A. and Irgens, F., "Thickness vibrations of sandwich plates and beams and delamination detection," *Journal of intelligent material systems and structures*, vol. 10, no. 1, p. 46, 1999.

[23] Kardomateas, G., "Wrinkling of wide sandwich panels beams with orthotropic phases by an elasticity approach," *Journal of Applied Mechanics*, vol. 72, p. 818, 2005.

[24] Kardomateas, G., "An elasticity solution for the global buckling of sandwich beams/wide panels with orthotropic phases," *Journal of Applied Mechanics*, vol. 77, p. 021015, 2010.

[25] Kardomateas, G. and Phan, C., "Three-dimensional elasticity solution for sandwich beams/wide plates with orthotropic phases: The negative discriminant case," *Journal of Sandwich Structures and Materials*, vol. 13, no. 6, pp. 641–661, 2011.

[26] Ley, R. P., Weichuan, L., and Mbanefo, U., "Facesheet wrinkling in sandwich structures," 1999.

[27] Li, R. and Kardomateas, G., "Nonlinear high-order core theory for sandwich plates with orthotropic phases," *AIAA journal*, vol. 46, no. 11, pp. 2926–2934, 2008.

[28] Nemat-Nasser, S., Kang, W., McGee, J., Guo, W., and Isaacs, J., "Experimental investigation of energy-absorption characteristics of components of sandwich structures," *International journal of impact engineering*, vol. 34, no. 6, pp. 1119–1146, 2007.

[29] Norris, C., Ericksen, W., March, H., Smith, C., and Boller, K., "Wrinkling of the facings of sandwich construction subjected to edgewise compression," *FPL Report No. 1810*, 1961.

[30] Pagano, N., "Exact solutions for composite laminates in cylindrical bending," *Journal of Composite Materials*, vol. 3, no. 3, pp. 398–411, 1969.

[31] Phan, C., Frostig, Y., and Kardomateas, G., "Analysis of sandwich panels with a compliant core and with in-plane rigidity-extended high-order sandwich panel theory versus elasticity," *Journal of Applied Mechanics*, in press.

[32] Phan, C. and Kardomateas, G., "Global buckling of a sandwich wide panel/beam based on the extended high order theory," *AIAA Journal*, in press.

[33] Plantema, F., *Sandwich construction: the bending and buckling of sandwich beams, plates, and shells*. Wiley, 1966.

[34] Schwarts-Givli, H., Rabinovitch, O., and Frostig, Y., "Free vibration of delaminated unidirectional sandwich panels with a transversely flexible core and general boundary conditionsa high-order approach," *Journal of Sandwich Structures and Materials*, vol. 10, no. 2, pp. 99–131, 2008.

[35] Sokolinsky, V., Nutt, S., and Frostig, Y., "Boundary condition effects in free vibrations of higher-order soft sandwich beams," *AIAA journal*, vol. 40, no. 6, pp. 1220–1227, 2002.

[36] Swanson, S. and Kim, J., "Comparison of a higher order theory for sandwich beams with finite element and elasticity analyses," *Journal of Sandwich Structures and Materials*, vol. 2, no. 1, pp. 33–49, 2000.

[37] Tekalur, S., Bogdanovich, A., and Shukla, A., "Shock loading response of sandwich panels with 3-d woven e-glass composite skins and stitched foam core," *Composites Science and Technology*, vol. 69, no. 6, pp. 736–753, 2009.

[38] Vinson, J., *The behavior of sandwich structures of isotropic and composite materials*. CRC, 1999.

[39] Vonach, W. and Rammerstorfer, F., "The effects of in-plane core stiffness on the wrinkling behavior of thick sandwiches," *Acta mechanica*, vol. 141, no. 1, pp. 1–10, 2000.

[40] Wang, E., Gardner, N., and Shukla, A., "The blast resistance of sandwich composites with stepwise graded cores," *International Journal of Solids and Structures*, vol. 46, no. 18, pp. 3492–3502, 2009.

[41] Zenkour, A., "Three-dimensional elasticity solution for uniformly loaded cross-ply laminates and sandwich plates," *Journal of Sandwich Structures and Materials*, vol. 9, no. 3, p. 213, 2007.

VITA

Catherine Phan received her Bachelor of Science degrees in Mechanical and Aerospace Engineering in 2007 from the University of California, Irvine. She received her Master of Science degree in Aerospace Engineering in 2009 from the Georgia Institute of Technology. She enjoys paragliding and surfing.